Age Determination of the Outer Lateral Moraines of Barun Glacier in Nepal

Cosmogenic Radionuclide Surface Exposure Dating of Moraines with ^{10}Be and Former ELA and Glacial Extent Reconstructions of Barun Glacier

GEO 511 Master's Thesis

Author
Laura Büchler
13-754-254

Supervised by
Dr. Frank Paul
Prof. Dr. Markus Egli

Faculty Representative
Prof. Dr. Markus Egli

30.04.2019
Department of Geography, University of Zurich

'Men argue. Nature acts.'
Voltaire

ABSTRACT

The Himalayan orogen is a most interesting study site in terms of tectonics, geomorphology and climate due to its extreme relief and location at the transition zone between the monsoon influenced region and the semiarid/arid Tibetan Plateau. The aim of this Master's Thesis is to gain information about the Quaternary glacial history of the Barun Glacier next to Mount Makalu in Nepal, with a special focus on the age determination of the sequence of moraines above the Makalu Base Camp. For this purpose, a dedicated field survey collected rock chips from large boulders deposited on three moraines outside the prominent Little Ice Age moraine of Barun Glacier and examined them geochronologically using ^{10}Be surface exposure dating, weathering rind depths and Schmidt-Hammer measurements. The dating revealed glacial advances during the Late Pleistocene (~ 12 ka), Early Holocene (~ 8 ka) and Late Holocene (~ 3 ka). However, there are at least six more moraines within this sequence, implying a very sensitive reaction of the glacier to changes in climate. Surprisingly, moraines from the Last Glacial Maximum (LGM) or pre-LGM moraines that have been found in the neighbouring Khumbu Valley are missing in the Barun Valley and have likely been removed by erosion or buried by thrusting.

Additionally, equilibrium line altitudes (ELAs) were estimated with data from mapped and dated glacier extents in the Khumbu Valley using the inversed THAR (toe to headwall altitude ratio) method to reconstruct glacial extents of Barun Glacier and illustrate/analyze them in a GIS. According to this analysis, ELA values dropped by 289, 132 and 19 m during the LGM, Early Holocene and Late Holocene, respectively, compared to the Little Ice Age ELA. A cross-comparison with the accumulation area ratio (AAR) method shows that a THAR value of 0.5 with glacier extents from the Randolph Glacier Inventory provided the most reasonable results for the Barun Valley. Additionally, using the mean elevation out of seven accumulation basins as the headwall altitude reveals the best results. Uncertainties are introduced by the unknown amount of debris cover, unconsidered tributaries, and missing terminal moraines so that the glacial extents derived here provide only a starting point for further investigations. Dating of the other moraines – including those on the opposite side of the valley – would certainly provide additional insights about past glaciological and thus also climatic variability in the Barun Valley.

CONTENT

FIGURES

TABLES

ABBREVIATIONS

AAR	Accumulation Area Ratio
A.D.	Anno Domini
AMS	Accelerator Mass Spectrometry
ANOVA	Analysis of Variance
^{10}Be	Radioactive Isotope of Beryllium
BP	Before Present (Present = 1950)
BR	Balance Ratio
CRN	Cosmogenic Radionuclide
DEM	Digital Elevation Model
EL	Equilibrium Line
ELA	Equilibrium Line Altitude
ENSO	El Niño/Southern Oscillation
ESA	European Space Agency
ETH	Eidgenössische Technische Hochschule
GAMDAM	Glacier Area Mapping for Discharge in Asian Mountains
GGI	GAMDAM Glacier Inventory
GLIMS	Global Land Ice Measurements from Space
GLOF	Glacier Lake Outburst Flood
GPS	Global Positioning System
GIS	Geographic Information System
HF	Hydrofluoric acid
HMA	High Mountain Asia
IPCC	Intergovernmental Panel on Climate Change
LGM	Last Glacial Maximum
LIA	Little Ice Age
LLGM	Local Last Glacial Maximum
MELM	Maximum Elevation of Lateral Moraines
MEG	Median Elevation of Glaciers
MIS	Marine Isotopic Stage
NSIDC	National Snow and Ice Data Center
OSL	Optically Stimulated Luminescence
RGI	Randolph Glacier Inventory
SLHL	Sea-level high-latitude
TCN	Terrestrial Cosmogenic Nuclide
THAR	Toe to Headwall Altitude Ratio
TP	Tibetan Plateau
TRAM	Toe to Ridge Altitude Method
TSAM	Toe to Summit Altitude Method
YD	Younger Dryas

1. INTRODUCTION

1.1 Relevance of Glaciers

Glaciers are receding globally (IPCC, 2007). Although the Himalayas is the most glacierized mountain range outside the poles (Haeberli *et al.*, 1988), the impact of climate change on glaciers is especially high in this region. These glaciers supply water to Indus, Ganges, Brahmaputra, Yangtze and Yellow rivers, where more than 1.4 billion people depend on (Immerzeel *et al.*, 2010; Brun *et al.*, 2017). Especially, the Brahmaputra and Indus basins are most susceptible to decreased waterflow in terms of drinking water supplies, food security, irrigation, mining, hydropower, agriculture and recreation (Immerzeel *et al.*, 2010; Brun *et al.*, 2017; Huss *et al.*, 2017). However, human dependence on glacier melt does not correlate with the highest population densities in most regions according to a study conducted by Kaser *et al.* (2010). Large uncertainties in future runoff occur due to variations in projected precipitation between different climate models (Immerzeel *et al.*, 2013; Radić and Hock, 2014). A study conducted in Nepal by Immerzeel *et al.* (2013) projects increasing runoff despite receding glaciers at least until 2050. Together with a positive change in precipitation, water availability is not likely to decrease in this region (Immerzeel *et al.*, 2013). Azam *et al.* (2018), Lutz *et al.* (2014) and Huss and Hock (2018) suggest a similar scenario with increasing glacier runoff predictions. However, they claim that in roughly half of their investigated basins the maximum ('peak water') has already been passed and thus runoff steadily declines (Huss and Hock, 2018). Additionally, they predict the globally largest reduction in runoff occurs in central Asia and the Andes (Huss and Hock, 2018). However, recent mass balance computations of High Mountain Asia revealed less negative estimates than previous estimations (Brun *et al.*, 2017). An anomaly takes place in the Pamir and Karakoram (Cogley, 2016), where at least for the last decade the overall mass balance is two to three times less negative than the global average for glaciers (Gardelle *et al.*, 2013) or according to other studies nearly balanced (Azam *et al.*, 2018). Bliss *et al.* (2014) highlight the variety of glacier runoff responses to climate change and emphasize that rain is a major contributor to runoff in the monsoon influenced region of Asia in contrast to most regions where glacier melt dominates annual glacier runoff. Hence, glaciers in the Himalayas play an important role in hydrology and might be severely impacted by future climate change, but knowledge about their past fluctuations is still sparse.

Glaciers react fast and pronounced to fluctuations in climate (Oerlemans, 2005), and their deposits (moraines) marking former extents are thus good indicators for past climatic conditions (Dong *et al.*, 2018). Such moraines have been dated to reconstruct climate fluctuations in glacierized regions such as the Himalayas or the Tibetan Plateau (Balco, 2011; Dong *et al.*, 2018). Although the glaciers in the Himalayas play an important role in climate reconstruction, knowledge about their dynamics and climatic controls is sparse (Finkel *et al.*, 2003; Owen and Dortch, 2014; Azam *et al.*, 2018). Especially the timing and extent of former glacier fluctuations are yet more unclear than in other mountain ranges, mainly due to limitations in logistical and political accessibility of the glacierized regions (Owen *et al.*, 2008; Zech *et al.*, 2009; Owen and Dortch, 2014). Additionally, glacial depositions from before the Little Ice Age (LIA) are poorly preserved due to the high erodibility of the material in high altitudes, steep terrain and large amounts of precipitation (Zech *et al.*, 2009). In addition, large landslides hinder the identification of some landforms and thus complicate their interpretation (Hewitt, 2009). The missing quantification of the timing and extent of past

glaciers is required for better linking Himalayan climate fluctuations to changes in global climate (Finkel *et al.*, 2003).

1.2 The Study Region

In contrast to the Alps and other glacierized mountain regions, the glaciers in the south of the Himalayas are influenced by the south Asian summer monsoon, which is responsible for heavy precipitation during summer (Benn and Owen, 1998). Whereas during winter the Himalayan orogen is dominated by mid-latitude westerly winds (westerlies), which generally bring cold and relatively dry air (Inoue, 1978; Benn and Owen, 1998; Maussion *et al.*, 2014). Hence, the timing of highest accumulation coincides with the highest ablation. Glaciers in this climatic regime have been named summer-accumulation type glaciers (Ageta and Higuchi, 1984). Increased moisture availability due to the south Asian summer monsoon might also be the reason why the glaciers in this region behaved asynchronously to glacial advances in the northern hemisphere (Finkel *et al.*, 2003; Owen *et al.*, 2008, 2009). To better understand the interaction between the two climate systems in the transition zone (i.e. influenced by the south Asian summer monsoon and the Eurasian mid-latitude westerlies) (Dong *et al.*, 2018), the Barun Valley in the Makalu National Park (Nepal) was chosen for this thesis to test if the timing of the glacier fluctuations found for the nearby Khumbu Valley could possibly be extended to the east. Barun Glacier is a ca. 17 km long valley glacier that is heavily debris covered in its lower part and located 19 km south east of Mount Everest next to Mount Makalu (8485 m). Barun Glacier produced a sequence of well-preserved lateral moraines well outside the dominating moraines from LIA, implying active and pronounced glacier fluctuations during the Holocene and maybe Pleistocene. Once dated, these glacial remnants, provide information about the timing and former extents of the glacier as well as related climatic fluctuations that can be derived from changes in mean or median elevation.

1.3 State of Knowledge

In the past two decades, numerous studies have been performed to analyse the glacial history of the Quaternary in the Himalayan and Tibetan orogen with the aim of a better understanding of the timing and extent of glaciations (Finkel *et al.*, 2003; Owen and Dortch, 2014; Dong *et al.*, 2018). Especially improvements in the cosmogenic surface exposure dating technique with the isotope Beryllium 10 (^{10}Be) give new and better insight in the timing of past glaciations (Dong *et al.*, 2018). Several glacial chronologies suggest that glaciers in this region reached much larger extents thousands of years prior to the Last Glacial Maximum (LGM) which occurred 19-23 ka ago and is also known as the Marine Isotope Stage 2 or MIS2 (Clark and Mix, 2002). It is speculated that this was due to the high sensitivity of glaciers to fluctuations in precipitation which are coming from changing monsoon intensities (Owen *et al.*, 2002a,b; Finkel *et al.*, 2003; Chen *et al.*, 2015; Dong *et al.*, 2017). A study by Finkel *et al.* (2003) conducted to the south of Mt. Everest on several glaciers in the Khumbu Valley revealed at least seven glacier advances during the Pleistocene and Holocene as derived from ^{10}Be surface exposure dating of large boulders within lateral and terminal moraines (*Fig. 1*). They argue that glaciation was most extensive during MIS 3 and earlier and quite limited during MIS 2 i.e. the LGM. This data implies an asynchronous behaviour of the glaciers in this

region compared to other glaciers in the Northern hemisphere, presumably due to changing monsoon intensities. The oldest moraine has been dated at 86 ± 6 ka during MIS 5 in the Khumbu Valley. The extent during MIS 2 was less pronounced than other extents and occurred locally at 23 ± 3 ka. Similar results were obtained by other studies as shown in *Fig. 2* (Sharma and Owen, 1996; Phillips *et al.*, 2000; Owen *et al.*, 2002a,b; Chen *et al.*, 2015).
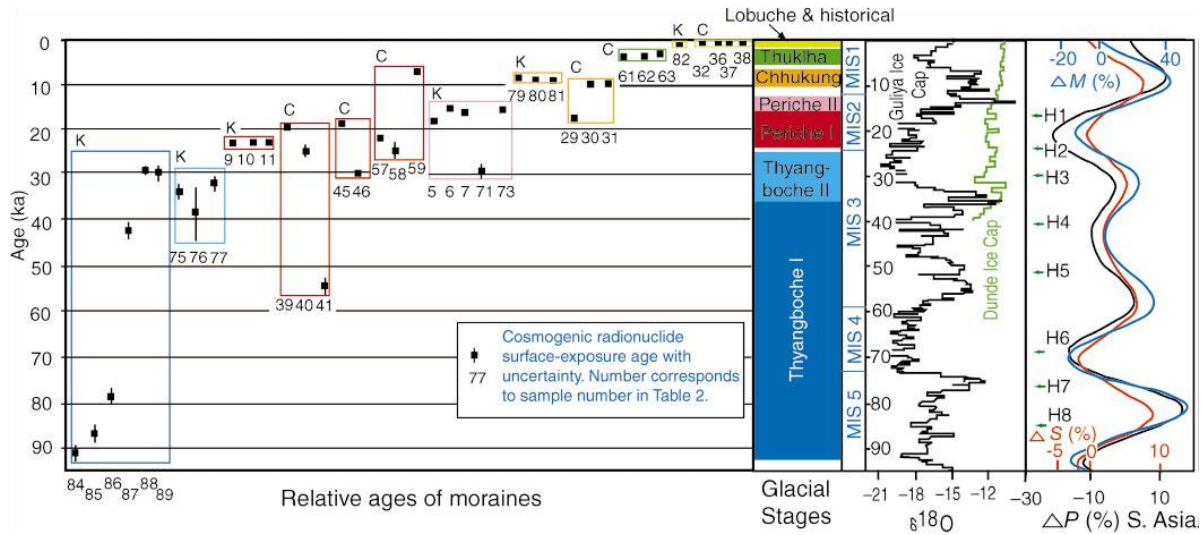
Fig. 1: Cosmogenic radionuclide (CRN) ages for moraines in Khumbu Himal south of Mt. Everest (Finkel et al. 2003).
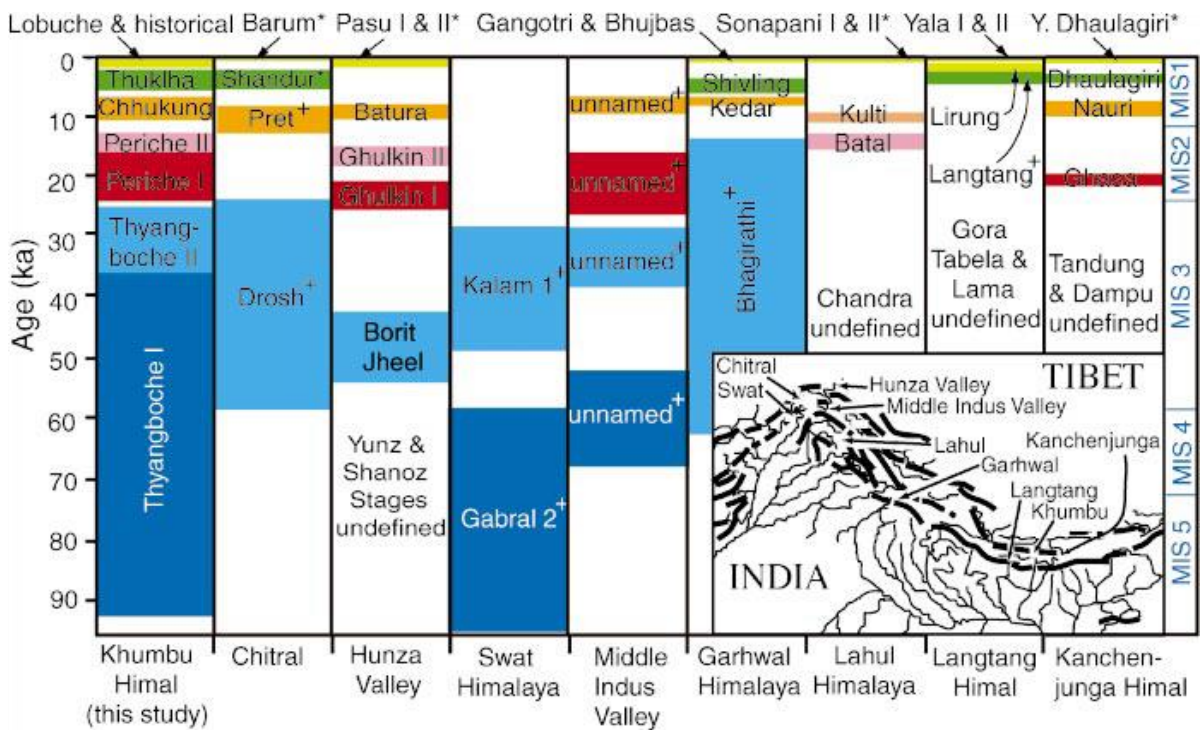
Fig. 2: Glacial chronologies in the Himalayan orogen that have been conducted with numerical dating techniques such as ^{10}Be (Finkel et al. 2003).

1.4 Research Questions

This thesis analyses the age of some lateral moraines in the Barun Valley next to the Makalu Base Camp at 5000 m a.s.l. in Nepal with cosmogenic radionuclide (CRN) surface exposure dating and relative dating techniques (Schmidt-Hammer measurements and weathering rind quantifications). In total, five rock samples of three moraines have been collected and dated with the ^{10}Be-method. The ages of the different moraines will show whether the Barun Glacier behaved similar to the glaciers south of Mount Everest during the last glaciations or not. A synchronous behaviour with the glaciers of Mt. Everest implies that during the LGM 23 ka years ago (MIS 2), Barun Glacier did not reach its largest extent and older moraines outside of the LGM moraine are still existing. The basic research question is thus:

1) How old are the outer lateral moraines of the Barun Glacier in Nepal?

Hypothesis: The oldest (or outermost) moraines of Barun Glacier were deposited before the LGM.

The results from the dated morphological evidence (moraines) from the Barun Valley are then compared to the Khumbu moraine ages. Adapting ELA depressions from the neighbouring Khumbu valley with the inversed THAR (toe to headwall altitude ratio) method enables estimating glacial extent in the Barun Valley using a digital elevation model (DEM) and a Geographic Information System (GIS). From this reconstruction, the following further research questions emerge for this study:

2) How large was Barun Glacier during the Late Pleistocene and Holocene glaciations?

3) How can the found moraine ages be interpreted in a climatic context when also considering the sequence of undated moraines?

1.5 Content of this Master's Thesis

In the beginning of this thesis a theoretical background is provided, where the focus lies on glacier characteristics and past glacial behaviour with a special attention on the Himalayan orogen. A short introduction in the surface exposure dating method with ^{10}Be and relative dating techniques is following. In Chapter 3 the physical setting and local climate of the study region is presented. Subsequently, the materials and methods applied are explained. Chapter 5 contains the results with a detailed description and illustrations of glacier fluctuations in graphs and figures, which are then discussed in Chapter 6. In the last chapter general conclusions of the study are presented and further research possibilities are highlighted.

2. THEORETICAL BACKGROUND

2.1 Glaciers

Glaciers offer giant and dynamic storages of water that are in continuous mass and energy exchange with the hydrosphere, the atmosphere and other spheres on Earth (Benn and Evans, 2013). According to Benn and Evans (2013) glaciers gain mass by the accumulation of snow or ice on the surface and lose mass (ablation) due to melting, sublimation and/or calving. Comprehending a glacier system and the relation of its mass balance to climate, enables scientists to reconstruct past environmental changes from former glacier fluctuations.

2.1.1 Origin, Mass Balance and Flow

If not mentioned otherwise, the contents of the following section is based on the work by Benn and Evans (2013). *Accumulation* on a glacier can occur in several ways but predominantly happens through snowfall. The amount of precipitation, however, varies significantly in space and time. Generally maritime regions tend to have heavy snowfalls und high accumulation rates due to cyclonic weather systems and orographic uplift, whereas inland regions tend to have more arid climates and thus have lower accumulation rates and lower temperatures. Avalanching affects accumulation in particular in steep mountain regions, where it can contribute large amounts of snow onto the glacier surface. The freezing of supercooled water drops, which results in the formation of ice crystals (most importantly the formation of *rime ice*), and the freezing of rainwater or groundwater can also contribute mass to a glacier. Over the course of one melt season the complex structure of snow crystals starts to transform into more simple-shaped aggregates, bulk density increases, the air-filled pores are decreased, and the snow turns to *firn*. Further compression due to successive accumulative layers of snow over the years finally converts the firn grains to ice. The time needed for the metamorphic process of ice formation depends on the governing climate and is enhanced by melting and refreezing processes.

Ablation incorporates several processes of ice and snow loss including melting, sublimation, evaporation, aeolian loss, calving and avalanching. Mountain glaciers that are not terminating in a lake (lacustrine) or the sea (tidewater or marine terminating), predominantly lose mass through melting.

The *mass balance* of a glacier designates the net gain or loss of mass over a specific time period (usually one year). Accumulated mass is transported under the force of gravity from the accumulation area at higher elevations downhill towards the ablation area (*Fig. 3*), fully replacing the melt under steady-state conditions. Thereby, the equilibrium line (EL) separates the two areas (Hooke, 2005). Its elevation at the end of the ablation period corresponds for most glaciers well with its mass balance in that year. If accumulation surpasses ablation, the glacier gains mass (positive mass balance) and vice versa if accumulation is smaller than ablation, the mass balance is negative.

The transport or *flow* of ice occurs in various ways, e.g. by sliding, deformation of ice and deformation of the glacier bed. With this fundamental characteristics glaciers are able to rework landscapes and carry debris from erosive into depositional areas (Oerlemans, 2001). The details of glacier flow, however, are still a topic of intense research.
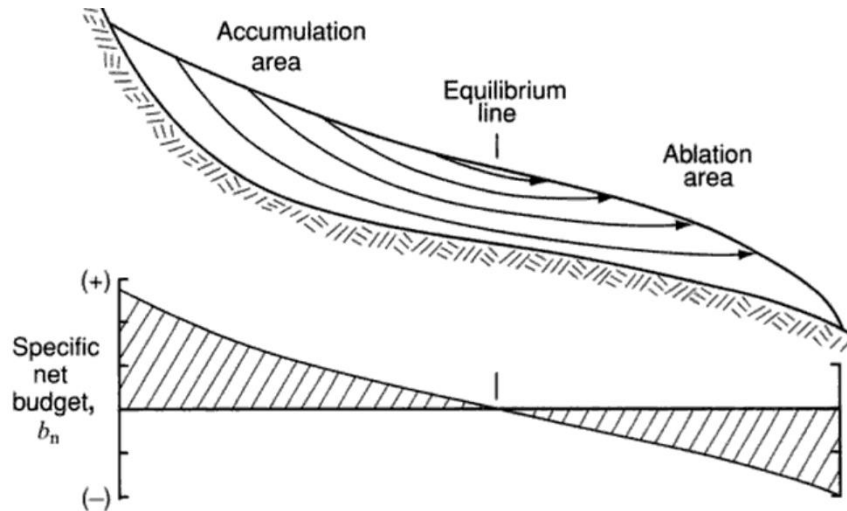
Fig. 3: A typical valley glacier with the accumulation area and ablation area, flow lines and equilibrium line (Hooke, 2005).

The *equilibrium line (EL)* connects the points on the glacier, where accumulation of snow and loss of ice is equal over the period of one year (Benn and Lehmkuhl, 2000). Its position on the glacier throughout a year is roughly at the lowermost end of the snow covered region. The equilibrium line altitude (ELA) is the averaged elevation of the EL. The ELA where the mass balance of a glacier is zero (ELA_0) is very closely linked to the local climate and can be approximated by the mean, mid-point or median elevation of a glacier (Raper and Braithwaite, 2009). This means that (a) for a mass balance close to zero at least 50% of the glacier surface must be covered by snow (i.e. its accumulation area) at the end of the ablation season and (b) that stable glacier extents (corresponding to a balanced mass budget) can be reconstructed from a change of the ELA_0 or median elevation. Whereas the ELA varies within a year and from year to year (indicative of positive or negative glacier mass balance) the ELA_0 is governed by mean climatic conditions. This is why changes in the altitude of the ELA_0 are considered as important indicators of glacier response to climate change and are consequently used for former climate reconstructions. The ELA_0, however, is not to be confused with the glacier's behaviour itself as it does not mean that the glacier is in a dynamic equilibrium. When a glacier has a zero annual mass balance over several years to decades (depending on its response time, it neither advances nor retreats. This is a very useful but theoretical concept to parametrize climatic conditions associated with glacial extents. Glacier's nourishment by avalanches in the accumulation area and thick debris cover at the tongue alter mass gain and loss locally and influence the glacier mass balance gradient. Under such condition reconstructions of glacier extents from ELA_0 changes are more complicated.

2.1.2 Transport and Deposition of Material

Glaciers are very effective in terms of erosion and transporting debris (silt, sand, gravel and boulders) several hundred of kilometres away from its origin. Thereby, the debris source can be extraglacial (e.g. from the surrounding mountains) or subglacial (e.g. through abrasion, overridden sediments or plucking). Debris is then transported along several ways glacially, through water ways, subaerially or subaqueously (Benn and Evans, 2013). The transport process determines particle

morphology and grain-size distribution (Boulton, 1978; Hoey, 2004). Further, this glacial material is then deposited in various geometries and extents (Benn and Evans, 2013).

The accumulation of ridge-like formations at the ice margins or on the ice surface of active glaciers is called *moraine* (Evans, 2013). The depositional moraine at the outermost boundary of the glacier terminus is referred to a terminal or end moraine (Gebhardt *et al.*, 2011; Benn and Evans, 2013). Further moraines within the boundary of the terminal moraine are named recessional moraines, due to the fact that they were formed during minor re-advances or stillstands but during a longer phase of general glacier retreat (Benn and Evans, 2013). Lateral moraines are formed around the entire lateral glacier tongue (below the ELA_0) and are widespread in high mountain regions such as the Himalayas (Gebhardt *et al.*, 2011; Benn and Evans, 2013). A combination of lateral and end moraine is called latero-frontal moraine (Barr and Lovell, 2014). Moraine structures are formed when either supra-, en-, or sub-glacial material is deposited at the ice margins (Benn, 1992), when proglacial material is flattened during glacial advance (Boulton, 1986) and further squeezed towards the glacier margins (Price, 1970) or when loose material beneath the glacier is thrusted proglacially during glacier advancement (Evans and England, 1991). Often a combination of these processes lead to a moraine ridge formation and thus to highly variable internal structures (Barr and Lovell, 2014). Morainic sediments (till) usually consist of unstratified material with a broad spectrum of grain sizes and blocks with rounded edges, slightly polished, and sometimes even scratched loads (Gebhardt *et al.*, 2011).

Thick, to a greater or lesser extent continuous *debris cover* on the glacier is a likely phenomenon on high-mountain glaciers (especially in the Himalayas). Thin debris cover (< 2 cm) increases the ablation rate due to a decreased albedo and an increased absorption of solar radiation in comparison to clean ice. On the other hand, debris cover thicker than about 2 cm insulates the ice and thus reduces glacier melt. (Benn and Lehmkuhl, 2000; Benn and Evans, 2013)
As a consequence, heavily debris-covered glaciers are disposed to have larger ablation areas than non-debris covered glaciers (Kayastha and Harrison, 2008). Other factors such as the catchment topography (with its shading effects and snow avalanching) and aspect (shading of precipitation and radiation) also affect glacier mass balance and thus control the position of the ELA (Sharma and Owen, 1996; Benn and Lehmkuhl, 2000).

2.2 Palaeoglaciation

The past climate has been highly variable since 2.5 Mio years with a cycling alternation of glacial periods and warmer intervals (Weissert and Stössel, 2015). According to Gebhardt *et al.* (2011) several natural drivers are likely to induce climate variability, amongst others increased volcanism or uprising of high mountain ranges. This results in radiation effects and increased silicate weathering conditions, which reduce the amount of CO_2 in the atmosphere and the greenhouse effect and thus induces global cooling. However, mostly accepted for the emergence of climate cycles is the oscillation of Earth's orbit parameters and its impact on the distribution of global solar radiation as a driver (referred to as Milankovitch cycles) (Gebhardt *et al.*, 2011). The current warm period, however, is most likely reinforced by anthropogenic factors such as the combustion of fossil resources, which increases the amount of CO_2 in the atmosphere (Gebhardt *et al.*, 2011).

2.2.1 The Last Glacial Maximum (LGM) and Past Ice Ages

Climate variations in the Quaternary caused major global ice ages. The *Quaternary* refers to the period on the geological timescale we are now in and the current epoch is called the *Holocene (Table 1)*. The Quaternary is subdivided into the Pleistocene (11'700 – 2.58 Mio years) and the ongoing Holocene (0 - 11'700 years) (Dawson, 1992). During the Pleistocene at least four major global ice ages (*Günz, Mindel, Riss* and *Würm* (Weissert and Stössel, 2015)) occurred with intermediate warm periods, whereas the Holocene represents the current warm interval (Gebhardt *et al.*, 2011). The transition from the last ice ages into the Holocene was not continuous, but interrupted through distinct cold period returns such as the Younger Dryas (YD) (Gebhardt *et al.*, 2011).

Table 1: Subdivisions of the Quaternary system (modified from: www.stratigraphy.org, 18.02.19).

Subdivisions of the Quaternary System				
Period	Epoch	Stage	Age (Ma years)	
Quaternary	Holocene	Meghalayan	Today	0.0042
		Northgrippian	0.0042	0.0082
		Greenlandian	0.0082	0.0117
	Pleistocene	Upper	0.0117	0.126
		Middle	0.126	0.781
		Calabrian	0.781	1.8
		Gelasian	1.8	2.58

Accumulated marine sediments provide a mostly undisturbed record of deposited calcareous and siliceous micro-organisms, which can be used for reconstructing former environmental changes through stable oxygen isotope ratios ($^{18}O/^{16}O$) (Dawson, 1992). The stable oxygen isotope composition of the carbonates are balanced with the isotopic composition of the sea water and depend on temperature and water depth during formation (Dawson, 1992; Gebhardt *et al.*, 2011). Due to the preferential evaporation of lighter oxygen isotopes (^{16}O), ^{18}O is enriched in the ocean water and thus in the marine sediments during an ice age as a lot of water is stored in ice on land (Dawson, 1992). Consequently, the relative deviation of the oxygen isotope ratio of marine sediments compared to the mean ratio of a standard value indicates former ice ages (Dawson, 1992; Gebhardt *et al.*, 2011).

Gebhardt *et al.* (2011) indicate that with the aid of stable oxygen isotope analysis in marine sediments, Milankovitch cycles and ice core drillings several ice ages could be detected, which are on a global scale numbered *Marine Isotopic Stages* (MIS) (*Fig. 4*). MIS 2 refers to the LGM, whereas MIS 1 is the current Holocene and MIS 5 the last interglacial period. During MIS 2 the sea level was around 120 - 130 m lower than today. During certain interglacial periods (e.g. MIS 5) the sea level might have been even higher than today.

The *Last Glacial Maximum* (LGM) means the last glacial cycle when glaciers and ice sheets globally advanced to their maximum extents (Bowen, 2009). It occurred between 19'000 and 23'000 years ago (Clark and Mix, 2002) and its cause is believed to be climate change in response to a changed orbital configuration (Bowen, 2009). The LGM occurred on both hemispheres more or less synchronously,   its extent and exact timing is still argued (Bowen, 2009). However, some studies conducted in the Himalayas and the Tibetan Plateau (TP) indicate that some glaciers had

their maximum extent earlier than the LGM, which indicates asynchronous behaviour compared to the variations of the northern hemisphere ice sheets (Owen *et al.*, 2002a, 2008; Finkel *et al.*, 2003; Hughes *et al.*, 2013; Owen and Dortch, 2014; Dong *et al.*, 2018).
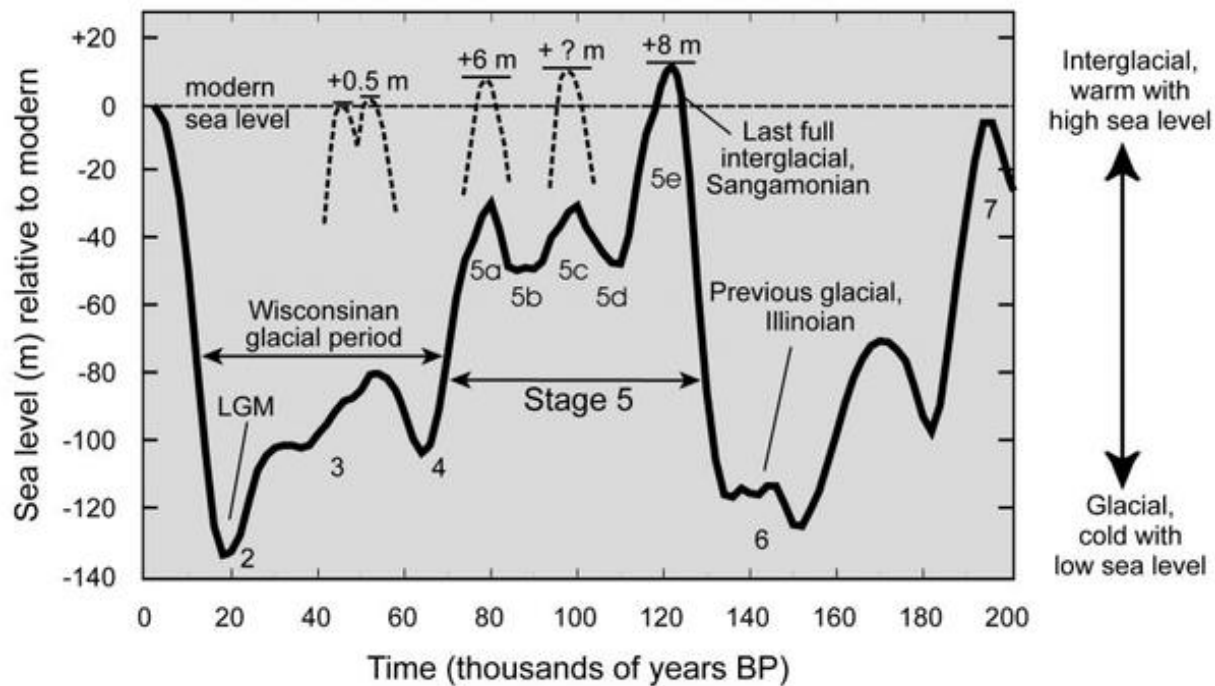
Fig. 4: Sea level change in connection with warm and cold periods over the past 200'000 years (Source:http://www.eeescience.utoledo.edu/Faculty/Krantz/Va_Coast_figures/Virginia_Coast_figures.htm, 22.08.2018).

2.2.2 Situation in the Himalayas / Tibetan Plateau vs. Alps

Glaciation in the Himalayas and Tibetan Plateau (TP) seems to behave differently in comparison to the glaciers in the Alps and the rest of the world (Zech *et al.*, 2009; Dong *et al.*, 2018). While during the LGM (Clark and Mix, 2002) mountain glaciers and ice sheets reached their maximum extents, and were thus overriding traces from earlier ice ages in most regions of the world, in the Himalayas and TP glacial remnants (e.g. lateral moraines) exist that are found outside the LGM deposits and were much older than the LGM (Finkel *et al.*, 2003; Owen *et al.*, 2008; Zech *et al.*, 2009; Dong *et al.*, 2018). A large number of surface exposure dating measurements (>2000 single measurements) contribute to the perception that the maximum glacial extent in this region occurred prior to the global LGM (Dong *et al.*, 2018). It is believed to have happened ca. 110 - 10 ka ago in some areas and is thought to be due to the high sensitivity of glaciers to precipitation changes occurring through intensity variations of the monsoon (Finkel *et al.*, 2003; Li *et al.*, 2014; Chen *et al.*, 2015; Dong *et al.*, 2018). Especially in arid areas glaciers tend to be more precipitation sensitive, whereas in humid areas glacier mass balance is largely controlled by temperature (Zech *et al.*, 2009). Therefore, reduced temperature during the Younger Dryas (YD) or the LGM led to glacial advances only in the eastern Himalaya, and was thus synchronous with the northern hemisphere growth of the ice sheets (Hu *et al.*, 2017). This effect was very restricted in extent in the remaining

part of the Himalayas due to a weaker monsoon at this time (Owen, Finkel and Caffee, 2002; Zech *et al.*, 2009). Towards the north and west, however, monsoon plays a more important role, due to a steep decreasing precipitation gradient (Zech *et al.*, 2009). Increased insolation and thus higher monsoonal precipitation amounts during MIS 3 in this region impacted positively on glacier mass balances and were responsible for glacial advance (Owen *et al.*, 2002a; Zech *et al.*, 2009). Additionally, the exact timing of the local maximum extent is still debated and differs regionally due to the mid-latitude westerlies, which have varying influences on glaciers, and Northern hemisphere climate variations (Hughes *et al.*, 2013; Zech *et al.*, 2013; Dong *et al.*, 2014; Owen and Dortch, 2014).

The extent of glaciation in the Himalayas and the TP was a highly debated topic over the last few decades (Owen and Dortch, 2014). Opinions differ from a totally covering ice sheet over the Tibetan Plateau (Kuhle, 1985) to only partially glacier covered regions (Klute, 1930; Frenzel, 1959; Li *et al.*, 1991; Shi *et al.*, 1992) (*Fig. 5*). However, nowadays it is mostly accepted that the TP was not totally ice covered during the past few glacial cycles (Lehmkuhl, 1998a; Owen *et al.*, 2008) due to glacial landforms that are still existing from previous ice ages detected through a large number of numerical dating results that have been conducted in the past years.
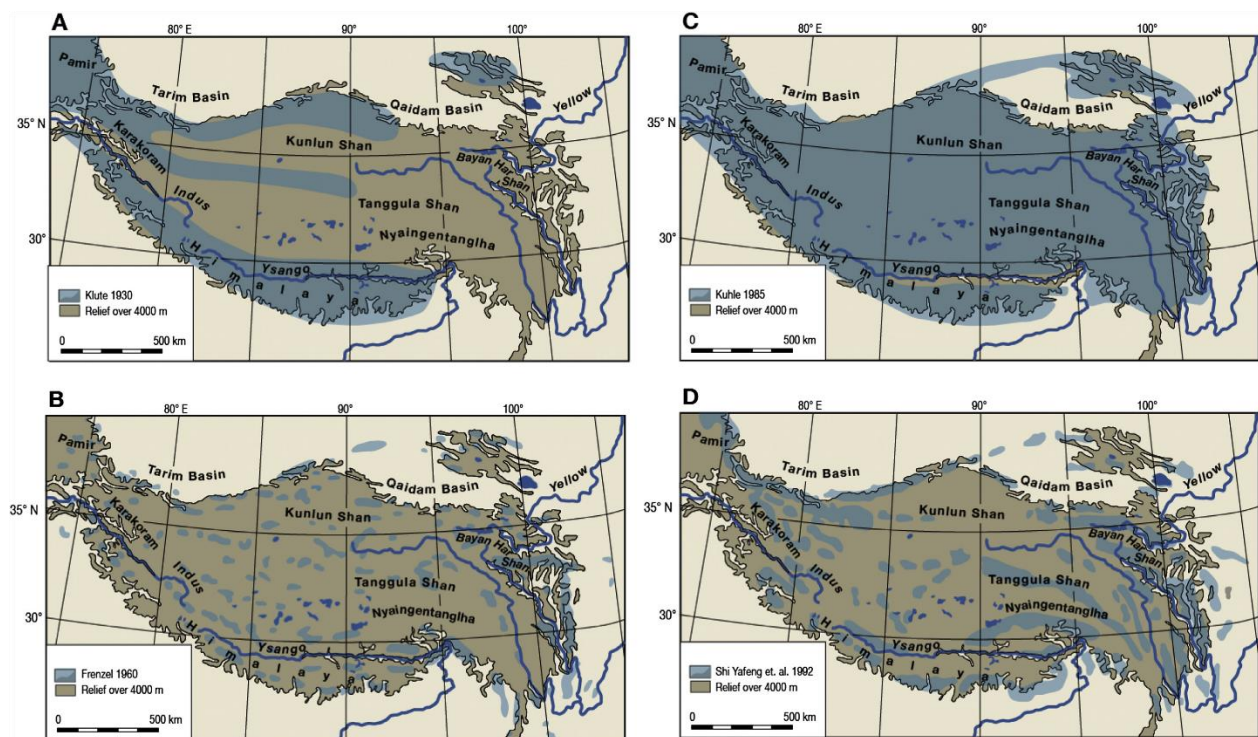
Fig. 5: Differing opinions about the maximum extents of glaciation during the LGM over the Tibetan Plateau and the Himalayas; greyish-blue: glaciated area; olive-brown: topography over 4000 m; A) glacier reconstruction of Klute (1930); B) glacier reconstruction of Frenzel (1960); C) glacier reconstruction of Kuhle (1985); D) glacier reconstruction of Shi, Zheng and Li (1992) and Li, Li and Cui (1991) (Owen and Dortch, 2014).

Such moraines would have been destroyed, if a large ice sheet over the TP existed (Owen and Dortch, 2014). Kuhle (2011), however, ignores these dating results, as he argues, that this technique

cannot be applied at high altitudes, therefore he still insists on a totally covering ice sheet (Kuhle, 1985). Additionally, large landslides are quite common in the Himalayan Tibetan orogen and tend to be misinterpreted due to their resembling appearance like moraines (Owen and Dortch, 2014). Therefore, a careful and sound interpretation of glacial landforms is necessary (Owen and Dortch, 2014).

The Alps and alpine foreland were repeatedly glaciated during the Quaternary (Ivy-Ochs *et al.*, 2008). More than four major ice ages (*Günz, Mindel, Riss* and *Würm* (Penck and Brückner, 1901-1909)) occurred, which have been detected through detailed analysis of glacial remnants (Schlüchter, 2004). The local maximum extent in most regions of the Swiss Alps correlates with the LGM during MIS 2, which was at its greatest extent at around 18.5 ka (Ivy Ochs *et al.*, 2000 cited by Schlüchter, 2004). Through lithostratigraphy interpretations and luminescence dating ice ages during MIS 5 and MIS 4 have been mingled, but terminal moraines or landforms are not preserved from that age because they were erased by later glaciations during MIS 2 (late Würm ice age) (Ivy-Ochs *et al.*, 2008). The Younger Dryas (YD) cold phase took place at around 12 ka and was characterized by depositing very distinct moraines across the Alps (Ivy-Ochs *et al.*, 1996, 1999, 2006, 2008).

2.2.3 Glacier Fluctuations Since the LIA

The *Little Ice Age* (LIA) refers to a period of time between 1400 and 1850 and indicates most recent globally occurring glacial advance (Grove, 2001; Ogilvie and Jónsson, 2001; Shindell, 2009; Sinha *et al.*, 2011). Spatial and temporal small-scale variations in climate were present, but mass balances were predominantly balanced or positive so glaciers stayed expanded and advanced repeatedly (Grove, 2001). During the LIA most glaciers formed distinct moraines (Shiyin *et al.*, 2003). Oxygen isotope records from central and northeast India manifest a period of break-dominated precipitation regime between 1400 - 1700 A.D. and an active-dominated regime from 1700 - 2007 A.D in terms of precipitation (Sinha *et al.*, 2011). These two regimes were abruptly crossed over at ~ 1650 - 1700 A.D. when monsoon winds suddenly increased in the Arabian Sea (Sinha *et al.*, 2011). This lead to increased moisture availability towards the end of the 17th century and together with cold conditions to global glacier advances during the LIA (Sinha *et al.*, 2011; Liu *et al.*, 2017). Prior to the LIA, during the Medieval Warm Period mass balances had likely been negative over an extended period of time and glacier extents were shrinking (Grove, 2001). However, there is a lack of agreement about the exact time of initiation of the Little Ice Age and its end (Grove, 2001; Ogilvie and Jónsson, 2001) and the exact period seems to be regionally variable (Rabatel *et al.*, 2008). Since the end of LIA glacier volumes are decreasing, runoff has increased and ELAs have risen due to higher temperatures and will continue to do so due to global warming (Yao *et al.*, 1997; Su and Shi, 2002; Shiyin *et al.*, 2003).

2.3 Surface Exposure Dating

Surface exposure dating with terrestrial cosmogenic nuclides (TCN) is gaining increasing prominence in the study of surface processes and landscape evolution (Ivy-ochs and Kober, 2008). Six broadly used cosmogenic nuclides (^{10}Be, ^{26}Al, ^{36}Cl, ^{3}He, ^{14}C and ^{21}Ne) are applied for exposure dating on rock surfaces of any rock type, independently of its latitude and altitude (Gosse and

Phillips, 2001; Ivy-ochs and Kober, 2008). Thereby exposure ages between 10^2-10^7 years can be dated, depending on the weathering rates (Gosse and Phillips, 2001; Ivy-ochs and Kober, 2008). A TCN measurement in a rock surface enables more knowledge about erosion rates, fluvial incision rates, denudation rates, landscape evolution and the age of moraines and alluvium sediments and thus provides geomorphologists and glaciologists a powerful tool (Gosse and Phillips, 2001; Ivy-ochs and Kober, 2008).

TCN concentration in the rock surface of boulders that were deposited on a moraine, represents how long the rock has been exposed to cosmic rays and thus the time span since glacial retreat (Lal, 1991; Gosse and Phillips, 2001; Böhlert *et al.*, 2011a). This method is based on the assumption that the rock was carried by the glacier, deposited on the moraine and since glacial retreat exposed to the bombardment by cosmic rays without any movement of the rock itself (Böhlert *et al.*, 2011b; Heyman *et al.*, 2011). Measured concentrations of TCN accumulation, which have spatial and temporal variations, can be converted into absolute exposure ages and describe the timing of deposition of a moraine; thus for a terminal moraine it more or less represents the maximum extent of a glacier (Gosse *et al.*, 1995; Gosse and Phillips, 2001; Balco *et al.*, 2008; Ivy-ochs and Kober, 2008; Owen *et al.*, 2008; Böhlert *et al.*, 2011b).

2.3.1 The Physical Principle of Dating with Beryllium Isotopes

Among several cosmogenic nuclides 10-Beryllium (^{10}Be) is ideally used for surface exposure dating when the dated rock type is granite or gneiss due to the fact that ^{10}Be builds up in silicate minerals especially quartz and is therefore often applied in geoscientific investigations (Tuniz, 1998; Nishiizumi *et al.*, 2007; Ivy-ochs and Kober, 2008). While cosmogenic ^{10}Be is radioactive and has a half-life time of 1.388 ± 0.018 Ma years, the ^{9}Be isotope is stable (Korschinek *et al.*, 2010). A steady flux of primary cosmic radiation consisting of highly energetic protons and α particles is bombarding the Earth and interacts with the air (N_2 and O_2) when entering the upper atmosphere (*Fig. 6*) (Wagner, 1998). The secondary radiation, which consists mainly out of protons, neutrons, muons and photons, further clashes with the atoms of the air, decreases in energy and then approaches the Earth's surface (Gosse and Phillips, 2001). When secondary cosmic rays hit
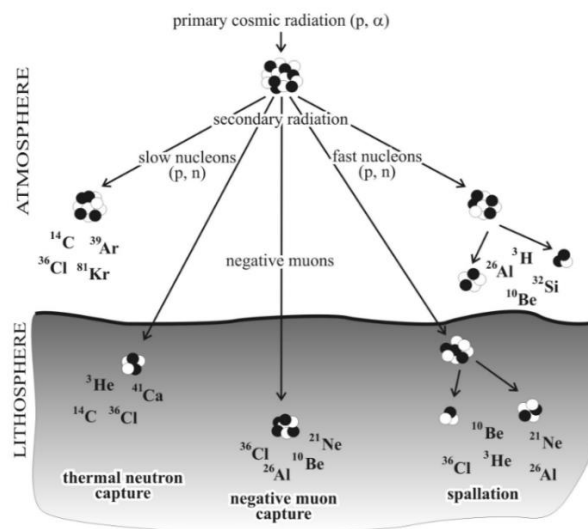
Fig. 6: Production of cosmogenic nuclides on Earth (Wagner, 1998).

the upper part of the lithosphere (target element in a mineral) with sufficient energy, one or several particles are ejected and the TCN (amongst others [10]Be) in the target element is produced (Ivy-ochs and Kober, 2008). This process is called spallation and decreases exponentially with depth (Lal, 1991; Ivy-ochs and Kober, 2008). Spallation next to the capture of slow muons are the main production and later accumulation process of TCN in rocks (Lal, 1991; Wagner, 1998; Gosse and Phillips, 2001; Ivy-ochs and Kober, 2008).

The simplified accumulation of [10]Be in the rock surface without inheritance nor erosion is expressed in the following equation:

$$N(t) = \frac{P}{\lambda} * (1 - e^{-\lambda t})$$
                Eq. 1

where N stands for the amount of accumulated [10]Be or any other TCN, P is the production rate at the sampling site, t is the duration of exposure and λ is the decay constant (Ivy-ochs and Kober, 2008; Zech *et al.*, 2009). However, when rock surface weathering (erosion) was likely, the following equation should be used:

$$N(t) = \frac{P}{\lambda + \frac{\rho \varepsilon}{\Lambda}} \times \left(1 - e^{-\left(\lambda + \frac{\rho \varepsilon}{\Lambda}\right)t}\right)$$
        Eq. 2

Here ρ is the density of the irradiated material, ε is the erosion rate and Λ stands for the attenuation length (Ivy-ochs and Kober, 2008). Assuming that the rock was not exposed to cosmic radiation previously, the calculated age identifies the event of interest (Gosse and Phillips, 2001; Zech *et al.*, 2009), in the case of this thesis the deposition of a moraine (*Fig. 7* a). The likelihood of pre-exposure which then results in an inherited older age (*Fig. 7* b) was found out to be small (only 3%) (Putkonen and Swanson, 2003). Surface instability (especially on terminal moraines) and erosion, which results in post-depositional exhumation of buried material, leads to a reduced TCN concentration and thus to an underestimated depositional age (*Fig. 7 c*) (Gosse and Phillips, 2001; Zech *et al.*, 2005; Owen *et al.*, 2009; Heyman *et al.*, 2011). Zech *et al.* (2005, 2009) and Owen *et al.* (2009) suggest selecting the oldest exposure age for the determination of the landform's age in such a case. In order to avoid that problem, it is proposed to sample the largest boulders ideally on the top of a glacial deposit (on the ridge) (Heyman *et al.*, 2011).

Latitude and altitude mainly influence the local production rate of TCNs (Gosse and Phillips, 2001), which have been calculated and described with different scaling factors including a reference production rate and to some extent by correction for variations in the time-dependent geomagnetic field and solar variability (Lal, 1991; Stone, 2000; Dunai, 2001; Desilets and Zreda, 2003; Lifton *et al.*, 2005; Desilets *et al.*, 2006). However, calculation of the production rate still causes problems and is much-debated (Owen *et al.*, 2008, 2009).
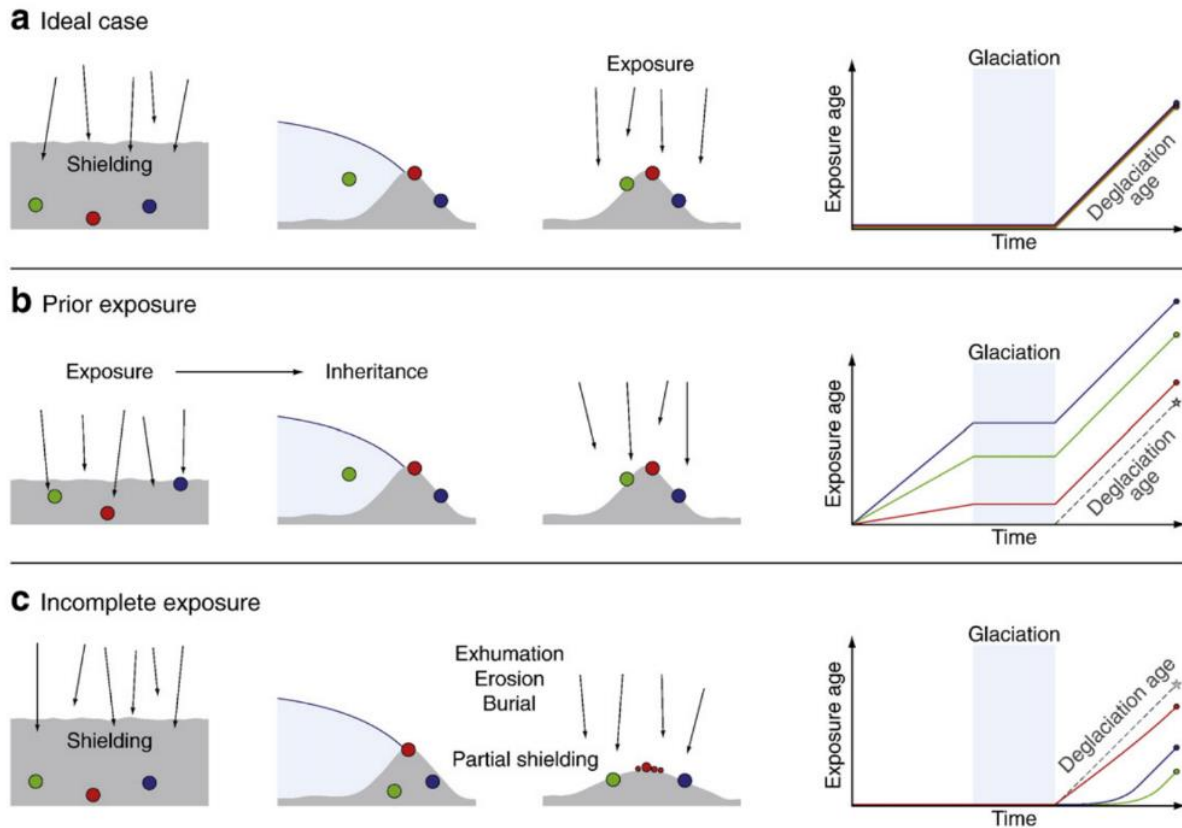
Fig. 7: Principle of pre-exposition and incomplete exposure resulting in an over- respectively un-der-estimation of the exposure age (Heyman et al. 2011).

2.3.2 Corrections to be Applied

The following factors need to be considered when calculating surface exposure ages and take part in the calibration of the scaling system:

Topographic shielding and *slope* from the surrounding mountains reduces the cosmic-ray influx to the rock surface (Balco *et al.*, 2008). This loss of TCNs, which is the production rate at the site in relation with the amount of TCNs that would exist in the rock if the surface was flat, needs to be corrected with a so called *shielding factor* (also see chapter 4.1.2 in Materials and Methods) (Balco *et al.*, 2008).

Elevation highly affects the amount of nuclide production due to the atmospheric depth at the sample site, whereas the mean atmospheric pressure is the controlling variable to estimate the production rate (Balco *et al.*, 2008). Since former atmospheric pressure is impossible to measure, the altitude combined with a standard atmosphere-elevation relationship is calculated (Balco *et al.*, 2008).

The *erosion rate* influences the reliability of the TCN surface exposure age and needs to be taken into account when calculating surface exposure ages (see Eq. 2) (Gosse and Phillips, 2001; Balco *et al.*, 2008).

Snow cover needs to be considered in regions where the dated landform is shielded significantly by its snow cover (Gosse and Phillips, 2001). When calculating the shielding by snow cover, snow depth ($Z_{snow,i}$), snow density ($\rho_{snow,i}$), the amount of months when snow exists, the effective attenuation length ($\Lambda_{f,e}$) and the height of the sampling boulder (Z_{sample}) need to be taken into account (Gosse and Phillips, 2001):

$$S_{snow} = \frac{1}{12} \sum_i^{12} e^{-((Z_{snow,i} - Z_{sample})\frac{\rho_{snow,i}}{\Lambda_{f,e}})} \qquad \text{Eq. 3}$$

The *geomagnetic field* influences the cosmic-ray intensity (Gosse and Phillips, 2001). There is a latitudinal effect and cosmic radiation varies longitudinally as well (Gosse and Phillips, 2001). The production rate of TCN rises with geomagnetic latitude (Gosse and Phillips, 2001).

2.4 Relative Dating Methods

Several different relative dating methods compare the age of rock layers or objects without actually measuring the absolute age. Amongst others lichen, rock weathering and soils offer the best relative dating methods on age (Birkeland, 1973). In this study the weathering rind and rock hardness were measured and the related methods are thus more thoroughly described in the following section.

2.4.1 Weathering Rind

When a rock is exposed to the atmosphere, alkali/alkaline earth metals are dissolved due to the availability of water and get washed out (Oguchi, 2001). This process is called (biogeo-) chemical weathering. The presence of CaO, MgO, Na_2O, K_2O and Al_2O_3 decreases in the weathering bands (Oguchi, 2001). Iron, however, persists as ferric hydroxide in the rock and due to oxidation processes an outer brown layer band is formed as soon as air is involved (Oguchi, 2001).

This brownish layer is called a weathering rind and is shown in *Fig. 8*. Such rinds are quantifiable after a few hundred years (depending on the type of rock) and its thickness depends on the degree of penetration of oxidation of minerals below the rock surface (Gellatly, 1984). Weathering rind thickness is measured in mm and mostly increases with the duration of exposure towards the rock centre (*Fig. 9*) (Laustela *et al.*, 2003). Generally, the mean, modal or median value of thickness is used to estimate surface ages (Laustela *et al.*, 2003). Apart from the duration of exposition, grain size and the degree of metamorphosis have the largest influence on the growth in depth (Chinn, 1981).

Fig. 8: Weathering rind of a granite (source: http://geologypics.com/we-29/, 22.08.2018).

Furthermore, boulder orientation in space, its height above the soil, vegetation cover, the rock type and the local climate may affect the development of a weathering rind (Colman, 1977; Chinn, 1981). Weathering rind measurements are particularly useful for relative age estimations of glacial and periglacial material deposits e.g. moraines or rock glaciers (Laustela *et al.*, 2003; Böhlert *et al.*, 2011b).
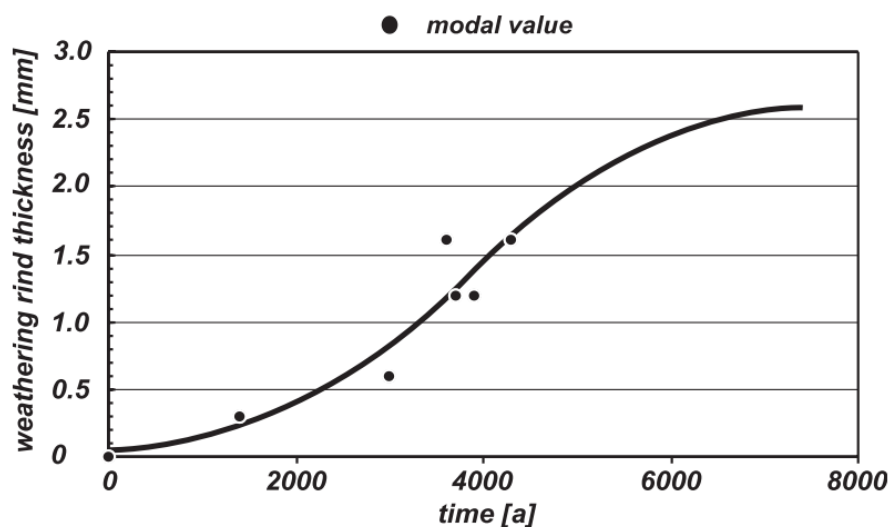
Fig. 9: Increasing weathering rind thickness with time (Laustela et al. 2003).

2.4.2 Schmidt-Hammer

The Schmidt-Hammer is a device which was originally engineered to test the quality of concrete without destroying it (Schmidt, 1951). This portable instrument can also be applied on rock surfaces to measure the rock hardness (*Fig. 10*) (Böhlert *et al.*, 2011a). A bolt strikes the surface and generates a rebound (R-value) (Böhlert *et al.*, 2011a). Generally, it is presumed that rock surfaces that have been exposed to weathering conditions for a longer time are softer and thus provide a lower R-value than fresh and unweathered rock surfaces (Böhlert *et al.*, 2011b,a; Tomkins *et al.*, 2016).

Fig. 10: Conducting rock hardness measurements with the Schmidt-Hammer (Photo: Pierre Lecomte, ESA photographer).

ComparingRr-values is only justifiable with rocks having an identical lithology which thus have equal surface hardness (McCarroll, 1987). Variations in climate may cause different chemical weathering processes and thus result in disparities of this relative dating technique in the event of an application on a larger scale (Winkler, 2005). Additionally, rock moisture and surface disconti-nuities (Sumner and Nel, 2002) as well as surface moisture content (Viles *et al.*, 2011) play a role on Schmidt-Hammer measurement results.
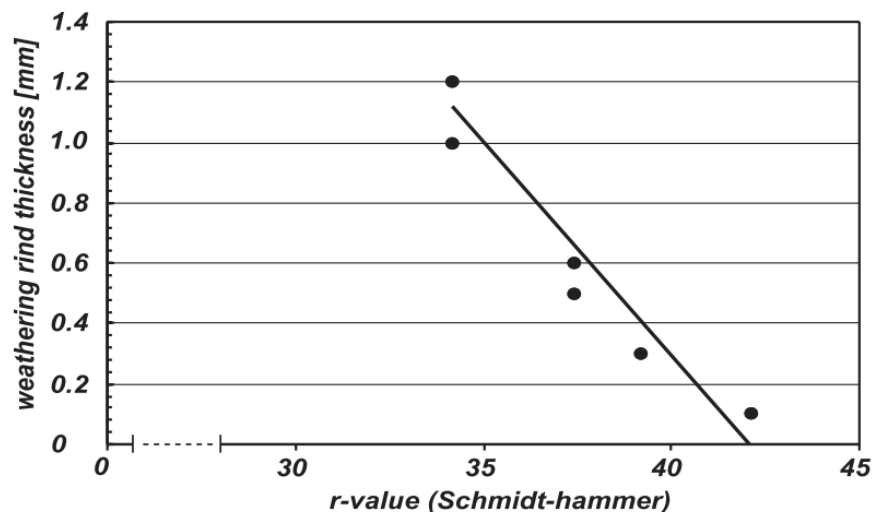
Fig. 11: The negative correlation between weathering rind thickness and rock hardness (Laustela et al. 2003).

The R-value and weathering rind thickness are negatively correlated to each other (Laustela *et al.*, 2003). A low R-value and thus a strongly weathered rock surface correlates with a larger weather-ing rind depth and vice versa (*Fig. 11*).

3. STUDY REGION

3.1 Location / Physical Setting of the Barun Valley

The Barun Valley is located around 150 km to the east of Kathmandu in the eastern part of Nepal (*Fig.12*). Mount Makalu (8485 m) is the highest mountain in this valley and gives the name to the Makalu Barun National Park which embraces the Barun Valley. The valley is embedded in the Himalayas and borders the Tibetan Plateau towards the north. Mount Everest (8848 m) is situated 19 km to the northwest of Mount Makalu.
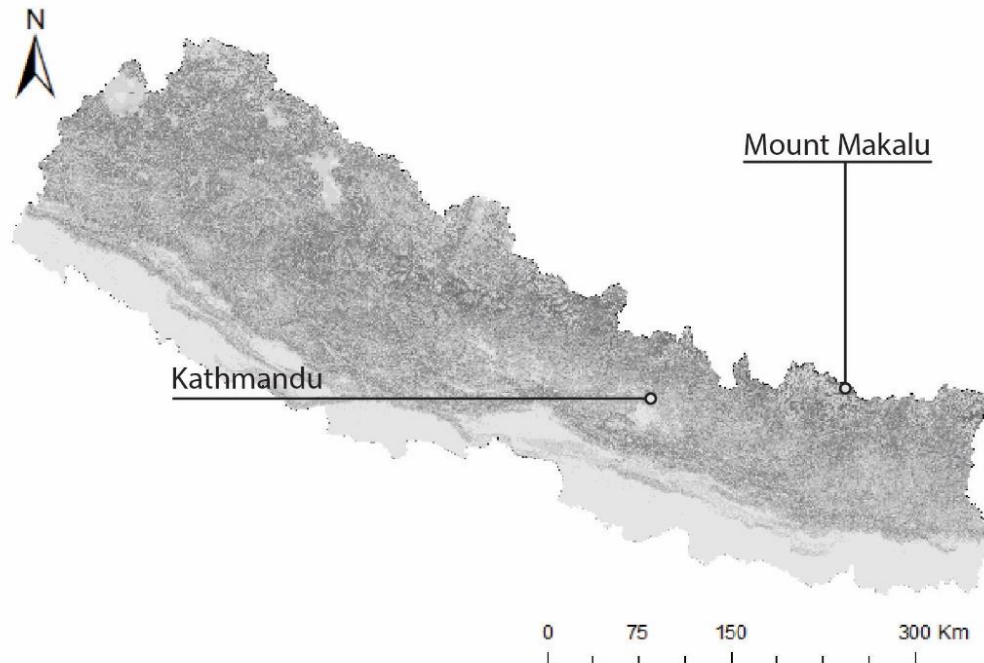
Fig.12: Map of Nepal with location of study site.

The Himalayan-Tibetan orogen arose through the tectonic collision of the Eurasian continental plate, the Indian plate and island arcs about 50 Mio. years ago (Yin and Harrison, 2000). This orogen has an average elevation of 5023 m a.s.l. (Fielding *et al.*, 1994). The mountains of the Himalayan orogen are the highest on Earth and this area is the most glacierised area aside from the polar region (Haeberli *et al.*, 1988; Dortch *et al.*, 2013). The Himalayan orogen predominantly consists of crystalline schists and gneiss from Precambrian and Palaeozoic rocks (Miehe, 2004). The highest mountains are composed of gneiss and granite nappes (Miehe, 2004). Sand- and lime-stone only exists in the Tibetan Himalayas (Miehe, 2004).

The Barun Khola (river) which originates in the glacier lake (Barun Pokhari) below the tongue of the Barun Glacier is part of a river system that flows into Arun river and eventually confluences with the river Ganges, which delivers freshwater to billions of people in Nepal, India and Bangla-desh.

The sequence of lateral moraines, where the rock samples are collected for the [10]Be measurements, is located next to the Makalu Base Camp (4870 m) at roughly 5000 m altitude at the end of Barun

Pokhari (*Fig.13*). Barun Pokhari is nearly completely enclosed by steep LIA moraines. Barun Glacier is situated to the north of the lake and has a south-eastern aspect (122°). Dead ice of the no longer active glacier terminus borders the lake. The glacier tongue is only very slowly melting away due to thick debris cover on top.

Fig.13: Overview over field site, blue: selected moraine ridges.
Photo: Pierre Lecomte, ESA photographer.

Lower Barun Glacier terminates into Barun Valley as well, however it is not part of this study and no measurements have been performed there. Lower Barun glacier is calving into the Lower Barun Glacier lake which is rapidly increasing in size since it has been observed in the 1960's (Haritashya *et al.*, 2018). Haritashya *et al.* (2018) show that between 2000 and 2017 the lake size has grown by 34%. Lower Barun Lake is likely to be the most voluminous and deepest glacial lake in the Nepal Himalaya. Due to the fact that this lake is hold back by an ice-cored moraine, it is prone to natural hazards such as catastrophic glacier lake outburst floods (GLOFs) and classified as one of the most dangerous lakes in Nepal.

There is no weather station in this region. However, a study conducted in the Rongbuk valley, which is located 25 km northwest of Makalu Base Camp, suggests that the monthly mean air temperatures above 5000 m a.s.l. are most likely below zero except for the months June, July, August and September (Mann *et al.*, 1996).

Vegetation in the upper part of the Barun Valley is sparse and limited to small shrubs, grass and moss. The tree line is at ca. 3800 m a.s.l. When moving downstream in the Barun valley the vegetation becomes more and more temperate until at an altitude of around 500 m the forest is tropical.

The Barun Valley is largely unpopulated, but several small clusters of tea houses are spread in the lower part of the valley. The management of such tea houses and tourism (e.g. Sherpa, travel guide, porter or cook) is the main income of the Nepalese population in this region. The largest small settlement is Yangri Kharka at 3600 m altitude.

3.2 Himalayan Climate

The Barun Valley is dominated by two climatic systems: the mid-latitude westerlies and the South Asian summer monsoon (Benn and Owen, 1998; Finkel *et al.*, 2003). Several studies underline the link between long-term and short-term variability of these two climatic systems with mountain glaciers advancing and retreating throughout the Quaternary (Owen *et al.*, 2008, 2009; Owen and Dortch, 2014). Long-term variability is related to changes in the Northern Hemisphere insolation, while short-term variability is linked to fluctuations within the climate system such as variations in the Eurasian snow cover, the El Niño/Southern Oscillation (ENSO) or tropical sea surface temperatures (Hahn *et al.*, 1976; Dey *et al.*, 1982; Prell and Kutzbach, 1987, 1992; Soman and Slingo, 1997; Owen *et al.*, 2008; Owen and Dortch, 2014). Glacial systems in the Himalayan-Tibetan orogen are strongly influenced by climate and topography (Owen and Dortch, 2014). Although this region plays a key role in the reconstruction of past glaciations and climate, knowledge is sparse and only available for selected sites (Zech *et al.*, 2009).

3.2.1 South Asian Summer Monsoon

The Monsoon (or south Asian summer monsoon) is a large-scale, seasonal change of wind and precipitation patterns and builds up an essential part of the general circulation of the Earth (Prell and Kutzbach, 1987; Soman and Slingo, 1997). Over one third of the tropical area is influenced by the monsoon for several months during the northern hemisphere summer (Soman and Slingo, 1997). Additionally, it exchanges a considerable mass of air between the southern and northern hemisphere (Soman and Slingo, 1997). Precipitation associated with the monsoon that occurs from June to September delivers the main amount of fresh water for billions of people in India and southeast Asia and thus has a great influence on their livelihood and economy (Soman and Slingo, 1997). However, the origin and dynamics of this climatic weather system are complex (Prell and Kutzbach, 1987).

In short, the yearly cycle of solar radiation results in a warming of the African and Asian landmasses during the northern hemisphere summer and cooling during the northern hemisphere winter (Prell and Kutzbach, 1987). Prell and Kutzbach (1987) explain that due to the increased heat capacity of adjacent ocean water in comparison to the landmasses, the continents are warmer than the oceans in the northern hemisphere summer and cooler in the northern hemisphere winter. The strong heating of the atmosphere over the continents in summer results in an upwards motion of the air and consequently responses with strong winds from the ocean to the landmasses (*Fig. 14 A*). Due to this inflow of air, large-scale convergence of the surface winds, low-pressure cells over the continents and a maximum summer monsoon precipitation in northern and eastern Africa and southern Asia are caused.

In contrast, the Himalayan-Tibetan orogen is dominated by mid-latitude westerly winds (westerlies) (*Fig. 14 B*) during the northern hemisphere winter that generally bring cold and relatively dry air (Inoue, 1978; Benn and Owen, 1998). However, heavy precipitation can fall as snow especially in the western part of the Himalayan-Tibetan orogen (*Fig. 14 B*) due to the westerly winds that bring moisture from the Mediterranean, Black and Caspian seas (Owen *et al.*, 2008).
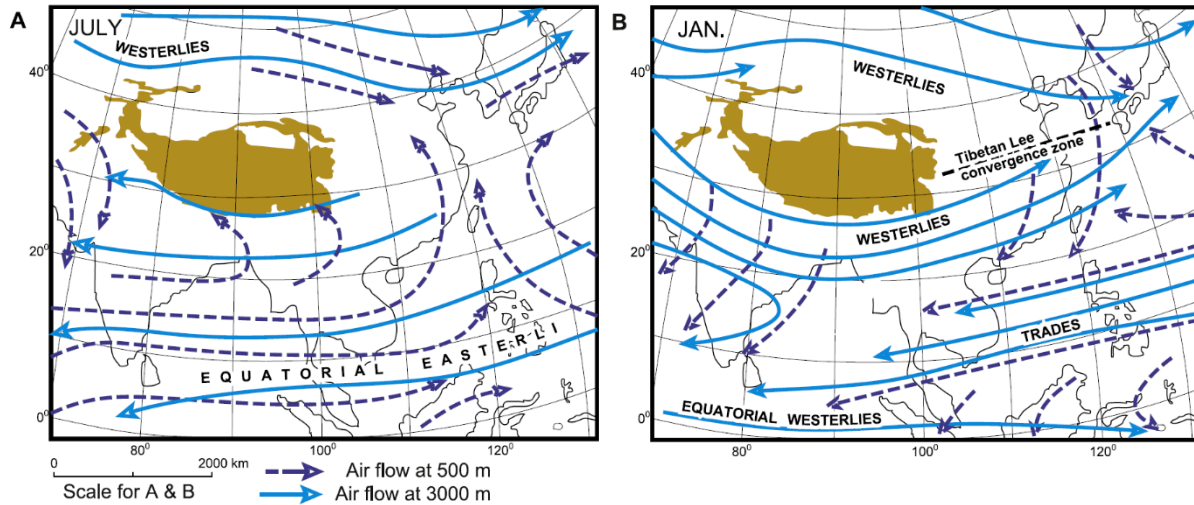
Fig. 14: Simplified model of the summer (A) and winter (B) air circulation over India and South-east Asia. Blue solid line: wind direction at about 6000 (summer) and 3000 (winter) m a.s.l.; dark blue dashed line: wind direction at about 600 m a.s.l. (Owen and Dortch, 2014).

3.2.2 Temperature and Precipitation Regime

The southern and Eastern parts of Asia are affected by a distinct summer precipitation maximum (*Fig. 15 B*), due to increased moisture availability during the south Asian summer monsoon coming from the Indian Ocean (Murakami, 1987). The summer precipitation maximum results in high snow accumulation in high altitudes of the Himalayas and western Tibet (Yasunari and Inoue, 1978; Higuchi and Inoue, 1982). However, there is a sharp decline in summer precipitation from south to north across the Himalayan orogen and reaches very low amounts over the Tibetan plateau (Owen *et al.*, 2008).

Similar to the Everest region, the Barun Valley is located at the transition zone and is therefore influenced by both climate systems, the mid-latitude westerlies and the south Asian summer mon-soon (Owen *et al.*, 2009). As shown in *Fig. 15 A* the mean annual precipitation in the Barun Valley amounts around 2000 mm. However, as there are no precipitation measurements nor temperature values available for this valley and due to the low resolution of the map (*Fig. 15*) the mean annual precipitation needs to be handled with care.

A study from the Lanchow Institute (1975) (cited in Mann, Sletten and Reanier, 1996) provide some precipitation measurements from the Rongbuk valley (25 km northwest of Barun Valley) for the 1950s and 1960s, where a semi-arid and cold climate dominates. The mean annual precipitation in 1959 at 5030 m altitude was 334 mm. This is at the same altitude as the dated moraines next to Makalu Base Camp. The mean annual precipitation on 5900 m altitude between 1966 and 1969 was 790 mm. However, as the Rongbuk Valley lies in the northern slope of Mount Everest and it is therefore protected from major precipitation events, these values are probably much lower than for the Barun Valley.
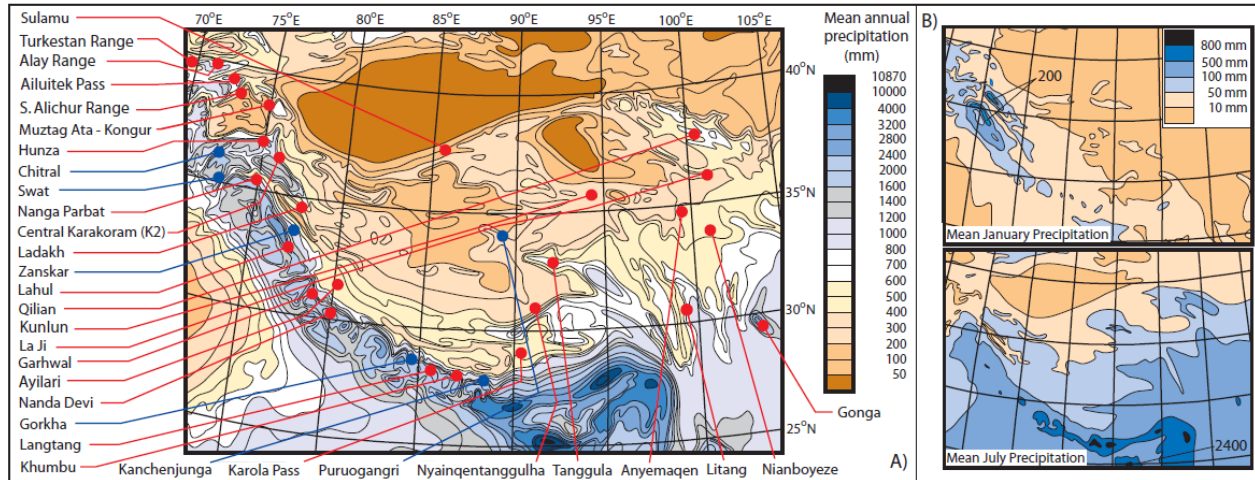
Fig. 15: A: Mean annual precipitation across the Himalayas and the Tibetan plateau. B: Mean January and mean July precipitation across the same region. (Owen et al., 2008)

Although this region experiences a distinct summer precipitation maximum and at the same time the main glacier accumulation, glacier ablation is also at its peak during the northern hemisphere summer (Webster, 1987a,b, cited in Owen *et al.*, 2008). This is due to the high temperatures resulting from direct solar radiation, as well as sensible and latent heat released by condensation (Webster, 1987a,b, cited in Owen *et al.*, 2008).

3.2.3 Recent Changes and Past Variability of Climate

Numerous studies in recent years suggest that glaciation throughout the Himalayan-Tibetan orogen is enforced by the interaction between the south Asian summer monsoon and mid-latitude westerlies (Benn and Owen, 1998; Finkel *et al.*, 2003; Owen *et al.*, 2009; Owen and Dortch, 2014). As these two dominant climate systems varied significantly during the Quaternary, phases of glaciation and deglaciation across the orogen occurred asynchronous (Benn and Owen, 1998; Owen and Dortch, 2014).

Finkel *et al.* (2003) explain that increased insolation and warmer climate leads to a more active south Asian summer monsoon. Thereby the moisture delivery is enlarged which results in glacial advances in the Himalayas where increased snowfall takes place at high altitudes. These findings assist to grasp the importance of the influence of global climate change and monsoon on the behaviour of glaciers in the Himalayan-Tibetan orogen and its sensitive response to climate change.

However, simultaneously the behaviour of some glaciers remains synchronous with Northern hemisphere ice sheet growth and decay due to spatially variable and topographically controlled precipitation patterns (Zech *et al.*, 2009; Sati *et al.*, 2014). Generally, glaciers that lay in orographically shielded regions tend to be more sensitive to variations in precipitation, while glaciers with high precipitation inputs tend to be more sensitive to variations in temperature (Zech *et al.*, 2009; Sati *et al.*, 2014).

The monsoon provokes periodical changes in strength over a geological time scale according to Prell and Kutzbach (1987). Studies indicate that during the LGM around 18'000 years ago the

Indian summer monsoon was significantly weaker. Whereas, during the Mid-Holocene around 9'000-10'000 years ago the strength of the monsoon was higher.

A study by Wang *et al.* (2001) proclaims that oxygen isotope archives of speleothem calcite from Hulu Cave in the eastern part of China show a similar behaviour as oxygen isotope records from Greenland ice cores (*Fig. 16*). This implies that the east Asian summer monsoon intensity changed more or less synchronous with Greenland temperatures, at least between 11'000 and 75'000 years B.P. A prominent drop in $\delta^{18}O$ in both records around 12'000 years B.P. correlates with the Younger Dryas (YD) glaciation. Stalagmites may assist to correlate older events once ice core records are more uncertain.
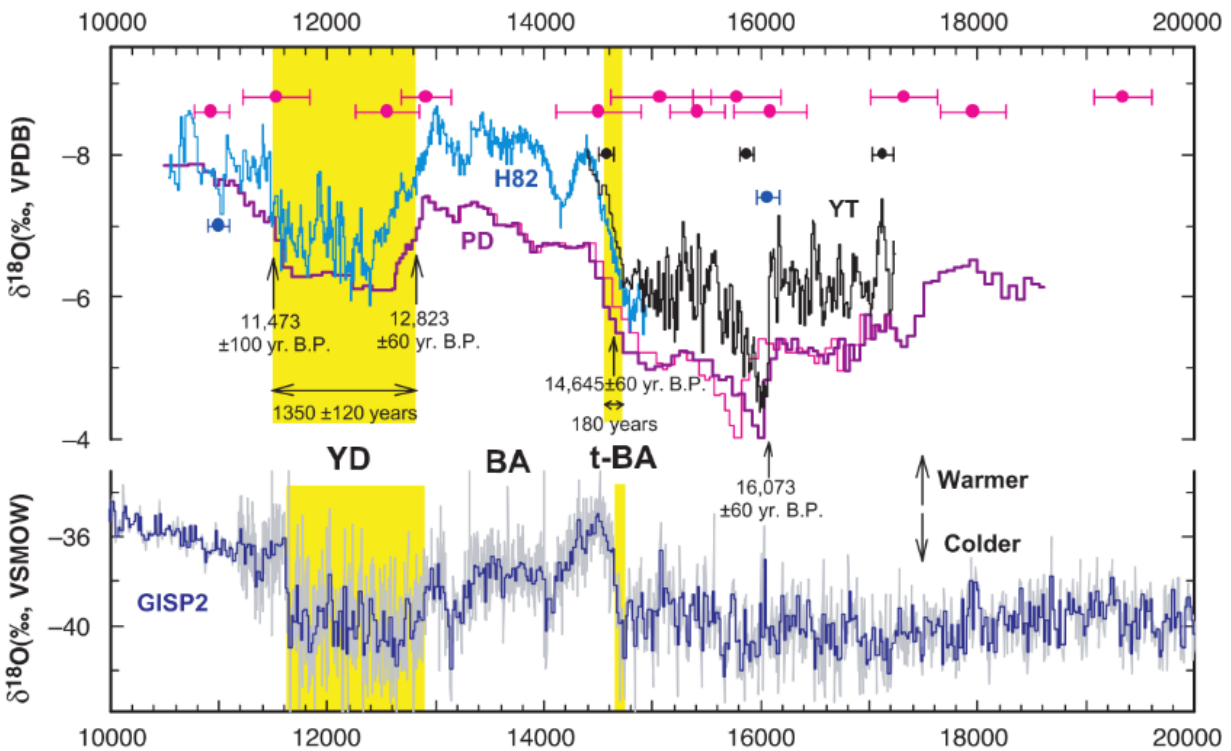
Fig. 16: Time series of $\delta^{18}O$ values; purple, blue and black: from Hulu Cave stalagmites; dark blue and grey: from the Greenland ice (Wang et al., 2001).

4. MATERIALS AND METHODS

4.1 Dating Moraines

4.1.1 Sampling Strategy

Prior to the fieldwork, we identified a series of eight glacial moraines on the orographically right hand side next to Makalu Base Camp using very high resolution satellite images from Google Earth and Flickr photos (*Fig. 17*), whereof three were selected to obtain rock samples for [10]Be measurements. When referring to the numbers shown in *Fig.17*, we sampled one boulder of moraine 1, two boulders of moraine 2 and two boulders of moraine 5. We preferentially took samples of the largest granitic boulders that lay on the highest point of the moraine, to increase the likelihood that it was deposited by the glacier and not through a rockfall event from the side. Large boulders have a higher chance of having escaped post-glacial shielding and therefore the likelihood of a more accurate exposure age is higher than for smaller boulders (Heyman *et al.*, 2016). Additionally, they are less likely to have moved or tipped sideways, which has to be avoided for the boulders selected for taking samples for surface exposure dating measurements.

Fig. 17: Sequence of moraines next to Makalu Base Camp (Photo: Oleg Bartunov, source: flickr.com).

4.1.2 Field Measurements

Once the boulders where located, a 20 x 20 cm raster with 2 – 3 cm depth was cut into the rock, preferentially on a flat area on top of the block. The raster was cut with a flex (diamond saw) and later carved out with a hammer and a chisel (*Fig. 18 E*). We collected between 1 - 2 kg of rock chips, which were later taken to the lab at the University of Zurich (Switzerland) for the [10]Be measurements.

From each block we noted the coordinates and altitude with help of a Garmin GPS, took photographs and described it. The description includes measurements of the shielding by the surrounding topography (where every 10° the topographic height was measured) (*Fig. 18 B*) and dip and strike

Fig. 18: Field measurements; A: weathering rind; B: topographic shielding; C+D: Schmidt-hammer; E: cutting rocks out with hammer and chisel; F: strike and dip; Photos: Pierre Lecomte, ESA photographer.

measurement of the area where we took the rock samples (*Fig. 18 F*) with a Suunto Tandem clinometer, if inclined. These parameters were later used for a calibration of the model to calculate the age of the moraines. In addition, we made 50 measurements around each block with the Schmidt-hammer (*Fig. 18 C+D*). Furthermore, we also measured the weathering rind of 50 smaller rocks around each block (*Fig. 18 A*). More detailed sample information about each sample site is provided in *Table 2*.

Table 2: Data information for each sample site.

Sample ID	Latitude (°N)	Longitude (°E)	Elevation (m.a.s.l.)	Topographic shielding	Dating	Snowfactor	Mean Sample Thickness (cm)	10Be (atoms/g Qz)	± atoms g-1
MAKA_1.A	27.8424	87.07313	5026	0.932	First	No	2	17197	17197
					First	Yes	13.1	694545	17197
					Second	No	2	654662	15992
					Second	Yes	13.1	726675	15992
MAKA_2.A	27.84275	87.07393	5034	0.959687	First	No	2.5	24819	24819
					First	Yes	13.6	485937	24819
					Second	No	2.5	378175	13491
					Second	Yes	13.6	423556	13491
MAKA_2.B	27.84288	87.07372	5040	0.963839	First	No	2.25	12413	12413
					First	Yes	13.35	503308	12413
					Second	No	2.25	434182	12060
					Second	Yes	13.35	484113	12060
MAKA_3.A	27.8377	87.07373	4995	0.972529	First	No	1.75	8478	8478
					First	Yes	12.85	192520	8478
					Second	No	1.75	159497	10747
					Second	Yes	12.85	176723	10747
MAKA_3.B	27.8382	87.07402	5001	0.971193	First	No	1.75	10190	10190
					First	Yes	12.85	339515	10190
					Second	No	1.75	293959	9163
					Second	Yes	12.85	325707	9163

We assumed the erosion rate the be 0.0001cm yr^{-1} and a rock density of 2.7 g cm^{-3} as the lithology is felsic granite (*Table 2*). Additionally, we calculated a snow cover correction factor for each site as we presume 2 m of snow with a density 0.3 g cm^{-3} over 6 months of the year. More detailed information about the data input parameters for CRONUS Earth (explained in section 4.1.4) is provided in the Appendix (*Table 11*).

In *Fig. 19* a panorama picture of each dated block with its surroundings is shown. As the photographs have been taken in panorama modus, the view is slightly distorted. The moraine ridges are orientated in north-south direction and have altitudes from 4995 m to 5040 m. As the sample site is located in the middle of the Himalayas, the surrounding mountains are relatively high (generally 6'000 - 7'000 m) with Mt. Makalu (8485 m a.s.l.) in the north, the topographic shielding amounts 0.93 - 0.97.

Fig. 19: Each sampled block with its surroundings; Photos: Pierre Lecomte, ESA photographer.

A close-up photograph of each dated block is presented in *Fig. 20*. Block MAKA_1.A, MAKA_2.A and MAKA_3.B are well embedded in the moraine, where as MAKA_2.B and MAKA_3.A lay on top. However, their size indicates that a tipping of the block can be largely excluded.

Dated Blocks in the Barun Valley

(Makalu Base Camp, Nepal)
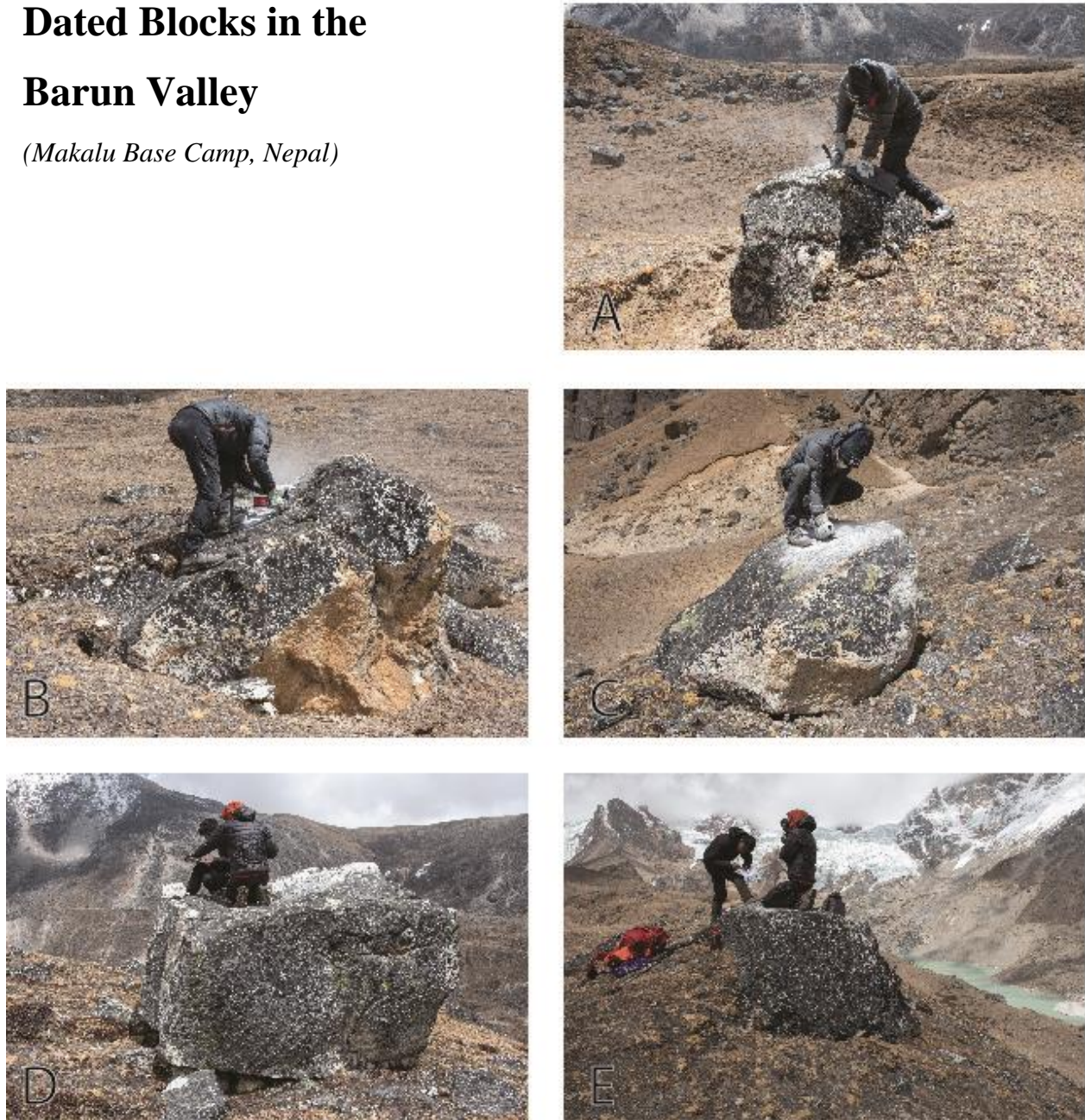
Fig. 20: Photograph of each dated block to locate the sampling area; A: MAKA_1.A, B: MAKA_2.A, C: MAKA_2.B, D: MAKA_3.A, E: MAKA_3.B; Photos: Pierre Lecomte, ESA photographer.

4.1.3 Preparation of the Samples/ AMS

The rock samples from the field were taken to the laboratory at the University of Zurich, Switzerland, where standard procedures for sample preparation and analysis followed (Kohl and Nishiizumi, 1992; von Blanckenburg *et al.*, 1996, 2004). In brief, this firstly involves crushing and sieving of the rock chips to obtain at least 400g of the 0.25-0.6mm fraction (*Fig. 21 D*). Afterwards the samples were treated with Aqua regia, which is a mixture of nitric acid and hydrochloric acid (*Fig. 21 A*). It is used for removing organic compounds and carbonates. The remaining samples were exerted with a method called *flotation*, which separates feldspar from the rest of the samples due to a difference in density. Thereafter, leaching with hydrofluoric acid (HF) was used to obtain pure quartz. This treatment has been repeated several times until the samples were as clean as possible. However, some particles were indestructible, which then have been removed by hand-picking. As HF is able to dissolve quartz, too, a carrier (^{9}Be) has been added, to quantify the loss of ^{10}Be in the end. An additional HF treatment was applied to completely decompose quartz as for the further processings quartz was used in liquid form. In a next step iron (Fe) was removed with an *anion exchange column* (with 2 ml of Biorad 1-X8 100-200 mesh) (*Fig. 21 C*). Then aluminium (Al) was separated from Be with help of a *cation exchange column* (with 1 ml Biorad AG50W-X8 200-400 mesh). After the removal of Fe and Al Beryllium was relatively pure. However, with an addition of NH^{4}OH Be precipitated and could be extracted after using the centrifuge (*Fig. 21 B*). After drying we got BeO which is the final product that was provided to the ETH at Hönggerberg for the accelerated Mass Spectrometry (AMS) measurement of the ^{10}Be/^{9}Be ratio. This whole procedure as well as the AMS measurement were applied twice to every sample in order to receive a more accurate exposure age and to be able to better confine the uncertainties.
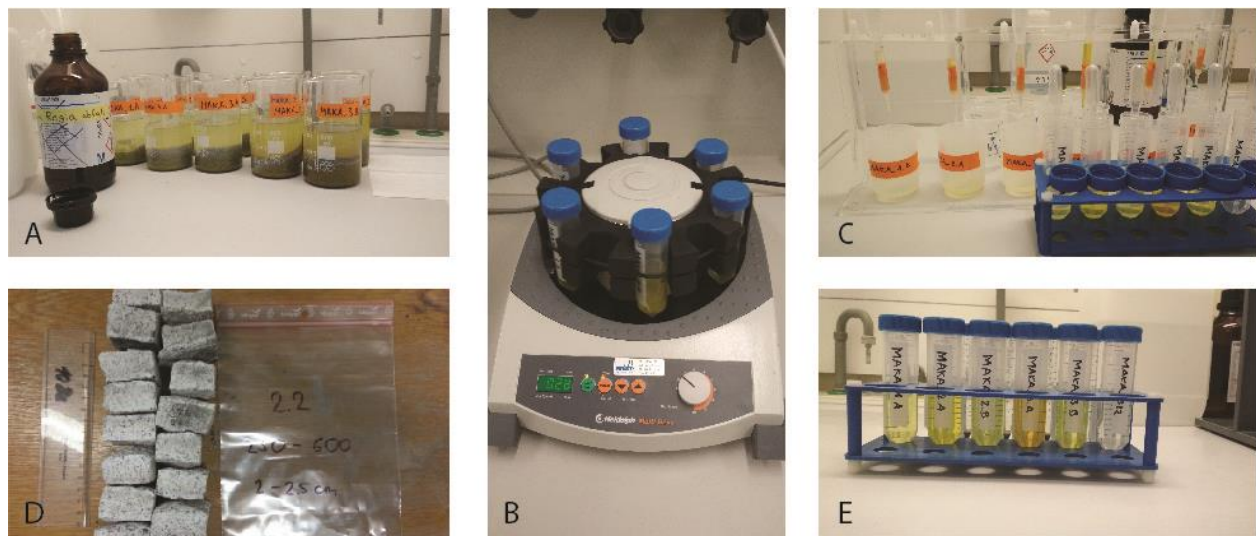
Fig. 21: Lab work; A: Aqua Regia, B: Centrifuge, C: Columns, D: samples before crushing and sieving, E: sample preparation before Fe removal; Photos: Laura Büchler.

4.1.4 Calibration and Scaling System

When calculating cosmogenic-nuclide production rates, a scaling system is required, which defines the variation of the production rate with time, location and altitude (Balco *et al.*, 2008). Secondly, a reference production rate at a certain time and location (which is typically the current time at sea level and in high latitude) is needed (Balco *et al.*, 2008). The simplest, earliest and most common production-rate scaling scheme is from Stone (2000) following Lal (1991) and comprises a variation in spallogenic production rates with latitude and atmospheric pressure but supposes the production rate to be constant through time (Balco *et al.*, 2008). Yet, the strength of the Earth's magnetic field has varied in the past and thus the production rate must have as well (Balco *et al.*, 2008). The scaling scheme of Lal (1991) and Stone (2000) is therefore not optimally adapted. Alternative scaling methods have been developed recently which consider changes in production rates due to elevation, variations in the magnetic field and solar variability (Dunai, 2001; Desilets and Zreda, 2003; Lifton *et al.*, 2005; Desilets *et al.*, 2006).

However, all ^{10}Be TCN ages from this study were calculated by the Lal (1991) and Stone (2000) constant production rate model using the CRONUS Earth 2.2 calculator with the Heyman (2014) calibration data set compilation, which is especially adapted to the Tibetan plateau and Himalayan region (http://hess.ess.washington.edu/math/al_be_v22/alt_cal/Heyman_compilation_input_aspublished.html). We used this model because Owen and Dortch (2014) suggested that studies focusing on the timing of glaciation and relations to climatic records ought to use the time-independent scaling model from Lal (1991) and Stone (2000). This provokes more thorough comparability between other studies as long as the geomagnetic correction and the sea-level high-latitude (SLHL) production rate uncertainties are not yet very well allocated (Owen and Dortch, 2014). Nonetheless, exposure ages from time varying production models from other studies (Lal, 1991; Stone, 2000; Dunai, 2001; Desilets and Zreda, 2003; Lifton *et al.*, 2005; Desilets *et al.*, 2006) are included in *Table 3*. Exposure ages derived from the younger developed scaling systems as from Desilets and Zreda (2003), Lifton *et al.* (2005) and Desilets, Zreda and Prabu (2006) are generally very similar, whereas Dunai (2001), Lal (1991) and Stone (2000) are slightly older for late Pleistocene and early Holocene events and slightly younger for late Holocene events.

Additional to the geomagnetic field, the topographic shielding, altitude, latitude, a snow cover correction and erosion are input parameters in CRONUS Earth when calculating the surface exposure age of a block (see also *corrections to be applied* in section 2.3.2).

In order to vanquish some problems with dating, a strategy taken by some researchers is to apply both optically stimulated luminescence (OSL) and TCN methods within one study (Owen and Dortch, 2014). Unfortunately, the OSL method was not performed within this study due to limited capacities on the expedition to Makalu Base Camp.

4.2 Glacier Outline and ELA Reconstruction

4.2.1 Methods to Estimate Former Glacier ELAs

The *balance ratio (BR)* explicitly addresses glacier mass balance calculations and is based on the assumption that (1) accumulation and ablation gradients of a glacier are more or less linear and (2) the ratio between accumulation and ablation gradient is identified (Furbish and Andrews, 1984; Benn and Lehmkuhl, 2000). Therefore, this method is only useful when topographic maps are accessible and thus the hypsometry of a (former) glacier is known or can be reconstructed with surface contours (Benn and Lehmkuhl, 2000). The BR method, however, is unsuitable for glaciers when a major amount of the accumulation is derived through avalanching and where the ablation gradient is highly influenced by debris cover (Benn and Lehmkuhl, 2000).

According to Benn and Lehmkuhl (2000), the *accumulation-area ratio (AAR)* is the relative size of the accumulation area compared to the total area of a glacier. Similar to the BR, the AAR requires contour lined maps of former glaciers and can thus only be applied where topographic data is available. Balanced budget AARs (AAR_0) in high mountain areas generally lie in the range 0.5 - 0.8 and around 0.58 in the global mean (Dyurgerov *et al.*, 2009). However, AAR_0 values are highly variable among glaciers due to variations in debris cover extent, hypsometry and different options for nourishment in the accumulation (snowfall or avalanching) Hence, constant AAR_0 values should be taken with care over a whole region (Benn and Lehmkuhl, 2000). Generally, debris-covered glaciers have lower AAR_0 values than clean glaciers, mostly resulting from the lower ablation and thus increasing extent of the ablation (Muller, 1980; Clark *et al.*, 1994).

The *maximum elevation of lateral moraines (MELM)* exerts the relationship between the ELA_0 and patterns of glacigenic deposition and thus offers an alternative to estimate the minimum altitude of the ELA of former glaciers (Benn and Lehmkuhl, 2000). This method can be used in areas where no topographic maps are available as no former glacier surface is required (Benn and Lehmkuhl, 2000). Due to the fact that glacier ablation and thus lateral moraine deposition occurs only below the ELA, the highest lateral moraine ridges reveal the minimum altitude of a former ELA (Lichtenecker, 1938). However, as morainic material may not be deposited instantaneously below the ELA, this method causes some complications (Benn and Lehmkuhl, 2000). Further problems are the fast degradation of lateral moraines on deglaciation and the steepness of the terrain which may prevent a morainic deposition, both leading to mistakenly low ELA estimations (Benn and Lehmkuhl, 2000). On the contrary, when glacier retreat is slow, continuous deposition of debris may overprint earlier lateral moraines and yield higher ELAs (Benn and Lehmkuhl, 2000).

The *toe-to-headwall altitude ratio (THAR)* presumes that the ELA_0 lies at a constant ratio between the altitude of the toe (A_t) which is the lowest point of a glacier and the headwall (A_h) which is the highest point (Meierding, 1982; Kayastha and Harrison, 2008):

$$ELA = A_t + THAR\,(A_h - A_t) \hspace{3cm} \text{Eq.4}$$

A THAR of 0.5 corresponds to the mid-point elevation of a glacier. Alternative THAR values between 0.35 - 0.5 were used for clean glaciers (Meierding, 1982; Porter, Pierce and Hamilton, 1983 in Porter, 1983). Debris-covered glaciers, however, have a higher THAR (0.5 - 0.8) due to

the increased ablation area size (Clark *et al.*, 1994; Benn and Lehmkuhl, 2000; Scherler *et al.*, 2010). Yet, defining the beginning of the headwall can be debatable or impossible sometimes (Benn and Lehmkuhl, 2000). This method does not consider glacier mass balance nor its hypsometry and is thus very basic (Benn and Lehmkuhl, 2000). Nevertheless, the THAR method gives a rapid general estimation about the ELA_0 in areas with poor or unreliable map coverage (Benn and Lehmkuhl, 2000).

The *toe-to-summit altitude method (TSAM)* is a similar method like THAR but tries to avoid the problem of defining the start of the headwall. The TSAM estimates the ELA by using the maximum altitude of the glacier catchment (peak) instead of the headwall of a glacier (Louis, 1955; Benn and Lehmkuhl, 2000). This method is very fast and provides good results where the map coverage is poor (Benn and Lehmkuhl, 2000). In the European Alps, ELA estimations tend to be slightly to high (Gross *et al.*, 1976) whereas in the Mongolian Altai the estimations fit well to the observed snowlines (Lehmkuhl, 1998b). Where the highest altitude of the catchment is unrepresentative and induces problems, the average elevation of a catchment can be taken instead. Nevertheless, the suitable THAR and TSAM values for each region/glacier are to be identified empirically as they vary considerably within the region and glacier type (Benn and Lehmkuhl, 2000).

4.2.2 Glacier Inventories

To improve calculations of past and future changes of glacier mass, the fifth assessment report (AR5) of the Intergovernmental Panel on Climate Change (IPCC) required a globally complete compilation of digital outlines of glaciers (Pfeffer *et al.*, 2014). Therefore, the glaciological community compiled the Randolph Glacier Inventory (RGI) in a comparably short time (1 - 2 years) with limited resources (Pfeffer *et al.*, 2014) based on existing datasets such as the GLIMS glacier database (Raup *et al.*, 2007). Around 198'000 glacier outlines were mainly derived from satellite imagery acquired over the 1999-2010 period. Seasonal snow and debris cover on the tongue led to misinterpretations and caused regionally area uncertainties (Pfeffer *et al.*, 2014).

Later in 2015, another glacier inventory for high-mountain Asia was presented by Nuimura *et al.* (2015). This new inventory called *Glacier Area Mapping for Discharge in Asia Mountains* (GAMDAM) contains 87'084 glacier outlines, which were processed manually using Landsat data, a digital elevation model (DEM) and Google Earth imagery. The GAMDAM glacier inventory (GGI) comprises 24% less surface area than the RGI due to the inequality in headwall definition, the exclusion of seasonal snow cover and shaded glacier zones, and general glacier retreat since the 1970s.

The GGI has currently been updated, improved and is presented in GAMDAM2 (Sakai, 2018). Both inventories – RGI and GAMDAM2 – are operated within this thesis. *Figure 22* shows the glacier outlines for Barun Glacier, its side glaciers and Lower Barun Glacier extracted from the two inventories. Disparities are mainly located at the tongue and in the headwall definition. As Barun Glacier is heavily debris covered, defining its glacier terminus remains difficult.
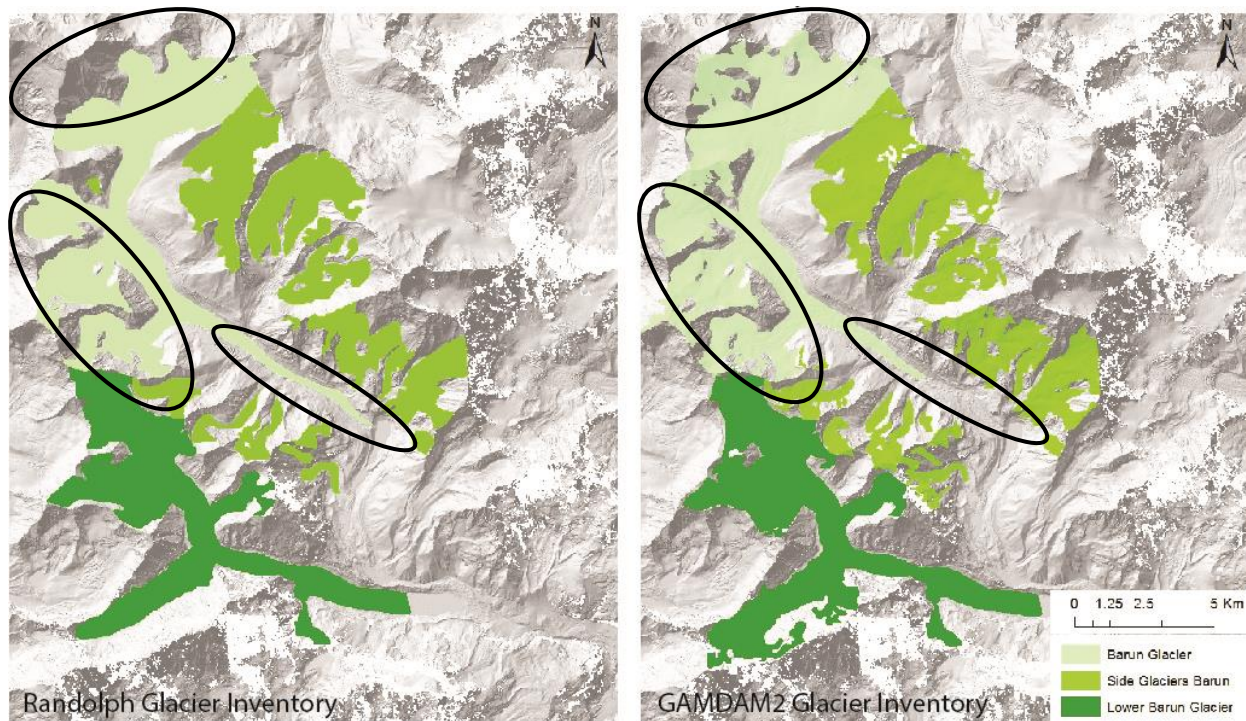
Fig. 22: Today's glacier outlines from two different glacier inventories for Barun Glacier, its side glaciers and Lower Barun Glacier. Left: Randolph Glacier Inventory. Right: GAMDAM2 Glacier Inventory.

While the RGI determines its terminus at the end of the lake where (probably dead) ice shows up, the GAMDAM2 Glacier Inventory places the glacier tongue roughly 140 m higher up. The same effect appears at the steep headwall of Barun Glacier. The accumulation area derived from GAMDAM2 is significantly larger and reaches higher altitudes than from the one from RGI. This discrepancy especially influences ELA_0 estimations when using methods like THAR or TSAM and needs to be kept in mind.

4.2.3 Inversed THAR Method

The age of lateral moraines is of limited use when it comes to the reconstructions of former glacier outlines. Dated terminal moraines are much more beneficial in this regard. However, as we have not found pre-LIA terminal moraines in the Barun Valley, we considered results from a study by Finkel *et al.* (2003) which was conducted in the neighbouring Khumbu Valley. They performed surface exposure dating with [10]Be on several lateral and terminal moraines from Khumbu Glacier, Ama Dablam Glacier, Nuptse Glacier, Kyubo Glacier and a nameless glacier which is henceforth called Hillary Glacier in this thesis (*Fig. 23*). These data were used to determine the toe of each glacier at the dated time periods (< 1 ka, ± 3 ka, ± 8 - 9 ka and ± 16 - 25 ka (Finkel *et al.*, 2003)). Headwall altitudes were derived from the glacier inventories (RGI and GAMDAM2) and were assumed being at the same altitude over the entire period. With these two input parameters (toe and headwall altitude) the THAR method could be applied to estimate former ELA_0 values of these glaciers. It was not clear which THAR values are best applied so values of 0.5, 0.6 and 0.7 were

32

used due to the heavy debris cover of these glaciers. Once the former ELAs from the neighbouring valley glaciers were calculated, we compared these estimations with today's ELA values and calculated their differences (ΔELA). The mean ΔELA of each time period (ice age) was then applied on today's ELA of Barun Glacier (out of both RGI and GAMDAM2) and consequently the former terminus of Barun Glacier could be estimated and modelled for different time periods with what we call here the *inversed THAR* method.
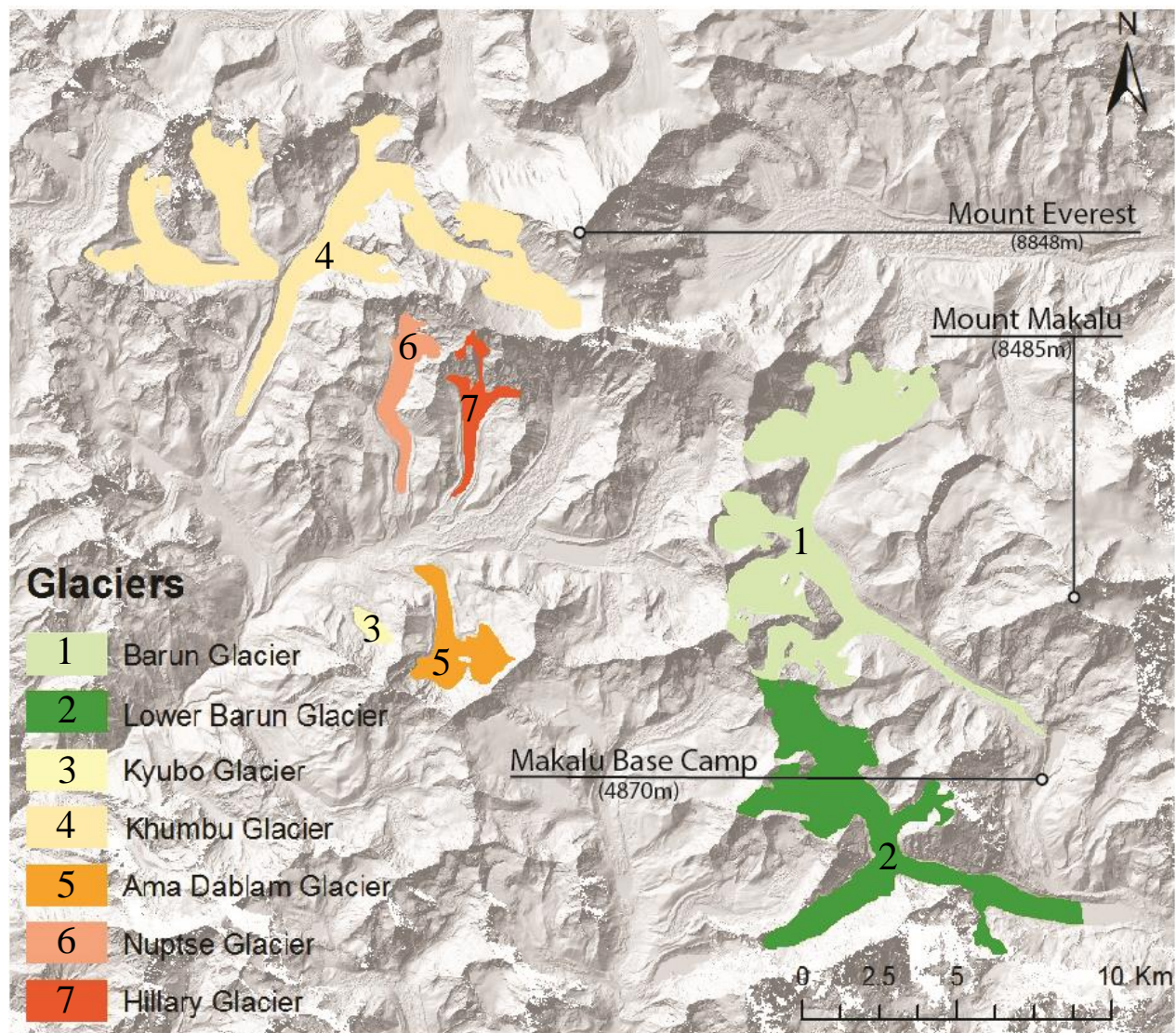
Fig. 23: Overview over incorporated glaciers from Finkel et al. (2003) and glaciers from the Barun Valley (without side glaciers) for ELA reconstruction purposes extracted from the Randolph Glacier Inventory (RGI)

Glaciers in this region, however, are currently not in steady state. In this regard, comparing former glacier ELAs with today's extents makes limited sense. Therefore, we additionally referenced the ΔELA on the LIA extent instead of today's ELA. The LIA moraines are very clearly detectable,

thus it was straightforward to define the LIA ELA of Barun Glacier and the glaciers from the Finkel *et al.* (2003) study.

To handle the headwall definition problem, we applied three different strategies. Firstly, the highest altitude of the whole glacier (7056 m for RGI and 7416.8 m for GAMDAM2) was used to calculate the former glacier terminus with the inversed THAR method, again with a THAR value of 0.5, 0.6 and 0.7. Secondly, the mean elevation of seven contributing basins in the accumulation area (6070 m, 6236 m, 6316 m, 6422 m, 6543 m, 6905 m, 7056 m) was calculated and resulted in a mean elevation of 6506 m. This is 550 m lower than with the highest peak method of the conventional THAR method and thus renders quite a different result. Thirdly, the ELA was estimated separately in each of the four main basins with locally different headwall altitudes (6315 m, 6316 m, 6905 m, 7056 m). The second and third headwall definitions were then calculated only with THAR values of 0.5 and 0.6 and only with the Randolph Glacier Inventory.

Once the former glacier toes of different ice ages were estimated, former glacier extents could be reconstructed in ArcGIS using a hill shading layer derived from the High Mountain Asia (HMA) 8-meter resolution DEM from National Snow and Ice Data Center (NSIDC) (http://dx.doi.org/10.5067/KXOVQ9L172S2, 01.09.2018), the dated lateral moraines and satellite images.

5. RESULTS

5.1 Surface Exposure Dating

The results from the TCN surface exposure dating of the sequence of moraines next to Makalu Base Camp are compiled in *Fig. 24*. They were all derived with the constant production rate model of Lal (1991) and Stone (2000). The first dating of the outermost moraine (block MAKA_1.A) revealed an age of 12.257 ± 0.751 ka including a snow correction and with the Heyman Model, which is especially accurate for the Himalayan region. The second dating produced a slightly higher age of 12.832 ± 0.773 ka. This moraine is from now on named *Late Pleistocene moraine*. Block MAKA_2.A on the second outermost moraine showed an age of 8.3 ± 0.63 ka in the first dating and 7.226 ± 0.464 ka in the second dating with an applied snow correction. The second block on the same moraine (MAKA_2.B) yielded a slightly higher age of 8.523 ± 0.52 ka in the first and 8.195 ± 0.5 ka in the second dating with a snow correction. Thus, the second outermost moraine is from now on called *Early Holocene moraine*. MAKA_3.A was dated to the age of 3.264 ± 0.231 ka in the first dating session and 2.995 ± 0.247 ka in the second dating with a snow correction. Block MAKA_3.B on the same moraine yielded a higher age of 5.764 ± 0.364 ka in the first and 5.528 ± 0.344 ka in the second dating with a snow correction. This latter moraine will be termed *Late Holocene moraine* henceforth.
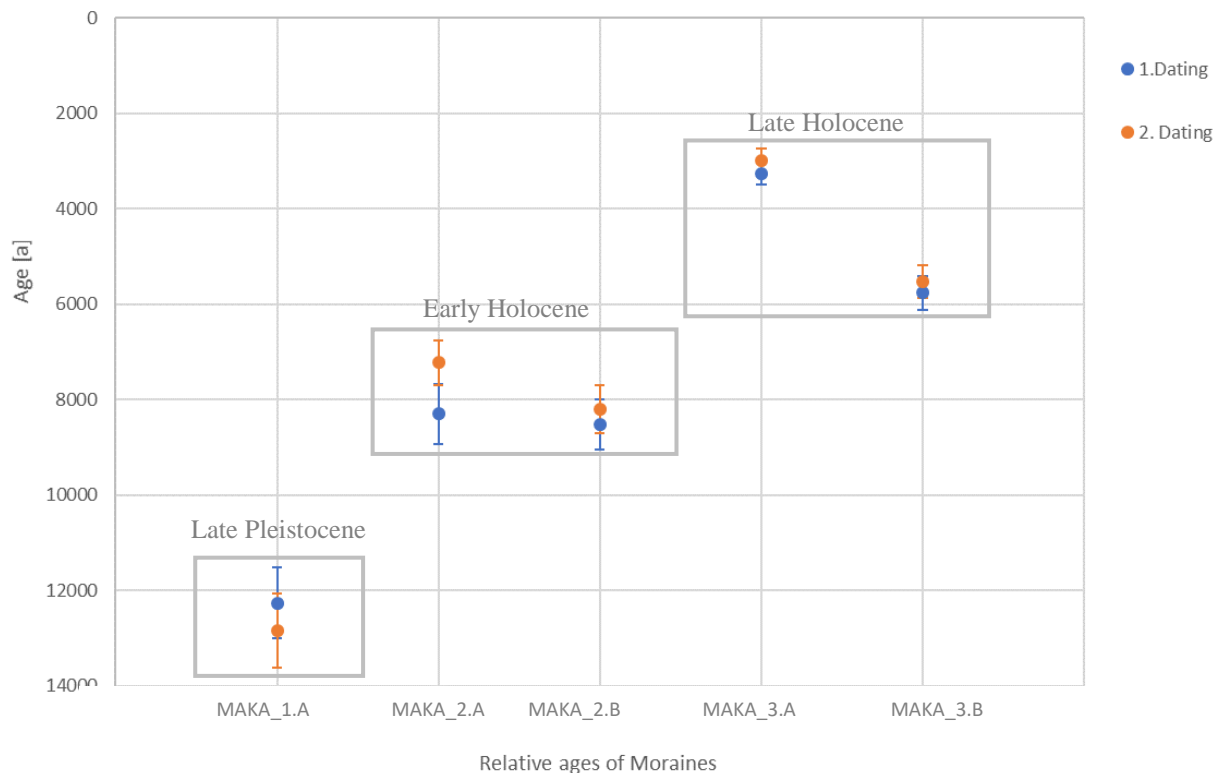
Fig. 24: Surface exposure ages of blocks on the moraines at Makalu Base Camp with a snow correction (with the Heyman Model adapted for the Himalayas).

Without snow correction the derrived ages from the blocks are younger than with a snow correction. MAKA_1.A was dated to 10.056 ± 0.626 ka in the first and 10.527 ± 0.642 ka in the second dating without any snow correction. MAKA_2.A showed an age of 6.755 ± 0.541 ka and 5.882 ± 0.389 ka in the second dating and the ages for MAKA_2.B are 6.966 ± 0.432 ka and 6.698 ± 0.417 ka. The Late Holocene moraine revealed an age of 2.687 ± 0.198 ka in the first and 2.466 ± 0.215 ka in the second dating for MAKA_3.A and 4.743 ± 0.307 ka in the first and 4.549 ± 0.29 ka in the second dating for MAKA_3.B without snow correction.

The derived ages from the first and second dating with a snow correction have been averaged to generate a more accurate surface exposure age of the dated blocks (see *Fig. 25*). Consequently, the Late Pleistocene moraine has an age of 12.5445 ± 0.762 ka, the Early Holocene moraine contains
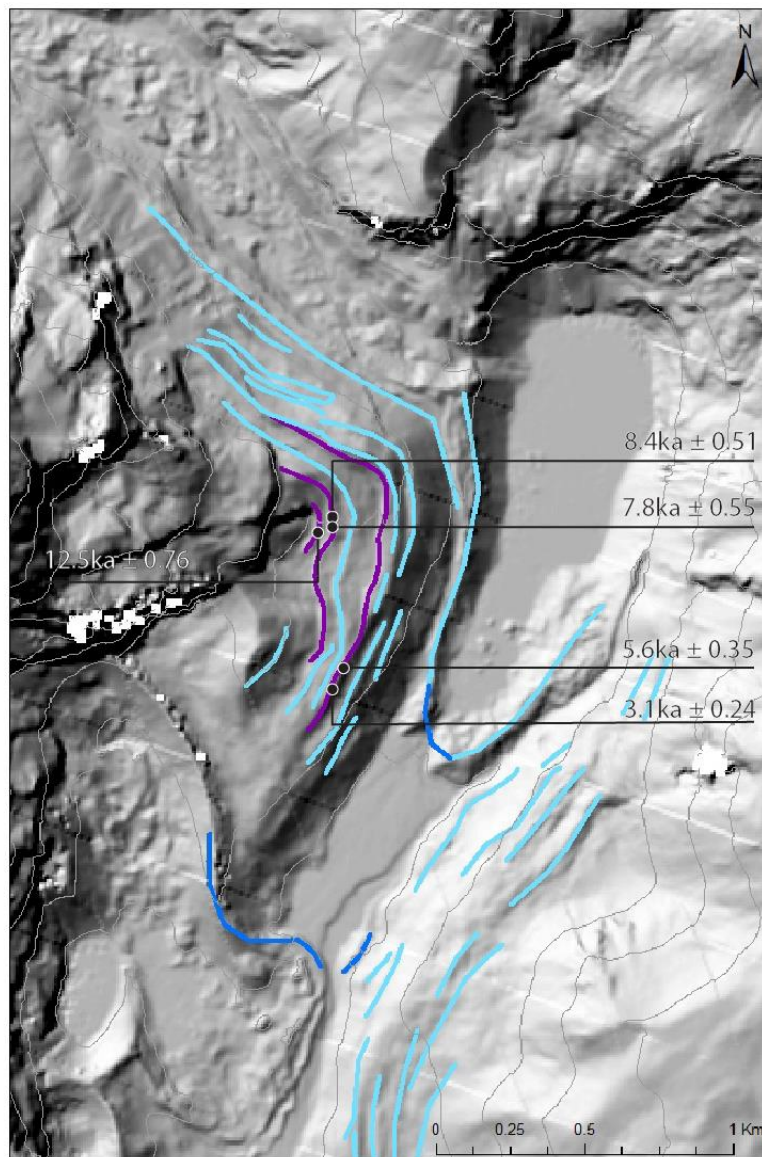
Fig. 25: Dated blocks next to Makalu Base Camp with surface exposure ages; purple: dated moraines within this study; light blue: existing lateral moraines derived from an in situ visual assessment, satellite images and a DEM (not dated); dark blue: potential terminal moraines (not dated).

of two blocks with the averaged ages 7.763 ± 0.547 ka and 8.359 ± 0.51 ka and the Late Holocene moraine comprises two blocks as well, with the averaged ages 3.1295 ± 0.239 ka and 5.646 ± 0.354 ka.

The constant production rate model from Lal (1991) and Stone (2000) has been applied in this thesis, however, ages derived from time varying production models are provided in *Table 3* (Lal, 1991; Stone, 2000; Dunai, 2001; Desilets and Zreda, 2003; Lifton *et al.*, 2005; Desilets *et al.*, 2006) with and without snow correction for both the first and second dating. The more lately developed scaling systems from Desilets and Zreda (2003), Lifton *et al.* (2005) and Desilets *et al.* (2006) generally have very similar exposure ages. Dunai (2001), Lal (1991) and Stone (2000) tend to get older ages for Late Pleistocene and Early Holocene events, whereas for Late Holocene events they tend to be younger than Desilets and Zreda (2003), Lifton *et al.* (2005) and Desilets *et al.* (2006).

The difference between the scaling models on the oldest and youngest derived age for one block in the Late Pleistocene moraines is between 0.709 – 1.195 ka. Scaling models differ between 0.296 – 0.580 ka in the Early Holocene moraine, in contrast to the Late Holocene moraine, where the difference amounts between 0.246 – 0.325 ka. Generally, the difference between the scaling system as well as the external uncertainty are both increasing with an increased age. CRONUS input data is provided in the appendix (*Table 11*).

Table 3: Exposure ages derived from different production rate scaling models (constant production rate model vs. time varying production models) with and without snow correction factor for the first and second dating of each block.

Sample ID	Dating	Snowfactor	Lal (1991)/Stone 2000) exposure age (yr)	External uncertainty (yr)	Production rate (spallation) (atoms/g/yr)	Desilets et al. (2003, 2006) exposure age (a)	external uncertainty (yr)	Dunai (2001) exposure age (a)	external uncertainty (yr)	Lifton et al. (2005) exposure age (a)	external uncertainty (yr)	Lal (1991)/Stone (2000) timedep. exposure age (a)	external uncertainty (yr)
MAKA_1.A	First	No	10056	626	62.13	9347	729	9906	748	9366	666	9826	573
	First	Yes	12257	751	56.69	11242	868	11812	883	11162	784	11968	685
	Second	No	10527	642	62.13	9761	751	10309	768	9757	683	10279	586
	Second	Yes	12832	773	56.69	11746	897	12318	910	11637	807	12527	703
MAKA_2.A	First	No	6755	541	63.94	6360	590	6869	623	6480	564	6612	509
	First	Yes	8300	630	58.34	7748	691	8306	723	7845	653	8049	585
	Second	No	5882	389	63.94	5630	456	5926	466	5726	426	5860	366
	Second	Yes	7226	464	58.34	6791	540	7333	565	6919	503	7025	424
MAKA_2.B	First	No	6966	432	64.52	6550	509	7077	533	6675	473	6794	395
	First	Yes	8523	520	58.87	7943	611	8502	633	8031	562	8271	471
	Second	No	6698	417	64.52	6308	491	6804	513	6426	456	6564	383
	Second	Yes	8195	500	58.87	7652	589	8210	611	7754	543	7944	453
MAKA_3.A	First	No	2687	198	64.08	2797	244	2950	251	2883	235	2913	206
	First	Yes	3264	231	58.47	3349	284	3530	291	3437	270	3478	235
	Second	No	2466	215	64.08	2572	255	2712	263	2653	249	2680	227
	Second	Yes	2995	247	58.47	3100	294	3260	302	3184	284	3218	256
MAKA_3.B	First	No	4743	307	64.17	4752	379	5045	391	4855	356	4857	296
	First	Yes	5764	364	58.54	5545	436	5837	445	5641	405	5758	342
	Second	No	4549	290	64.17	4585	362	4874	373	4685	339	4679	280
	Second	Yes	5528	344	58.54	5369	418	5642	425	5458	388	5554	324

5.2 Schmidt-Hammer

Around each dated block, rock hardness measurements with the Schmidt-Hammer have been conducted and are illustrated in a boxplot in *Fig. 26*. The rock hardness of block MAKA_1.A varies between an R-value of 18 – 49 with a mean of 34.28 and the median at 34 (n = 50). Block MAKA_2.A reveals higher rock hardness values with R-values ranging from 31 – 54. Its mean R-value lies at 42.68 and the median at 42 (n = 50). Block MAKA_2.B on the same moraine has a lower rock hardness with a mean of 32.52 and median of 33, but a broader range of single rock hardness measurement values fluctuating between 18-54 (n = 50). Block MAKA_3.A on the late Holocene moraine has R-values between 16 - 54 with a mean of 38.38 and a median of 40 (n = 50), whereas the other block on the same moraine (MAKA_3.B) has R-values between 26 - 56, a mean of 41.88 and a median of 42 (n = 50). Detailed information about Schmidt-Hammer results is provided in the appendix (*Table 12*).
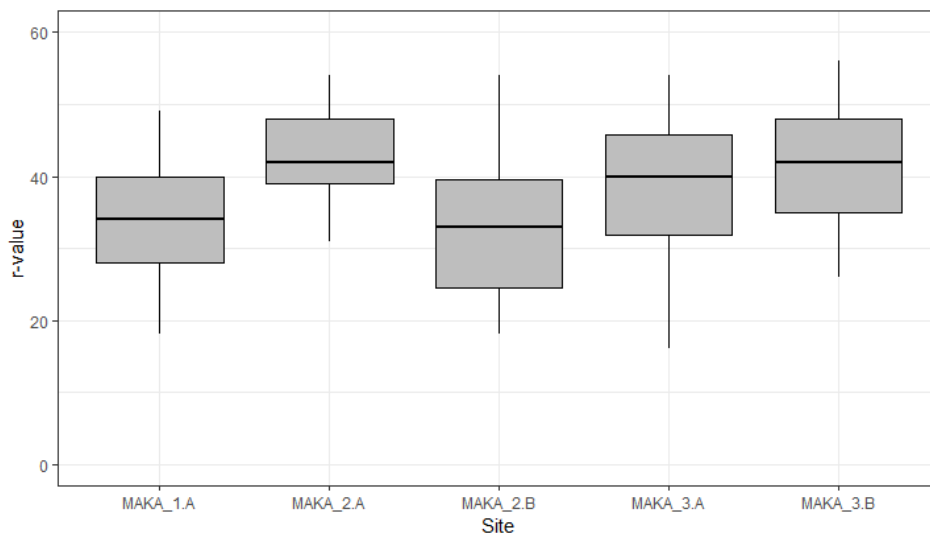
Fig. 26: Schmidt-Hammer measurements per dated block.

The Shapiro-Wilk normality test of every single site showed that they are normally distributed. MAKA_1.A has a p-value of 0.4855 (W = 0.97802), MAKA_2.A features a p-value of 0.2838 (W = 0.9722), MAKA_2.B shows a p-value of 0.1083 (W = 0.96205), MAKA_3.A has a p-value of 0.06035 (W = 0.96205) and MAKA_3.B produced a p-value of 0.1267 (W = 0.96367). They are all higher than 0.05 and are thus normally distributed which favors the application of a one-way ANOVA analysis. The results of the analysis of the variances confirms that the means of the rock hardness measurements of the five sites are significantly (***) different with $F_{(4,244)} = 15.92$ and $p = 1.36*10^{-11}$. The linear trendline of the means, however, reveals a low coefficient of determination (R^2) of 0.1468 and has the following appearance $y = 1.09x + 34.678$. However, when looking at the data (Boxplot) eventhough MAKA_2.A and MAKA_2.B are located on the same moraine and should therefore have identical R-values, they are very different. A Mann-Whitney rank sum test confirms that there is a statistically significant difference between these two sites (P = < 0.001). MAKA_3.A and MAKA_3.B are situated on the same moraine as well. They are according to a Mann-Whitney rank sum test statistically not significantly different (p = 0.092).

Regardless to the fact that the two blocks located on the same moraine are statistically different, they are gathered and compiled in *Fig. 27*. The Late Pleistocene moraine (12 ka) still has the same mean of 34.28 and median of 34 (n = 50). The Early Holocene moraine (8 ka) however, features a mean R-value of 37.6 and a median of 39 (n = 100). The Late Holocene moraine (3 ka) holds the highest mean of 40.13 and a median of 41 (n = 100). These Schmidt-Hammer results demonstrate a negative correlation between the rock hardness and duration of rock surface exposure to weathering conditions. The longer a rock surface has been exposed to the atmosphere, the lower are its R-values and thus the weaker or softer is the rock surfaces and vice versa.
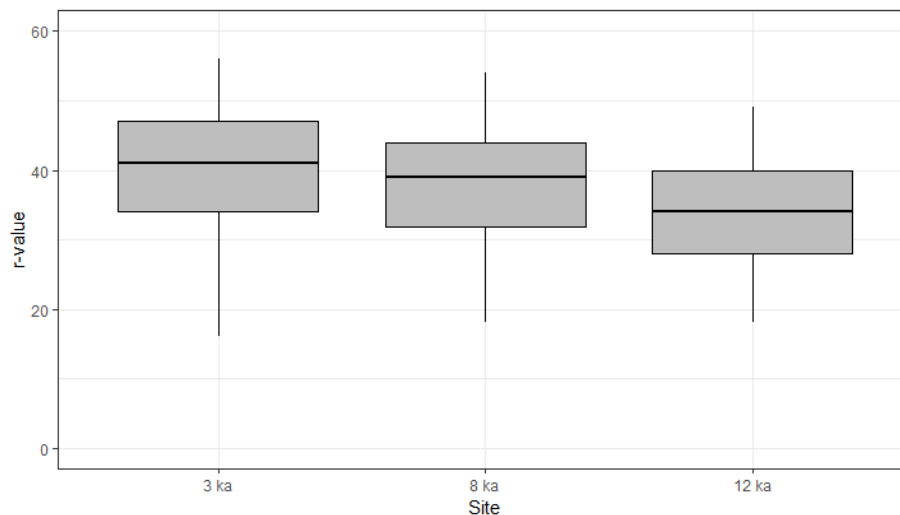
Fig. 27: Schmidt-Hammer measurements per moraine.

A Shapiro-Wilk normality test and a histogram analysis of each site but also per moraine indicates that all data are more or less normally distributed. The late Pleistocene moraine has a p-value of 0.4855 (> 0.05) in the Shapiro-Wilk normality test (W = 0.97802), the Early Holocene moraine in fact discloses a p-value of 0.01648 (< 0.05) in the Shapiro-Wilk normality test (W = 0.96832), but when considering the histogramm the data looks more or less normally distributed. The Late Holocene moraine has a p-value of 0.06535 (> 0.05) in the Shapiro-Wilk normality test (W = 0.97606). An analysis of variance (one-way ANOVA) was be performed which showed that the means of the three moraines are significantly (***) different with $F(2,246) = 8.022$ and $p = 0.000422$. The linear trendline of the means reveals a coefficient of determination (R^2) of 0.994 and has the following appareance $y = 2.925x + 31.487$. However, since one dataset was not normally distributed according to the Shapiro-Wilk normality test, aditionally, a Kruskal-Wallis one-way analysis of variance on ranks was performed. The result shows that the difference in the median values among the three moraines are statisticall significantly different as well (H = 15.121, 2 d.f., P = < 0.001). But a multiple comparison procedure (Dunn's method) indicated that even though Late Pleistocene moraine is statistically different to the Late Holocene moraine, between the Late Pleistocene and the Early Holocene plus between the Early Holocene and the Late Holocene no statistically significant difference occurs.

5.3 Weathering Rinds

Quantification of the weathering rind has only been made around blocks on the Late Pleistocene and Early Holocene moraines, since the Late Holocene moraine is too young for producing an apparent weathering rind. Weathering rind thickness measurements per block are illustrated in *Fig. 28*. The weathering rind of block MAKA_1.A varies between 0.1 – 0.8 mm with a mean of 0.305 mm and the median at 0.2 mm (n = 20). Block MAKA_2.A has the same range of depth measurements but a mean rind thickness of 0.212 mm and a median at 0.1 mm (n = 50). Block MAKA_2.B on the same moraine has a larger range of 0.1-1.0 mm, a mean of 0.294 mm and a median of 0.2 mm (n = 50). More detailed information about the weathering rind measurements is provided in the appendix (*Table 12*).

A Shapiro-Wilk normality test and the histogram analysis of each site indicates that the data are not normally distributed. MAKA_1.A has a p-value uf 0.002364 (<0.05) in the Shapiro-Wilk test (W = 0.82123). MAKA_2.A features a p-value of $5.309*10^{-10}$ (<0.05) (W = 0.62862) and MAKA_2.B has a p-value of $3.407*10^{-7}$ (<0.05) (W = 0.78171). Therefore, a Kruskal-Wallis one-way analysis of variance on ranks was undertaken and resulted in the perception that there is no statistically significant difference in the median values (H = 3.479, 2 d.f., P = 0.176). Thus, there is a possibility that the existing difference is due to random sampling variability.
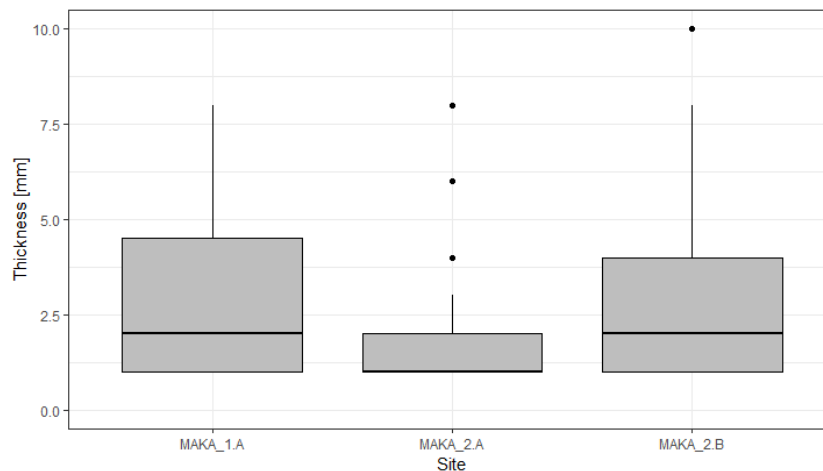
Fig. 28: Weathering rind thickness [mm] per dated block.

Since MAKA_2.A and MAKA_2.B are located on the same moraine, they are merged (8 ka moraine) and illustrated together with the 12 ka moraine (Late Pleistocene moraine) in *Fig. 29*. The gathered Early Holocene moraine has a mean of 0.253 mm and a median of 0.1 mm (n = 100). These results show that the weathering rind thickness slightly increases with increasing age (positive correlation). The linear trendline of the means reveals a low coefficient of determination (R^2) of 0.0117 and has the following appearance y = 0.055x + 2.5933. When comparing the weathering rinds of the two moraines (Late Pleistocene and Early Holocene moraine) a t-test can be applied. Due to the not normally distributed dataset, we used a Mann-Whitney rank sum test. The median values between the two moraines are not statistically significantly different (P = 0.273), which indicates random sampling variability. However, when looking at the data (boxplot) the median of the Late Pleistocene moraine is slightly increased compared to the Early Holocene

moraine which, although not significantly, suggests an increased weathering rind formation with increased exposure duration to the atmosphere and thus to weatheirng conditions.
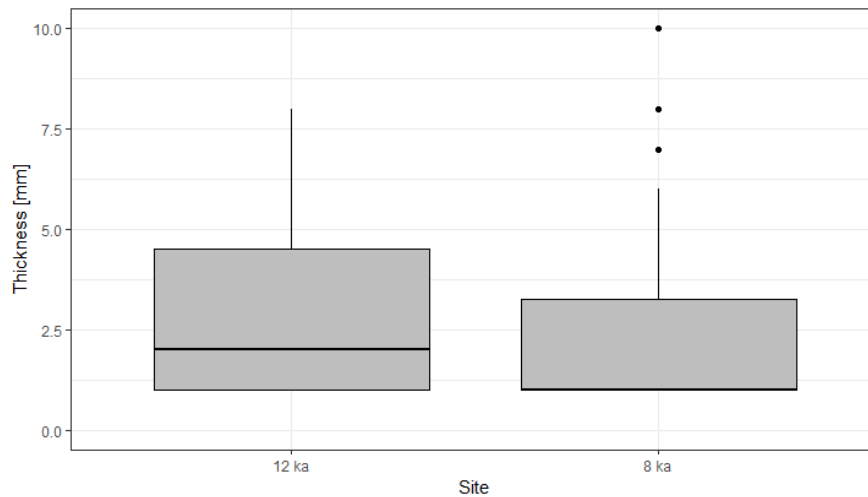
Fig. 29: Weathering rind thickness [mm] per moraine.

5.4 Reconstructions of Glacial Extents and Former ELAs

In this section the results from the ΔELA calculations based on the former ELA of the LIA with the RGI and extent reconstructions are presented. Details about the incorporated glaciers used for these reconstructions are provided in *Fig. 23* and section 4.2. ΔELA calculations conducted on the base of today's equilibrium line altitude with the Randolph Glacier Inventory (RGI) and the GAMDAM2 glacier inventory (GGI) will not further be presented here but are included in the appendix.

5.4.1 Reconstructions with the RGI Based on the ELA of the LIA

In contrast to today, glaciers were more or less to a steady-state during the Little Ice Age. Therefore, ELA depressions and glacier reconstructions are referred to the LIA using the RGI. Reconstructions with the THAR method based on the GGI are assumed to be less accurate in this region, because the accumulation areas are overrepresented. Therefore, reconstructions with the GGI are in the appendix and not further provided in this section. *Table 4* illustrates the ELAs from the different glaciers from the Khumbu Valley, which then have been used to calculate the ΔELA per glacial advance. Information about the current glacier characteristics for each glacier is described in *Table 4*. Out of these five incorporated glaciers, only Khumbu Glacier is comparable to the Barun Glacier in its size. The others are a lot smaller, which makes a comparison complicated. During the LIA the ELA in the Khumbu Valley was between 4907 - 6348 m. The ELA dropped down to 4662 – 6013 m during the LGM. This results in a mean ΔELA of -289 m during the LGM (THAR 0.5). During the Early Holocene (8 ka) the mean ΔELA in the Khumbu Valley was -132 m and during the Late Holocene (3 ka) -19 m, always calculated with a THAR value of 0.5. THAR values of 0.6 and 0.7 are provided in *Table 4*, too.

Table 4: Calculated ELAs and ΔELAs from the Khumbu Valley with the THAR method (RGI).

	Current	LIA	Δ ELA [m]	3ka	Δ ELA [m]	8ka	Δ ELA [m]	LGM	Δ ELA [m]
Ama Dablam Glacier									
Inventory	RGI								
Date	36829								
Area [km2]	5								
Headwall [m]	5873					5873			
Toe [m]	4774					4514			
Slope [°]	19								
Aspect [°]	338								
Lmax [km]	4								
ELA [m]									
THAR 0.5		5323				5193	-130		
THAR 0.6		5433				5329	-104		
THAR 0.7		5543				5465	-78		
Nuptse Glacier									
Date	37261								
Area [km2]	4								
Headwall [m]	5786			5786					
Toe [m]	4966			4929					
Slope [°]	12								
Aspect [°]	199								
Lmax [km]	6								
ELA [m]									
THAR 0.5		5376		5358	-19				
THAR 0.6		5458		5443	-15				
THAR 0.7		5540		5529	-11				
Hillary Glacier									
Date	37261								
Area [km2]	3								
Headwall [m]	7217			7217					
Toe [m]	4929			4890					
Slope [°]	22								
Aspect [°]	196								
Lmax [km]	4								
ELA [m]									
THAR 0.5		6073		6053	-20				
THAR 0.6		6302		6286	-16				
THAR 0.7		6530		6518	-12				
Kyubo Glacier									
Date	37181								
Area [km2]	1								
Headwall [m]	5096					5096		5096	
Toe [m]	4718					4631		4229	
Slope [°]	14								
Aspect [°]	307								
Lmax [km]	2								
ELA [m]									
THAR 0.5		4907				4863	-44	4662	-245
THAR 0.6		4945				4910	-35	4749	-196
THAR 0.7		4982				4956	-26	4836	-147
Khumbu Glacier									
Date	37261								
Area [km2]	32								
Headwall [m]	7832					7832		7832	
Toe [m]	4864					4419		4195	
Slope [°]	18								
Aspect [°]	262								
Lmax [km]	15								
ELA [m]									
THAR 0.5		6348				6125	-222	6013	-334
THAR 0.6		6644				6467	-178	6377	-267
THAR 0.7		6941				6808	-133	6741	-201
Overall mean ELA depression THAR 0.5					-19		-132		-289
THAR 0.6					-15		-106		-232
THAR 0.7					-11		-79		-174

Inversed THAR Method Applied on Barun Glacier

The generated and averaged ΔELA from the neighbouring Khumbu Valley have then been applied on the ELA of Barun Glacier from the LIA for the three different glacial stages with the inversed THAR method (*Fig. 30*). The headwall altitude is assumed to having been stable at the same altitude (7056 m) over the observed period of time (highest point method). Therefore, with the inversed THAR method the glacier terminus for each glacial stage can be determined and is provided in *Table 5*. Additionally, the ΔELA between the LIA and today (year 2000) of Barun Glacier has been calculated and amounts -37 m (THAR 0.5). The glacier toe was situated at an altitude of
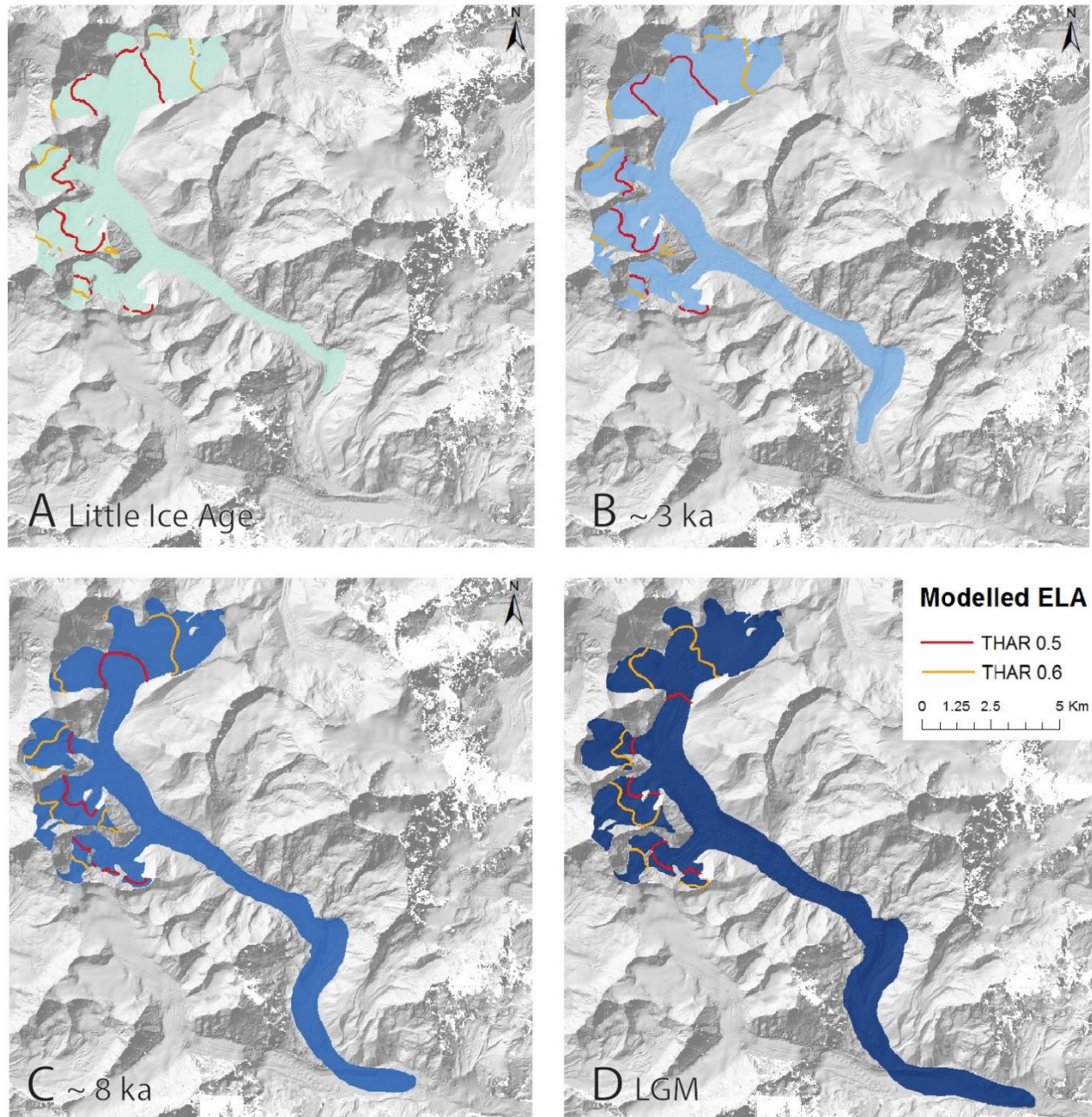
Fig. 30: Reconstructed glacial extents of Barun Glacier (with the RGI) and modelled ELAs with the highest point as headwall definition.

Table 5: Calculated ELAs and former glacier terminus of Barun Glacier.

Barun Glacier		Current	LIA	Δ ELA [m]	3ka	Δ ELA [m]	8ka	Δ ELA [m]	LGM	Δ ELA [m]
	Inventory	RGI								
	Date	30.10.2000								
	Area [km2]	30.0	32.2							
	Headwall [m]	7056	7056		7056		7056		7056	
	Method	Highest point of the accumulation area								
	Toe [m]	4875	4801		4763		4537		4222	
	Slope °	13.9								
	Aspect [°]	122								
	Lmax [km]	13.8								
ELA [m]										
	THAR 0.5	5965	5929	-37	5909	-19	5797	-132	5639	-289
	THAR 0.6	6184	6154	-29	6139	-15	6049	-106	5923	-232
	THAR 0.7	6402	6380	-22	6368	-11	6300	-79	6206	-174

4222 m during the LGM (*Fig. 30* D), whereas during the LIA the glacier terminus was at 4801 m.

Inversed THAR Method Applied on Barun Glacier with an alternative headwall definition

Instead of the highest elevation of the whole accumulation area, a mean of the headwalls of the seven accumulation basins was taken for the overall headwall altitude. This alternative was undertaken because a single high peak can highly influence and distort the THAR method. The seven accumulation basins have altitudes of 6905 m, 7056 m, 6316 m, 6232 m, 6070 m, 6422 m, 6543 m, which results in a mean of 6506 m. This headwall altitude combined with the same terminus altitudes from the RGI referred to the LIA and the same ΔELAs renders alternative ELAs for the four glacial stages and the LIA as shown in *Table 6* and illustrated in *Fig. 32*. Using the alternative headwall definition, the ELAs are generally 275 m lower than with the highest point method. During the LGM the ELA of Barun Glacier was at 5364 m and during the LIA at 5654 m (THAR 0.5). Due to the lower headwall altitude of this method, the ΔELA difference between the LIA and today's ELA is increased. The ELA depression calculated with a THAR value of 0.5 amounts

Table 6: Calculated ELAs and former glacier terminus of Barun Glacier with the alternative headwall definition.

Barun Glacier		Current	LIA	Δ ELA [m]	3ka	Δ ELA [m]	8ka	Δ ELA [m]	LGM	Δ ELA [m]
	Inventory	RGI								
	Date	30.10.2000								
	Area [km2]	30.0	32.2							
	Headwall [m]	6506	6506		6506		6506		6506	
	Method	Mean of 7 basins								
	Toe [m]	4875	4801		4763		4537		4222	
	Slope [°]	13.9								
	Aspect [°]	122	122							
	Lmax [km]	13.8								
ELA [m]										
	THAR 0.5	5965	5654	-312	5634	-19	5522	-132	5364	-289
	THAR 0.6	6184	5824	-359	5809	-15	5719	-106	5593	-232
	THAR 0.7	6402	5995	-407	5983	-11	5915	-79	5821	-174

-312 m between the LIA and today.

A third headwall definition method has been applied, where the ELA has been estimated separately for each of the four basins with the inversed THAR method, which results in separate ELA altitudes for each basin, too. The results, however, were not useful, due to the strong variation in the altitudes of the accumulation basins between the basins. Therefore, they are not further illustrated here, but provided in the appendix (*Table 9*). Additionally, a ΔELA -360 m scenario (Liu *et al.*, 2017) has been applied, to identify how far the Barun Glacier would advance. In such a case, the glacier had its ELA at 5294 m (THAR 0.5) and its terminus at an altitude of 4081 m (*Fig. 31*), which is 141 m lower than the modelled LGM extent of Barun Glacier with data from the Khumbu Valley. Within this scenario the Barun Glacier would have a size of 47.5 km^2 and a glacier length of 29.5 km.
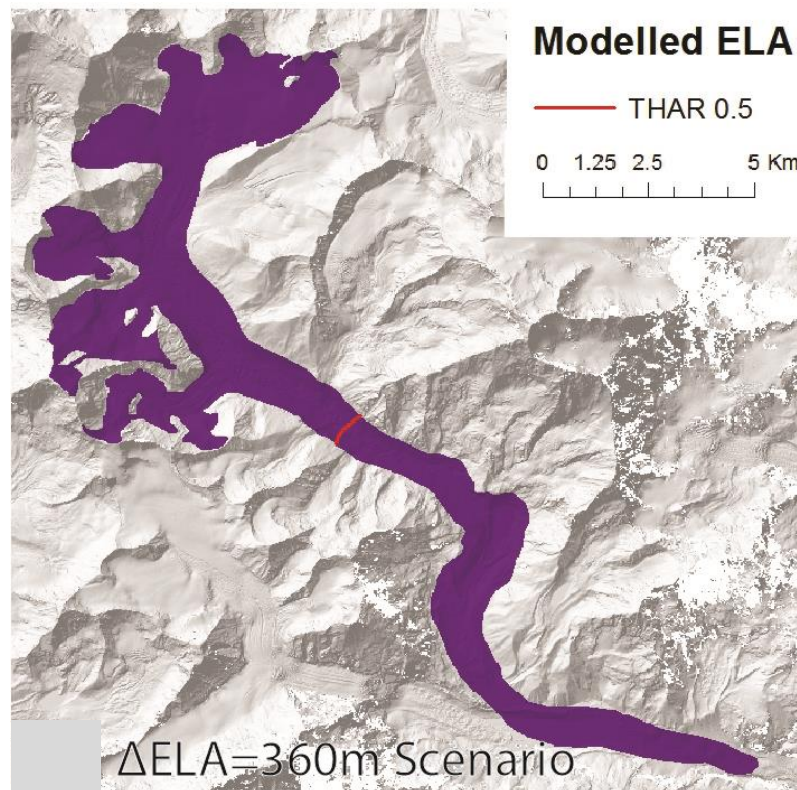
Fig. 31: ΔELA of -360 m scenario.
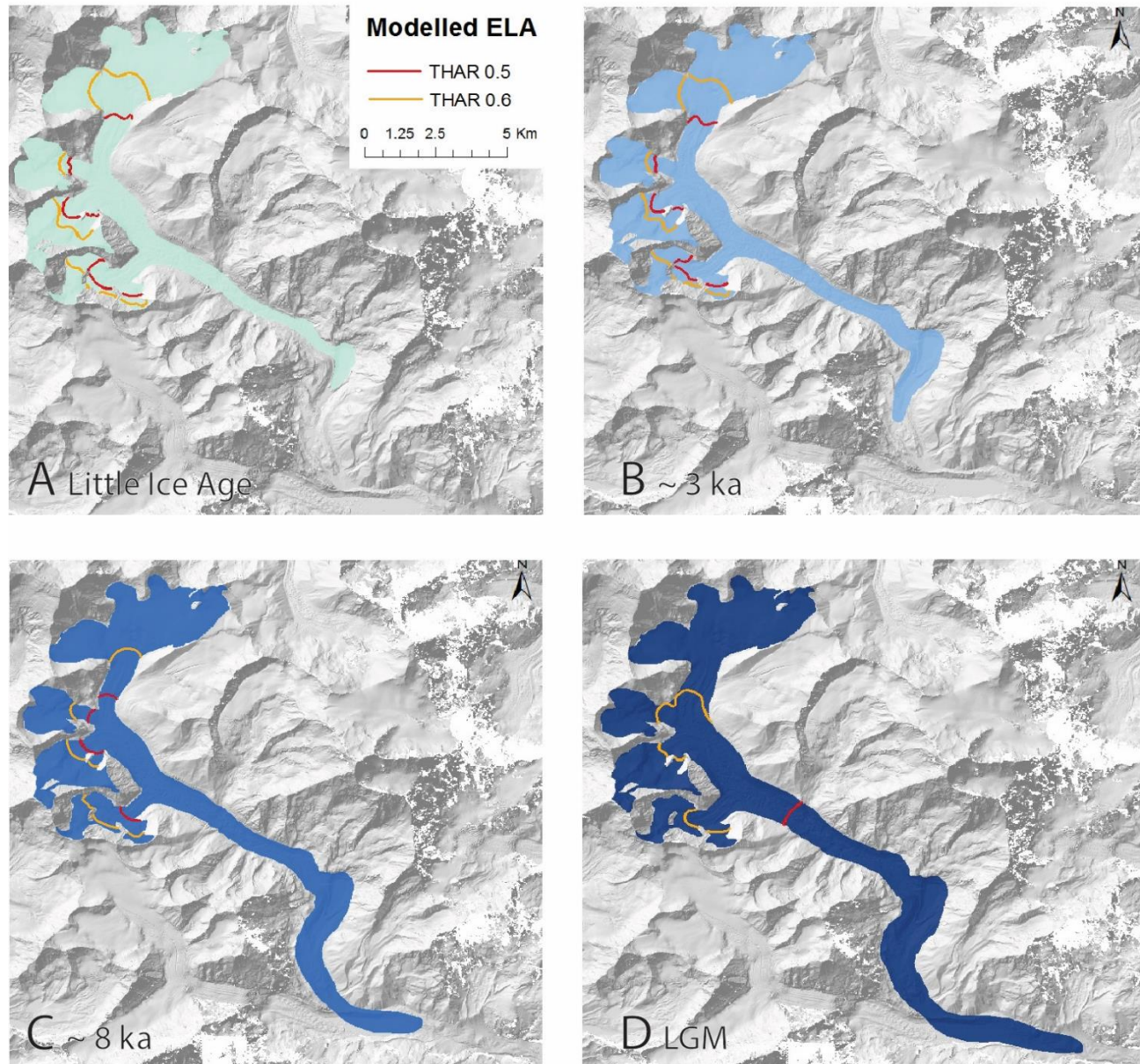
Fig. 32: Reconstructed glacial extents of Barun Glacier (with the RGI) and modelled ELAs with the mean of the seven basins as an alternative headwall definition.

5.4.2 Zonal Statistics of Glacier Reconstructions

Detailed topographic information has been calculated for the various glacier extents using the concept of zonal statistics. Calculations are only performed for the reconstructed stages of Barun Glacier referred to the ELA of the LIA (*Table 7*). According to these reconstructions the glacier area varied between 32.2 – 47.1 km^2. The mean elevations from the zonal statistics are between the ELA with a THAR of 0.5 and a THAR of 0.6. The standard deviations lie between 400 – 562 m. The median elevations are roughly on the same altitude as the ELAs calculated with a THAR of 0.6 and with the alternative headwall definition (mean of seven basins). However, compared to the ELAs calculated with the normal THAR method (highest elevation of the whole accumulation area), they are roughly 100 m lower than with the THAR 0.5 method. The glacier length rises from an initial 19.4 km during the LIA up to 28.7 km during the LGM. In the Δ360 m scenario the Barun Glacier would have a length of 29.5 km.

Table 7: Topographic information of the reconstructed Barun Glacier referred to the ELA of the LIA with the RGI.

	Area [km2]	Min [m]	Max [m]	Range [m]	Mean [m]	Median [m]	Glacier-length [km]
LIA	32.2	4801	7056	2255	5733	5829	19.4
~ 3ka	35.0	4756	7053	2297	5668	5766	21.3
~ 8ka	41.1	4493	7056	2563	5540	5629	26.3
LGM	47.1	4217	7052	2835	5468	5524	28.7

Additionally, in order to cross-examine and verify the estimated ELAs, the accumulation area ratios (AAR) have been calculated for both methods (mean of seven accumulation basins and the highest point method) referred to the LIA with the RGI (*Table 8*). The AARs for the normal THAR method (highest point) are very low for the THAR value of 0.6 and reasonably low for the THAR value of 0.5, varying between 0.44 and 0.09. The AARs of the glacier reconstruction for the alternative headwall definition method (mean of the seven basins) varies between 0.44 and 0.49 for a THAR value of 0.6 and between 0.55 and 0.68 for a THAR value of 0.5. When considering the balanced budget AARs in high mountain areas, which is generally in the range 0.5 - 0.8 and around 0.58 in the global mean (Dyurgerov *et al.*, 2009) the THAR value of 0.5 with the alternative headwall definition (mean) gives the best results. The Δ360 m scenario of Barun Glacier has an accumulation area ratio of 0.69.

Table 8: Accumulation area ratios (AAR) of several different glacier reconstructions for Barun Glacier conducted with different methods (mean and highest point).

	Mean		Highest point	
THAR	0.5	0.6	0.5	0.6
LIA	0.64	0.48	0.38	0.09
~ 3ka	0.60	0.49	0.39	0.11
~ 8ka	0.55	0.44	0.40	0.14
LGM	0.68	0.47	0.44	0.26

6. DISCUSSION

Prior to the discussion some major assumptions for this study need to be clarified. (1) The headwall altitude is assumed to be constant over time. (2) When applying the ELA depressions from the neighbouring Khumbu Valley, it is assumed that climatic conditions and trends (precipitation and temperature) are very similar in the neighbouring Barun Valley, although they may be different for several reasons (e.g. exposition, surrounding topography, hypsometry). However, the Barun Valley is likely somewhat drier than the Khumbu Valley due to increased rain shadow effects. (3) The Barun Glacier converged with the Lower Barun Glacier during its maximum post-glacial extents, which has an influence on several input parameters such as accumulation, ablation and ELA. Smaller yet disconnected glaciers around the Barun Glacier converged and formed tributaries which changed input parameters. However, the confluence of other glaciers was not considered here, but should be taken into account in subsequent glacier reconstructions. (4) It is also assumed that Barun Glacier was equally debris covered in the past as today and thus the THAR was not adapted for the glacial reconstructions. However, the amount of debris cover on the glacier surface changes over time and increases when a glacier is in retreat (Scherler *et al.*, 2018). Given that distinct lateral moraines have been deposited, it can be assumed that the surface of Barun Glacier was also (partly) debris covered after the LGM. Additionally, due to high and possibly always ice-free rock walls in the accumulation region of Barun Glacier, debris supply and thus debris cover on the tongue is likely for previous glacial stages, which facilitated moraine deposition. (5) As debris cover, the accumulation through avalanches, cloud coverage and the strength of the monsoon all influence the mass balance of Barun Glacier (but are unknown for the past), the here applied assumption of a constant climate sensitivity might not be justified. The presented geometric reconstructions have thus to be seen as a first rough guess only. (6) All [10]Be surface exposure dating ages are estimated with a snow correction factor as a lot of snow in this region is assumed, which influences the cosmogenic ray input into the rock surface.

6.1 Late Holocene

During the Late Holocene the Barun Glacier deposited several lateral moraines next to the Makalu Base Camp of which one was dated within this thesis. The two blocks that were dated on this moraine, however, revealed statistically different ages. One block is 3.1 ± 0.24 ka and the other block is 5.6 ± 0.35 ka. For the following reasons we decided to assign the 3.1 ka block as determinant and the relevant age for this moraine. Firstly, the 3.1 ka block appeared ideal for surface exposure dating using [10]Be, because it is large, flat at bottom (which makes toppling very unlikely) and no obvious signs of erosion exists. Additionally, the dip angle of the area where the rock sample has been extracted is low (10°). The block itself is placed on top of the moraine ridge, which indicates that is was deposited by the glacier and not by a posterior rock fall. It is also unlikely that this block has been buried before and excavated later to the surface. Moreover, a cross comparison across the Himalayan orogen reveals more or less synchronous glacial advances during this time. Surface exposure dating in the Khumbu Valley yielded a similar age of 3.5 ± 0.3 ka (Thuklha stage), whereas 5 ka blocks have not been found within the study of Finkel *et al.* (2003). Glacial history on the northern slope of Mount Everest of the Rongbuk Valley shows a slightly younger glacial advance than on the southern slope, with 2.4 ± 0.2 ka (TCN dating) and 2.3 ± 0.1 ka (OSL dating) (Owen *et al.*, 2009). Liu *et al.* (2017) detected a glacial advance using cosmogenic [10]Be

surface exposure dating around the Karola Pass in the eastern Lhagoi Kangri range (Tibet) dated to an age of 2.5 ± 0.2 ka (Neoglacial). An extensive glaciation was also found in the Langtang Valley in Nepal from $3.65 – 3.0$ ka (Langtang Stage) in the late Quaternary (Shiraiwa *et al.*, 1991). As dated 5 ka blocks have not been found in either of these sites and due to the physical characteristics mentioned above, we suppose that the 5.6 ka block has undergone pre-exposition and is thus ignored in this study.

Schmidt-hammer measurements revealed high R-values (mean: 40.13), which additionally indicates that this moraine is likely to be younger than the other sampled moraines. No weathering rind could be detected due to the young age, i.e. exposition to weathering conditions was relatively short. Both relative dating techniques endorse an age of 3 ka for this Late Holocene moraine.

Between the Late Holocene moraine and the LIA moraine are at least five younger moraines (see Fig. 25), which have not yet been dated, but seem very interesting. A high moraine deposition rate during this short time-period suggests a very sensitive reaction of the glacier to changes in climate. Since the accumulation of Barun Glacier occurs merely in summer, the glacier reacts very sensitively to temperature change (as both ablation and snow amounts are influenced). Higher temperatures during insolation maxima increase the moisture availability and thus increase precipitation amounts that will fall as snow at high altitudes, which results in mass gains and possibly glacial advances (Benn and Owen, 1998; Finkel *et al.*, 2003; Hu *et al.*, 2017). Lower temperatures, on the other hand, result in less ablation at the tongue and, at the same time less precipitation in higher altitudes.

The ELA shift of -19 m (THAR 0.5 referred to the Little Ice Age and with the RGI) is small compared to Liu *et al.* (2017), who found an ELA depression of 195 m during the Neoglacial (2.5 ± 0.2 ka). However, Liu *et al.* (2017) referred their ΔELA value to today's extent which was around the year 2010. Adding the -37 m (THAR 0.5) difference between the LIA and today of Barun Glacier, ΔELA is -56 m during the Late Holocene compared to today (2000). However, considering the fact that the RGI most likely overestimates glacier extent, as it includes dead ice parts of the heavily debris covered tongue, its glacier terminus and thus also the ELA would increase in altitude and thus increase the difference between the ELA of today and the 3 ka extent. Furthermore, the tributaries of the Barun Glacier and the potential merging with the Lower Barun Glacier (see Fig. 22) would further offset the glacier terminus. For these reasons a larger ΔELA than the here calculated -56 m can be assumed for Barun Glacier when compared to today's extent.

6.2 Early Holocene

During the Early Holocene glacial advances earmarked the Himalayan orogen (Finkel *et al.*, 2003; Owen *et al.*, 2009; Scherler *et al.*, 2010; Liu *et al.*, 2017). These extensive glaciations mostly began during the Younger Dryas (YD) period and continued until the Early Holocene (Sati *et al.*, 2014). In the Barun Valley two blocks were dated on an Early Holocene moraine. One block revealed an age of 7.763 ± 0.547 ka and the other one 8.359 ± 0.51 ka. Block MAKA_2.A which yielded a lower age of 7.763 ± 0.547 ka has slight traces of enhanced erosion. It might be that even a part

broke off, which gave rise to it is younger compared to the other block. However, it is still in the range of error and thus acceptable. The older block seems to be decent for surface exposure dating, as no sign of erosion or toppling is evident. Additionally, it is deposited on top of the moraine ridge, where only a glacier can have deposited it. The average age of the two blocks with each two dating ages reveals an age of 8.06 ka for the Early Holocene moraine. This age fits into the picture when compared to other studies within this region. Scherler *et al.* (2010) conducted ^{10}Be measurements in western Garhwal (India) and found five glacial episodes of which one was at ~ 8 - 9 ka. Surface exposure dating around the Karola Pass in central Himalaya revealed a glacial advance event between $8.2 \pm 0.4 - 9.7 \pm 0.4$ ka, as well (Liu *et al.*, 2017). Finkel *et al.* (2003) dated their Early Holocene moraine slightly older to an age of 9.2 ± 0.2 ka (Chhukung). The Early Holocene glacial advance is mostly attributed to a decrease in summer temperatures due to changes in solar insolation and an increase in monsoon precipitation (Rupper *et al.*, 2009). Sati *et al.* (2014) speculate that the ice-albedo feedback (Colin *et al.*, 1998) additionally reduced radiative heating (Adams *et al.*, 1999) and thus lowered temperature. Slightly younger moraines were found by Owen *et al.* (2009) in the Rongbuk Valley north of Mount Everest. OSL and TCN dating revealed an age of $6.8 – 7.7$ ka (Samdupo I). However, in contrast to the southern slope of Mount Everest, where glacial advances during the Early Holocene were distinct, no moraine was deposited in the Rongbuk Valley during this time. This is presumably due to increased monsoon precipitation in the Khumbu Himal, which resulted in positive glacier mass balances, whereas the Rongbuk Valley remained sheltered from the monsoon moisture and thus, did not allow glaciers to grow. According to Owen *et al.* (2009), glaciers in the northern slopes of Mount Everest are more sensitive to climatic change, especially to a change in precipitation linked to the monsoon dynamics. These findings support the view of Zech *et al.* (2009) and Sati *et al.* (2014), who claim that glaciers in more orographically shielded regions tend to be more sensitive to variations in precipitation, while glaciers with high precipitation inputs tend to be more sensitive to variations in temperature. However, apart from the Early Holocene, glacial advances around the Everest massif were broadly synchronous (Owen *et al.*, 2009). Since the dated moraines in the Barun Valley are roughly synchrounous with the glacial behavior of the southern slope of Mount Everest, it suggests that this region is influenced by the monsoon as well, in contrast to the northern slope, that is sheltered from high precipitation inputs and thus behaved asynchronously.

Between the Early and the Late Holocene moraine resides another moraine which is probably linked to the Mid Holocene glaciation, that occurred between 7.5 ka and 4.5 ka (Sati *et al.*, 2014). During this period, glacier advances were accounted for low temperatures and thus reduced ablation due to increased cloudiness and evaporative cooling, although precipitation was low (Rupper *et al.*, 2009). A Mid Holocene surge, however, has not been found pervasively across the Himalayan orogen, e.g. in the neighbouring Khumbu Valley (Finkel *et al.*, 2003) nor around the Karola Pass (Liu *et al.*, 2017). The Samdupo I moraines in the Rongbuk Valley ($6.8 – 7.7$ ka) (Owen *et al.*, 2009), however, as well as the ~ 5 ka glacial episode in Garhwal, India (Scherler *et al.*, 2010) can be placed in the Mid Holocene glaciation.

Schmidt-hammer measurements reveal high R-values with a mean of 37.6 and a median of 39, which indicates that this moraine is highly likely to be younger than the Late Pleistocene moraine but older than the Late Holocene moraine. However, this difference in the mean is not statistically

significant. The median thickness of the weathering rind between to Early Holocene and Late Pleistocene moraines are not statistically significantly different either, however a small trend towards an increased weathering rind with increased exposure duration is visible. The Late Pleistocene and Early Holocene moraine depositions might be temporally too close to build statistically different weathering rind depths.

The ELA depression value of -132 m (THAR 0.5 referred to the Little Ice Age and with the RGI) is lower than reported in Liu *et al.* (2017), who calculated an ELA depression of -265 m during the Early Holocene (8.2 ± 0.4 – 9.7 ± 0.4 ka). However, as well as during the Late Holocene, they referred their ΔELA to today's extent (2010). When adding the -37 m difference between the LIA and today (2000) of Barun Glacier, we obtain a ΔELA of -169 m for the Early Holocene. Due to a likely overestimations of today's glacial extent of the Barun Glacier in the RGI, the ΔELA of 8 ka would even be larger, but still lower than the ELA depression of Liu *et al.* (2017). Scherler *et al.* (2010) found contradictory ELA depressions in two close valleys in northern India. The Jaundhar Glacier has a ΔELA of -83 ± 12 m compared to today (2010), whereas Bandarpunch Glacier in the neighbouring valley has a ΔELA of -317 ± 21 m during the Early Holocene (Scherler *et al.*, 2010). When considering the uncertainties due to the ignorance of the tributaries and Lower Barun Glacier, the overestimation due to the debris covered tongue and thus the vaguely defined glacier terminus of the RGI, the ELA depression in the Barun Valley during the Early Holocene is located somewhere in the average between the Jaundhar Glacier and the Bandarpunch Glacier.

6.3 Late Pleistocene

The Late Pleistocene moraine adjoins the Early Holocene moraine and is the outermost and thus oldest moraine of this sequence of lateral moraines next to the Makalu Base Camp. Surface exposure dating of this moraine revealed an age of 12.257 ± 0.751 ka. No sign of erosion was found at the location where the samples were taken. Sati *et al.* (2014) found the same age of 12.2 ± 1.0 ka in the Dunagiri Valley in central Himalaya in India. In Garhwal, India, as well a ~ 11 - 12 ka glacial episode was found by Scherler *et al.* (2010) through surface exposure dating. However, such a moraine does not exist or was not found in the neighbouring Khumbu Valley (Finkel *et al.*, 2003). Due to the large size of this Late Pleistocene moraine in the Barun Valley, it is quite unlikely that such a glacier advance is not present in the southern region of Mount Everest. It is also unlikely that Finkel *et al.* (2003) have overlooked and not dated this moraine. Given the variability of the dating for the other two moraines, it might also be possible that the age of the moraine in the Barun Valley is indeed somewhat younger or older. A younger age would then be closer to the Chhungkung moraine in the Khumbu Valley that has been redated to 10.1 ± 0.4 ka (Owen *et al.*, 2009), whereas an older age could fit to the LGM (e.g if the dated rock has been buried within the moraine for some time). There is also a possibility that the Late Pleistocene in the Khumbu Valley has been eroded due to a high frequency of landsides and natural hazards during monsoon season (Sati *et al.*, 2014). However, since other studies have found similar ages across the Himalayan orogen, we assume that the surface exposure ages of the outermost moraine in the Barun Valley is realistic. Additionally, this period is in the Younger Dryas (YD), which was a global cold phase that left distinct moraines across the European Alps, eastern Himalaya and many other parts of the world (Ivy-Ochs *et al.*, 1996, 1999, 2006, 2008; Hu *et al.*, 2017).

The Late Pleistocene moraine has statistically significant lower Schmidt-Hammer values than the Late Holocene moraine, however to the Early Holocene moraine no statistically difference is found, because their ages are too close together. These results demonstrate a negative correlation between rock hardness and the duration of exposition. Low R-values and thus a weaker or softer rock surface is achieved with a longer exposition to the atmosphere.

ELA depressions and thus glacial extents for the Late Pleistocene have not been calculated in the Barun Valley, since this glacial event was not recorded by Finkel *et al.* (2003) in the Khumbu Valley. As their study provide the input data for this method, the inversed THAR method could not be applied on Barun Glacier. However, the ΔELA during the late Pleistocene would likely be located somewhere between the LGM (-289 m) and the Early Holocene (-132 m). Scherler *et al.* (2010) who analyzed two glaciers in Garhwal, India, estimated an averaged ELA depression of -301 ± 44 m during ~ 11 – 12 ka (Jaundhar Glacier: -190 ± 27 m; Bandarpunch Glacier: -419 ± 10 m). This ELA depression is slightly higher than what we would get in the Barun Valley.

6.4 Last Glacial Maximum

Since the outermost (and thus oldest) moraine has been dated and attributed to the Late Pleistocene, the question arises: Where is the LGM moraine or how large has Barun Glacier been during the LGM? Several possibilities exist: (1) The extent during the LGM was smaller than later extents, which means that its moraines were thrusted or pushed over and are thus now invisible on the surface. This case is rather unlikely, since the LGM moraine represents the maximum extents in many parts of the world and in the Himalayan orogen younger extents than the LGM have never exceeded the LGM extent (Finkel *et al.*, 2003; Owen *et al.*, 2009; Hu *et al.*, 2017; Liu *et al.*, 2017). (2) The glacier had the same extent during the LGM as during the Late Pleistocene and thus the lateral moraines are mixed up and thrusted. This case could be proofed with further surface exposure dating measurements, which might reveal some blocks with Late Pleistocene ages and other blocks with LGM ages. (3) Slightly above the outermost moraine lies another range of hills, which has a moraine-like appearance. This hill could be the LGM moraine (see *Fig. 34*). However, only few meters of this moraine are preserved due to erosion and the steep terrain. Surface exposure dating measurements or OSL measurements on this moraine would clarify the situation. Since the LGM moraine does very prominently exists in the neighbouring Khumbu Valley, it is quite probable that it is or was available in the Barun Valley, too. Therefore, it is supposed that cases (2) or (3) are more likely.

Nevertheless, glacial reconstructions and ELA depressions were calculated in the Barun Valley with the inversed THAR method using data from the Khumbu Valley. During the LGM the Barun Glacier would have had an ELA depression of -289 m (THAR 0.5 with the RGI and referred to the LIA). As well as during other ice ages, this ELA depression is lower compared to other studies conducted in the Himalayan orogen (Hu *et al.*, 2017; Liu *et al.*, 2017). While on Karola Pass the ΔELA was -360 m during the LGM (Liu *et al.*, 2017), in the eastern Himalaya the ELA depression even went down to -690 m (Hu *et al.*, 2017). Due to the above discussed uncertainties and underestimations, the ELA depression of Barun Glacier during the LGM might be slightly larger. This means that the ELA might have been slightly lower than modelled. A ΔELA of -360 m scenario from Liu *et al.* (2017) has been additionally modelled and applied on the Barun Valley, yielding a

slightly larger glacial extent. However, as the convergence zone of Barun Glacier and Lower Barun Glacier is not well constrained, highly erosive and now covered with sediments, it is difficult or impossible to identify a former terminal moraine and thus to correlate a moraine to that glacial stage. Therefore, defining the glacier terminus of the LGM remains speculative and can only be estimated by modelling. The LGM in the Khumbu Valley was very pronounced and occurred 23 ± 3 ka ago (Finkel *et al.*, 2003). Glaciers reached their maximum extent a little earlier in the Rong-buk Valley but are to a greater or lesser extent in sync at 24 – 27 ka (Jilong moraine) and correlate well with the Periche I glacial stage in the Khumbu Valley and with the global LGM (Finkel *et al.*, 2003; Owen *et al.*, 2009). Surface exposure dating measurements on the Tibetan Plateau have revealed similar glacial events at 23.8 ± 4.0 ka in the Nyainqentanglha mountains (Dong *et al.*, 2014) or 21.8 ± 1.3 ka east of Mount Jaggang in the Xainza range (Dong *et al.*, 2018). However, both sites on the TP exhibit older moraines which indicates that glacier extents on the TP during the LGM were smaller than during later stages (Gillespie and Molnar, 1995; Dong *et al.*, 2014, 2018). Yet, whether glacial advances in the Himalayan orogen were in phase with the northern hemisphere ice sheet maximum extent during the LGM is discussed in the next chapter.

6.5 Pre – Last Glacial Maximum

Whether glaciation in the Himalayan and Tibetan orogen was synchronous with the northern hemisphere ice sheets has been in debate since the first absolute dating measurements have revealed older moraine ages than the LGM (Gillespie and Molnar, 1995; Finkel *et al.*, 2003; Owen *et al.*, 2009; Dong *et al.*, 2014, 2018). Glaciers around the Xainza range in central Tibet reached their local maximum extent during MIS 4 (~ 61.9 ± 3.8 ka) and produced subsequent glacial advances during MIS 3 (~ 43.2 ± 2.6 ka and ~ 35.1 ± 2.1 ka) and during the transition MIS 3/2 another glacial re-advance / standstill occurred (~ 29.8 ± 1.8 ka) (Dong *et al.*, 2018). Other [10]Be exposure ages from the Nyainqentanglha mountains confirm asynchronous glacial behaviour on the TP with maximum extents during MIS 3 (18.0 ± 1.6 to 39.9 ± 3.7 ka) (Dong *et al.*, 2014). The increasing number of glacial chronologies suggest that the timing maximum extent across the TP is asynchronous probably due to different local influences of the mid-latitude westerlies and south Asian summer monsoon (Dong *et al.*, 2018). Glaciers in the valleys south of Mount Everest were most extensive during MIS 3 and earlier, and limited during the LGM (i.e. MIS 2) as cosmogenic radionuclide surface exposure dating of moraine successions have revealed (Finkel *et al.*, 2003). They were thus not synchronous with build up phase of the northern hemisphere ice sheets (Finkel *et al.*, 2003). Finkel *et al.* (2003) found two glacial advances older than the LGM, Thyangboche I (older than 30 ka) and Thyangboche II (MIS 3, 35 ± 3 ka), with a single measurement up to 91.75 ± 1.66 ka. Enhanced moisture delivery due to an active south Asian summer monsoon and thus more precipitation as snow in high altitudes is reasoned by Finkel *et al.* (2003) to be responsible for positive mass balances and the existence of glacial advances in the Himalayas albeit an increased insolation and higher temperatures. Similar dating ages have been discovered in the Rongbuk Valley in the northern region of Mount Everest by Owen *et al.* (2009). They have dated the Tingri moraine to > 330 ka and the Dzakar moraine to > 41 ka, which indicates that moraine preservation is well in the sheltered northern slopes of Mt. Everest and glacial advances were broadly synchronous across the entire Everest massif. These findings support the view of Gillespie and Molnar (1995), who

claim that glaciation throughout the Himalayas was not synchronous with the northern hemisphere ice sheets.

However, no such old ages have been found in the Barun Valley despite its proximity to the Everest massif. This could have several reasons: (1) Pre-LGM moraines once existed in the Barun Valley and former glaciations had larger extents than the LGM, but due to the steep terrain, high erosivity during monsoon season and possibly frequent landslides, former glacial remnants were excavated. (2) Pre-LGM moraines exist, but they have not been discovered and dated yet. (3) Glaciation prior to the LGM did not exceed the LGM extent in the Barun Valley. An explanation why glacial advances are so different compared to the neighbouring valley could be found in the local climatic and topographic characteristics and/or being located in the transition zone between the monsoon dominated region and the influence of the westerlies. Khumbu Glacier, Nuptse Glacier and Hillary Glacier have a south /south-west exposition and a high topography in their northern parts, whereas Kyubo Glacier, Ama Dablam Glacier and Rongbuk Glacier are exposed to the north. Barun Glacier on the other hand has its exposition towards the south-east and is surrounded by high peaks towards the west and south, which might have a sheltering effect on the glacier during monsoon. This difference in exposition may explain why during increased moisture availability throughout MIS 3 Barun glacier did not advance as much as other glaciers in the region (Kayastha and Harrison, 2008). Additionally, absolute ELAs are lower than in the Barun Valley, i.e. their sensitivity for climate changes is higher. (4) Glaciation prior to the LGM did not exceed the LGM extent in the Barun Valley, nor did it in the neighbouring valley. Surface exposure ages from Finkel *et al.* (2003) and other studies (Owen *et al.*, 2009) conducted in the Himalayan orogen that exceed the LGM could be wrong, due to pre-exposition or due to a misinterpretation of the landscape, e.g. the presumed moraine or glacial remnants was in fact a landslide or rockfall event. Since no other moraines except the presumed LGM moraine have been spotted in the Barun Valley – neither on site, nor on satellite images or with the hill shade version of the DEM - it is assumed that assumption (2) can be excluded. That the local climate has such a high small-scale variability is possible, but rather unlikely. On the other hand, as we have seen on the moraine deposition rate of Barun Glacier during the late Holocene, while in the Khumbu Valley the glaciers were inert, local climate and accumulation was different at times. Therefore, assumption (3) is possible. But what is more likely is that conditions were very similar in both valleys. This leads us to the assumption that either the pre-LGM moraines have been carried away in the Barun Valley (1) or that incorrect surface exposure dating has been conducted on the moraines in the neighbouring Khumbu Valley (4).

6.6 Glacier Reconstructions

Reconstructions of the Barun Glacier have been done using two different inventories, based on glacier extents from today and the LIA, with different headwall altitude definitions and different THAR values.

Disparities between the RGI and the GGI are mainly located at the tongue and in the headwall definition. Defining the terminus of Barun Glacier is difficult due to its heavy debris cover and results in a 140 m difference of the terminus position between the two inventories for today's extents. Similarly, the steep headwall of Barun Glacier is at different locations and reaches 360 m

higher in GAMDAM2 than in the RGI. Both discrepancies influence ELA estimations and result in differences between 250 – 300 m depending on the THAR value. Single outliers in altitude as for example a small couloir, which is not representative for the whole accumulation area, highly influences the ELA estimations when calculated with the THAR method. Therefore, we conclude that the RGI is the better choice when applying the THAR method.

Although the THAR method is rather simple and does not consider glacier mass balance or hypsometry, it gives a rapid estimation of the ELA and is thus a suitable first approach in regions with poor map coverage and limited glacial input parameters for modelling (Benn and Lehmkuhl, 2000). No consensus prevails about which THAR value is best for debris covered glaciers (Scherler *et al.*, 2010), but such glaciers generally have a larger ablation area and thus a higher THAR of 0.5 - 0.8 (Clark et al., 1994; Benn and Lehmkuhl, 2000; Scherler et al., 2010). Within this thesis THAR values of 0.5, 0.6 and 0.7 have been applied to accommodate for this uncertainty. The cross-comparison of the reconstructed glacial extents with the AAR method reveals AARs between 0.55 and 0.68 for the THAR of 0.5 with the mean altitude of the accumulation basins. In general, clean-ice glaciers have an AAR of 0.58 (Dyurgerov *et al.*, 2009) and debris covered glaciers have lower AARs (Benn and Lehmkuhl, 2000). Scherler *et al.* (2010) disposed an AAR of 0.45, 0.55 and 0.65 which corresponds well with the AARs of the THAR 0.5 and mean headwall altitude definition. Therefore, a THAR of 0.5 and the mean headwall altitude definition is considered as the best method to calculated ELAs in the Barun Valley. These findings fit well with the quality analysis of ELAs by Loibl & Lehmkuhl (2015) using a TRAM of 0.5. Qiao & Yi (2017) adapted the 0.5 value on the THAR, too. The mean elevation of the seven contributing basins in the accumulation area has proven to be more suitable and yields a better AAR than the highest altitude of the whole glacier. The third headwall definition, where the ELA was calculated separately in each of the four major accumulation basins did not work due to intersections of ELAs in the same glacier branch.

The *inversed* THAR method on the other hand has newly been applied within this thesis and is a good first approach to estimate ELA depressions and former glacial extents when no information about former glacier terminus positions are available. However, because of a large variability of ELA depressions within short distance, this method should only be applied with data from glaciers nearby, at best from neighbouring glaciers as in this study. Additionally, only glaciers with similar characteristics and exposition should be used.

Due to the assumed steady-state of Barun Glacier during the LIA, it makes more sense to refer the ELA depressions to the LIA than on to today's extent. Moreover, the time 'today' differs in every publication or study, which makes comparisons more difficult. Additionally, the glacier terminus is difficult to determine for today's glacier, due to its heavily debris-covered tongues and the related difficult identification of dead-ice bodies. Furthermore, LIA moraines are very prominently developed and clearly detectable across the whole Himalayan orogen. Therefore, it is suggested that LIA extents should be used as a reference when estimating ELA depressions. For that reason, it is proposed to digitize LIA extents for the whole orogen for further research and a better comparison between studies.

6.7 Methodological Uncertainties

Surface exposure dating, relative dating techniques and ELA reconstructions as well as glacial extent reconstructions are facing several uncertainties, which strongly influence the result and need to be discussed. Along with uncertainties in the laboratory that accumulate with each step during sample preparation of the ^{10}Be measurements, uncertainties are already introduced during field-work. The height of the horizon is measured only every 10° which has an impact on the calculated topographic shielding. However, related uncertainties are relatively small. A correction for snow cover was made, since a snow pack might be present in this region for at least 6 months of the year, thus we presumed 2 m of snow with a density of 0.3 g cm^{-3}. Other studies, however, assume only a thin snow pack because of an abrasion due to strong winds and thus do not consider a snow correction factor in their calculations (Owen *et al.*, 2009). However, since the lateral moraines next to Makalu Base Camp are protected from strong winds and due to their high altitude, a snow cover correction seems sensible, but might be slightly too large. The dated ages without snow correction are lower (see *Table 3*) but are placed in the same period and thus would not largely influence the result. Over- and underestimation owing to pre-exposure, erosion or exhumation complicate the interpretation of surface exposure ages and can result in large errors (Zech *et al.*, 2009; Owen and Dortch, 2014). Although Murari *et al.* (2014) argue that only around 10% of all glacial boulders in the monsoon influenced climatic regions of the Himalayan orogen exhibit inheritance, and although Zech *et al.* (2009) assert to choose the oldest age of the deposition in the absence of more exposure ages, we interpret one of the dated blocks next to Makalu Base Camp to have suffered pre-exposure and thus chose the younger block as appropriate. Within this study an erosion rate of 0.0001 cm yr^{-1} was assumed. Assuming zero erosion an exposure age of 10 ka would underestimate the true age by 1 – 4 %, whereas an age of 20 ka would be underestimated by 2 – 9 % (Finkel *et al.*, 2003). However, it was aimed to sample blocks with low evidence of erosion to reduce this uncertainty. The time-independent scaling model from Lal (1991) and Stone (2000) was used as it was proposed by Owen and Dortch (2014). However, choosing the right production rate and scaling scheme is under debate and it is not yet proven which one is the most accurate. Additionally, the CRONUS Earth 2.2 calculator with the Heyman (2014) calibration data set compilation was used due to its special adaption to the Tibetan Plateau and Himalayan region. However, extrapolation to high el-evated sites (> 4000 m) should be taken with caution (Owen and Dortch, 2014).

7. CONCLUSION AND OUTLOOK

In summary, TCN surface exposure dating with [10]Be in the Barun Valley helps defining the timing of three glacial advances during the Late Pleistocene (~ 12 ka), Early Holocene (~ 8 ka) and Late Holocene (~ 3 ka). Relative dating methods with the Schmidt-Hammer and weathering rind depths implicate the same chronological sequence. The dating correlates well with other studies conducted in the neighbouring Khumbu Valley and other regions. However, there are at least six further moraines within this sequence of moraines next to Makalu Base Camp that have not been dated but would provide additional information about the landscape/climate history of this part of the Barun Valley. The high moraine deposition rate during this period suggests a sensitive reaction of the glacier to a change in climate. This sensitivity is likely due to the summer-accumulation type of the glacier and a high variability of the monsoon. In contrast to other mid-latitude regions, the higher temperatures during insolation maxima increase the moisture availability and thus the amount of precipitation falling as snow at high altitudes, which results in a positive mass balance and related glacial advances. Due to the high and possibly always ice-free rock walls in the accumulation region of Barun Glacier, a certain debris supply and thus debris cover on the tongue can also be assumed for previous glacial stages. This debris has likely facilitated moraine deposition and is thus partly responsible for the dense time series found here. The absence of a dated LGM moraine or older pre-LGM moraines is somewhat strange compared to the neighbouring Khumbu Valley and not easy to explain. From the various possibilities, the erosion of previous deposits by a glacier that had similar extents later on, is the most reasonable explanation. Dating further moraine ridges (possibly also along the other side of the valley) and additional blocks on the already dated moraines would likely strengthen the results obtained here. Additionally, the moraine-like feature above the outermost moraine needs to be examined in more detail and should be dated as well. In any case, it could be shown that the hypothesis formulated in the beginning is wrong as the dated moraines (incl. the outermost) are all younger than LGM.

Equilibrium line altitudes (ELA) were estimated with data from the neighbouring Khumbu Valley with the inversed THAR method and related glacial extents were reconstructed. ELA values dropped by 289, 132 and 19 m for the LGM, Early Holocene and Late Holocene extents compared to the LIA. A cross-comparison with the AAR method shows that a THAR value of 0.5 applied to the RGI works best. Additionally, using the mean elevation from the seven main accumulation basins to determine the headwall altitude provided the best results. The inversed THAR method provides a useful tool to reconstruct former glacial extents of other glaciers in the Himalayan orogen if similar characteristics predominate (debris covered, exposition, form of accumulation, monsoon influenced, featuring tributaries, etc.). This study could show the former extents of Barun Glacier during the Late Pleistocene and Holocene glaciations. However, methodological uncertainties and its limitations need to be considered. Especially tributaries need to be integrated in future reconstructions for a better representation of additional accumulation areas in previous times. Additionally, further surface exposure dating with [10]Be of other glaciers would provide improved knowledge about the glacial history of this region and its local variability. There is a larger number of other valley glaciers in the region exhibiting dense sequences of moraine deposits outside their LIA maximum extent.

Whereas termini of heavily debris-covered and non-calving glaciers have been about stable over the past decades, elevation changes derived from DEM differencing revealed substantial surface lowering for nearly all glaciers in the Khumbu region, largely independent of the debris cover and also including Barun Glacier (Brun *et al.*, 2017). As the current morphology of the lower tongue of Barun Glacier is also indicating on-going mass loss, it can be safely assumed that glaciers in the region will continue shrinking in the next decades, i.e. their extents are not yet in balance with current climatic conditions and thus of limited use for reconstructions of former glacier extents.

Publisher's note: This Master's Thesis remains neutral with regard to jurisdictional claims in published maps and institutional affiliations.

8. ACKNOWLEDGMENTS

9. LITERATURE

Adams, J., Maslin, M. & Thomas, E. (1999). Sudden climate transitions during the Quaternary. *Progress in Physical Geography: Earth and Environment*, **23**, 1–36.

Ageta, Y. & Higuchi, K. (1984). Estimation of Mass Balance Components of a Summer-Accumulation Type Glacier in the Nepal Himalaya. *Geografiska Annaler: Series A, Physical Geography*, **66**, 249–255.

Azam, M.F., Wagnon, P., Berthier, E., Vincent, C., Fujita, K. & Kargel, J.S. (2018). Review of the status and mass changes of Himalayan-Karakoram glaciers. *Journal of Glaciology*, **64**, 61–74.

Balco, G. (2011). Contributions and unrealized potential contributions of cosmogenic-nuclide exposure dating to glacier chronology, 1990–2010. *Quaternary Science Reviews*, **30**, 3–27.

Balco, G., Stone, J.O., Lifton, N.A. & Dunai, T.J. (2008). A complete and easily accessible means of calculating surface exposure ages or erosion rates from 10Be and 26Al measurements. *Quaternary Geochronology*, **3**, 174–195.

Barr, I.D. & Lovell, H. (2014). A review of topographic controls on moraine distribution. *Geomorphology*, **226**, 44–64.

Benn, D.I. (1992). The genesis and significance of 'hummocky moraine': Evidence from the Isle of Skye, Scotland. *Quaternary Science Reviews*, **11**, 781–799.

Benn, D.I. & Evans, D.J.A. (2013). *Glaciers & Glaciation*. 2nd edn. Routledge.

Benn, D.I. & Lehmkuhl, F. (2000). Mass balance and equilibrium-line altitudes of glaciers in high-mountain environments. *Quaternary International*, **65**, 15–29.

Benn, D.I. & Owen, L.A. (1998). The role of the Indian summer monsoon and the mid-latitude westerlies in Himalayan glaciation: review and speculative discussion. *Journal of the Geological Society*, **155**, 353–363.

Birkeland, P.W. (1973). Arctic and Alpine Research Use of Relative Age-Dating Methods in A Stratigraphic Study of Rock Glacier Deposits, Mt. Sopris, Colorado. *Arctic and Alpine Research*, **5**, 401–416.

Blanckenburg, F. von, Belshaw, N.S. & O'Nions, R.K. (1996). Separation of 9Be and cosmogenic 10Be from environmental materials and SIMS isotope dilution analysis. *Chemical Geology*, **129**, 93–99.

Blanckenburg, F. von, Hewawasam, T. & Kubik, P.W. (2004). Cosmogenic nuclide evidence for low weathering and denudation in the wet, tropical highlands of Sri Lanka. *Journal of Geophysical Research*, **109**, F03008.

Bliss, A., Hock, R. & Radić, V. (2014). Global response of glacier runoff to twenty-first century climate change. *Journal of Geophysical Research: Earth Surface*, **119**, 717–730.

Böhlert, R., Compeer, M., Egli, M., Brandová, D., Maisch, M., Kubik, P.W. & Haeberli, W. (2011a). A Combination of Relative-Numerical Dating Methods Indicates Two High Alpine Rock Glacier Activity Phases After the Glacier Advance of the Younger Dryas. *The Open Geography Journal*, **4**, 115–130.

Böhlert, R., Egli, M., Maisch, M., Brandová, D., Ivy-Ochs, S., Kubik, P.W. & Haeberli, W. (2011b). Application of a combination of dating techniques to reconstruct the Lateglacial and early Holocene landscape history of the Albula region (eastern Switzerland). *Geomorphology*, **127**, 1–13.

Boulton, G.S. (1978). Boulder shapes and grain-size distributions of debris as indicators of transport paths through a glacier and till genesis. *Sedimentology*, **25**, 773–799.

Boulton, G.S. (1986). Push-moraines and glacier-contact fans in marine and terrestrial environments. *Sedimentology*, **33**, 677–698.

Bowen, D.Q. (2009). Last Glacial Maximum. *Encyclopedia of Paleoclimatology and Ancient Environments*.

Brun, F., Berthier, E., Wagnon, P., Kääb, A. & Treichler, D. (2017). A spatially resolved estimate of High Mountain Asia glacier mass balances from 2000 to 2016. *Nature Geoscience*, **10**, 668–673.

Chen, Y., Li, Y., Wang, Y., Zhang, M., Cui, Z., Yi, C. & Liu, G. (2015). Late Quaternary glacial history of the Karlik Range, easternmost Tian Shan, derived from 10Be surface exposure and optically stimulated luminescence datings. *Quaternary Science Reviews*, **115**, 17–27.

Chinn, T.J.H. (1981). Use of Rock Weathering-Rind Thickness for Holocene Absolute Age-Dating in New Zealand. *Arctic and Alpine Research*, **13**, 33–45.

Clark, D.H., Clark, M.M. & Gillespie, A.R. (1994). Debris-Covered Glaciers in the Sierra Nevada, California, and Their Implications for Snowline Reconstructions. *Quaternary Research*, **41**, 139–153.

Clark, P.U. & Mix, A.C. (2002). Ice sheets and sea level of the Last Glacial Maximum. *Quaternary Science Reviews*, **21**, 1–7.

Cogley, J.G. (2016). Glacier shrinkage across High Mountain Asia. *Annals of Glaciology*, **57**, 41–49.

Colin, C., Kissel, C., Blamart, D. & Turpin, L. (1998). Magnetic properties of sediments in the Bay of Bengal and the Andaman Sea: impact of rapid North Atlantic Ocean climatic events on the strength of the Indian monsoon. *Earth and Planetary Science Letters*, **160**, 623–635.

Colman, S.M. (1977). The development of weathering rinds on basalts and andesites and their use as a Quaternary dating method western United States.

Dawson, A.G. (1992). *Ice Age earth : late Quaternary geology and climate*. Routledge.

Desilets, D. & Zreda, M. (2003). Spatial and temporal distribution of secondary cosmic-ray nucleon intensities and applications to in situ cosmogenic dating. *Earth and Planetary Science Letters*, **206**, 21–42.

Desilets, D., Zreda, M. & Prabu, T. (2006). Extended scaling factors for in situ cosmogenic nuclides: New measurements at low latitude. *Earth and Planetary Science Letters*, **246**, 265–276.

Dey, B., Bhanu Kumar, O.S.R.U., Dey, B. & Kumar, O.S.R.U.B. (1982). An Apparent Relationship between Eurasian Spring Snow Cover and the Advance Period of the Indian Summer Monsoon. *Journal of Applied Meteorology*, **21**, 1929–1932.

Dong, G., Xu, X., Zhou, W., Fu, Y., Zhang, L. & Li, M. (2017). Cosmogenic 10Be surface exposure dating and glacier reconstruction for the Last Glacial Maximum in the Quemuqu Valley, western Nyainqentanglha Mountains, south Tibet. *Journal of Quaternary Science*, **32**, 639–652.

Dong, G., Yi, C. & Caffee, M. (2014). 10Be dating of boulders on moraines from the last glacial period in the Nyainqentanglha mountains, Tibet. *Science China Earth Sciences*, **57**, 221–231.

Dong, G., Zhou, W., Yi, C., Fu, Y., Zhang, L. & Li, M. (2018). The timing and cause of glacial activity during the last glacial in central Tibet based on 10Be surface exposure dating east of Mount Jaggang, the Xainza range. *Quaternary Science Reviews*, **186**, 284–297.

Dortch, J.M., Owen, L.A. & Caffee, M.W. (2013). Timing and climatic drivers for glaciation across semi-arid western Himalayan–Tibetan orogen. *Quaternary Science Reviews*, **78**, 188–208.

Dunai, T.. (2001). Influence of secular variation of the geomagnetic field on production rates of in situ produced cosmogenic nuclides. *Earth and Planetary Science Letters*, **193**, 197–212.

Dyurgerov, M., Meier, M.F. & Bahr, D.B. (2009). *A new index of glacier area change: a tool for glacier monitoring*.

Evans, D.J.A. (2013). GLACIAL LANDFORMS | Moraine Forms and Genesis. In: *Encyclopedia of Quaternary Science*. Pp. 769–779. Elsevier.

Evans, D.J.A. & England, J. (1991). High Arctic Thrust Block Moraines. *The Canadian Geographer/Le Géographe canadien*, **35**, 93–97.

Fielding, E., Isacks, B., Barazangi, M. & Duncan, C. (1994). How flat is Tibet? *Geology*, **22**, 163.

Finkel, R.C., Owen, L.A., Barnard, P.L. & Caffee, M.W. (2003). Beryllium-10 dating of Mount Everest moraines indicates a strong monsoon influence and glacial synchroneity throughout the Himalaya. *Geology*, **31**, 561–564.

Frenzel, B. (1959). Vegetations- und Landschaftszonen Nord-Eurasiens während der letzten Eiszeit und während der postglazialen Wärmezeit.

Furbish, D.. & Andrews, J.T. (1984). The Use of Hypsometry to Indicate Long-Term Stability and Response of Valley Glaciers to Changes in Mass Transfer. *Journal of Glaciology*, **30**, 199–211.

Gardelle, J., Berthier, E., Arnaud, Y. & Kääb, A. (2013). Corrigendum to "Region-wide glacier mass balances over the Pamir-Karakoram-Himalaya during 1999&ndash;2011" published in The Cryosphere, 7, 1263&ndash;1286, 2013. *The Cryosphere*, **7**, 1885–1886.

Gebhardt, H., Glaser, R., Radtke, U., Reuber, P. & Meyer, S. (2011). *Geographie physische Geographie und Humangeographie*. 2nd edn. Spektrum, Akad. Verl.

Gellatly, A.F. (1984). The Use of Rock Weathering-Rind Thickness to Redate Moraines. *Arctic and Alpine Research*, **16**, 225–232.

Gillespie, A. & Molnar, P. (1995). Asynchronous maximum advances of mountain and continental glaciers. *Reviews of Geophysics*, **33**, 311.

Gosse, J.C., Klein, J., Evenson, E.B., Lawn, B. & Middleton, R. (1995). Beryllium - 10 Dating of the Duration and Retreat of the Last Pinedale Glacial Sequence. *Annu. Rev. Astron. Astrophys*, **268**, 1329–1333.

Gosse, J.C. & Phillips, F.M. (2001). Terrestrial in situ cosmogenic nuclides: theory and application. *Quaternary Science Reviews*, **20**, 1475–1560.

Gross, G., Kerschner, H. & Patzelt, G. (1976). Methodische Untersuchungen über die Schneegrenze in alpinen Gletschergebieten. *Zeitschrift für Gletscherkunde und Glazialgeologie*, **12**, 223–251.

Grove, J.M. (2001). The Initiation of the "Little Ice Age" in Regions Round the North Atlantic. *Climatic Change*, **48**,

53–82.

Haeberli, W., Bösch, H., Scherler, K. & Wallén, C.C. (1988). World Glacier Inventory Status 1988: A contribution to the Global Environment Monitoring System (GEMS) and the International Hydrological Programme Compiled by the World Glacier Monitoring Service Edited by.

Hahn, D.G., Shukla, J., Hahn, D.G. & Shukla, J. (1976). An Apparent Relationship between Eurasian Snow Cover and Indian Monsoon Rainfall. *Journal of the Atmospheric Sciences*, **33**, 2461–2462.

Haritashya, U., Kargel, J., Shugar, D., Leonard, G., Strattman, K., Watson, C., Shean, D., Harrison, S., Mandli, K., Regmi, D., Haritashya, U.K., Kargel, J.S., Shugar, D.H., Leonard, G.J., Strattman, K., Watson, C.S., Shean, D., Harrison, S., Mandli, K.T. & Regmi, D. (2018). Evolution and Controls of Large Glacial Lakes in the Nepal Himalaya. *Remote Sensing*, **10**, 798.

Hewitt, K. (2009). Rock avalanches that travel onto glaciers and related developments, Karakoram Himalaya, Inner Asia. *Geomorphology*, **103**, 66–79.

Heyman, J. (2014). Paleoglaciation of the Tibetan Plateau and surrounding mountains based on exposure ages and ELA depression estimates. *Quaternary Science Reviews*, **91**, 30–41.

Heyman, J., Applegate, P.J., Blomdin, R., Gribenski, N., Harbor, J.M. & Stroeven, A.P. (2016). Boulder height – exposure age relationships from a global glacial 10Be compilation. *Quaternary Geochronology*, **34**, 1–11.

Heyman, J., Stroeven, A.P., Harbor, J.M. & Caffee, M.W. (2011). Too young or too old: Evaluating cosmogenic exposure dating based on an analysis of compiled boulder exposure ages. *Earth and Planetary Science Letters*, **302**, 71–80.

Higuchi, K. & Inoue, J. (1982). *Characteristics of precipitation during the monsoon season in high-mountain areas of the Nepal Himalaya**. IAHS Publ.

Hoey, T.B. (2004). *The Size of Sedimentary Particles. In: A practical guide to the study of glacial sediments*. Arnold.

Hooke, R.L. (2005). *Principles of glacier mechanics*. Cambridge University Press.

Hu, G., Yi, C., Zhang, J., Dong, G., Liu, J., Xu, X. & Jiang, T. (2017). Extensive glacial advances during the Last Glacial Maximum near the eastern Himalayan syntaxis. *Quaternary International*, **443**, 1–12.

Hughes, P.D., Gibbard, P.L. & Ehlers, J. (2013). Timing of glaciation during the last glacial cycle: evaluating the concept of a global 'Last Glacial Maximum' (LGM). *Earth-Science Reviews*, **125**, 171–198.

Huss, M., Bookhagen, B., Huggel, C., Jacobsen, D., Bradley, R.S., Clague, J.J., Vuille, M., Buytaert, W., Cayan, D.R., Greenwood, G., Mark, B.G., Milner, A.M., Weingartner, R. & Winder, M. (2017). Toward mountains without permanent snow and ice.

Huss, M. & Hock, R. (2018). Global-scale hydrological response to future glacier mass loss. *Nature Climate Change*, **8**, 135–140.

Immerzeel, W.W., Beek, L.P.H. van & Bierkens, M.F.P. (2010). Climate change will affect the Asian water towers. *Science (New York, N.Y.)*, **328**, 1382–5.

Immerzeel, W.W., Pellicciotti, F. & Bierkens, M.F.P. (2013). Rising river flows throughout the twenty-first century in two Himalayan glacierized watersheds. *Nature Geoscience*, **6**, 742–745.

Inoue, J. (1978). Gales over the Nepal Himalayas in 1976. *Journal of the Japanese Society of Snow and Ice*, **40**, 56–59.

IPCC. (2007). *Climate change 2007 : impacts, adaptation and vulnerability : contribution of Working Group II to the fourth assessment report of the Intergovernmental Panel on Climate Change*. Cambridge University Press.

Ivy-Ochs, S., Kerschner, H., Reuther, A., Maisch, M., Sailer, R., Schaefer, J., Kubik, P.W., Synal, H. & Schlüchter, C. (2006). The timing of glacier advances in the northern European Alps based on surface exposure dating with comogenic Be-10, Al-26, Cl-36 and Ne-21, 146.

Ivy-Ochs, S., Kerschner, H., Reuther, A., Preusser, F., Heine, K., Maisch, M., Kubik, P.W. & Schlüchter, C. (2008). Chronology of the last glacial cycle in the European Alps. *Journal of Quaternary Science*, **23**, 559–573.

Ivy-ochs, S. & Kober, F. (2008). Surface exposure dating with cosmogenic nuclides. *Quaternary Science Journal*, **57**, 157–189.

Ivy-Ochs, S., Schluchter, C., Kubik, P.W. & Denton, G.H. (1999). Moraine Exposure Dates Imply Synchronous Younger Dryas Glacier Advances in the European Alps and in the Southern Alps of New Zealand. *Geografiska Annaler, Series A: Physical Geography*, **81**, 313–323.

Ivy-Ochs, S., Schlüchter, C., Kubik, P.W., Synal, H.A., Beer, J. & Kerschner, H. (1996). The exposure age of an Egesen Moraine at Julier Pass, Switzerland measured with the cosmogenic radionuclides Be-10, Al-26 and Cl-36. *Eclogae Geologicae Helvetiae*, 1049–1063.

Kaser, G., Grosshauser, M. & Marzeion, B. (2010). Contribution potential of glaciers to water availability in different climate regimes. *Proceedings of the National Academy of Sciences of the United States of America*, **107**, 20223–7.

Kayastha, R.B. & Harrison, P.S. (2008). Changes of the equilibrium-line altitude since the Little Ice Age in the Nepalese Himalaya. *Annals of Glaciology*, **48**, 93–99.

Klute, F. (1930). Verschiebung der Klimagebiete der letzten Eiszeit. *Petermanns mit Ergänz.*, 166–182.

Kohl, C.. & Nishiizumi, K. (1992). Chemical isolation of quartz for measurement of in-situ -produced cosmogenic nuclides. *Geochimica et Cosmochimica Acta*, **56**, 3583–3587.

Korschinek, G., Bergmaier, A., Faestermann, T., Gerstmann, U.C., Knie, K., Rugel, G., Wallner, A., Dillmann, I., Dollinger, G., Lierse Von Gostomski, C., Kossert, K., Maiti, M., Poutivtsev, M. & Remmert, A. (2010). A new value for the half-life of 10 Be by Heavy-Ion Elastic Recoil Detection and liquid scintillation counting.

Kuhle, M. (1985). Ein subtropisches Inlandeis als Eiszeitauslöser. Südtibet- und Mt. Everest-Expedition 1984. *Georgia Augusta*, **1985**, 35–51.

Kuhle, M. (2011). The High Glacial (Last Ice Age and Last Glacial Maximum) Ice Cover of High and Central Asia, with a Critical Review of Some Recent OSL and TCN Dates. *Developments in Quaternary Sciences*, **15**, 943–965.

Lal, D. (1991). Cosmic ray labeling of erosion surfaces: in situ nuclide production rates and erosion models. *Earth and Planetary Science Letters*, **104**, 424–439.

Laustela, M., Egli, M., Frauenfelder, R., Kääb, A., Maisch, M. & Haeberli, W. (2003). Weathering rind measurements and relative age dating of rockglacier surfaces in crystalline regions of the Eastern Swiss Alps. *Permafrost*.

Lehmkuhl, F. (1998a). Extent and Spatial Distribution of Pleistocene Glaciations in Eastern Tibet. *Quaternary International*, **45**, 123–134.

Lehmkuhl, F. (1998b). Quaternary glaciations in central and western Mongolia. *Mountain Glaciation*, 153–167.

Li, J., Li, B. & Cui, Z. (1991). Quaternary glacial distribution map of Qinghai-Xizang (Tibet) plateau. *Quaternary Glacier and Environment Research Center, Lanzhou University*.

Li, Y., Liu, G., Chen, Y., Li, Y., Harbor, J., Stroeven, A.P., Caffee, M., Zhang, M., Li, C. & Cui, Z. (2014). Timing and extent of Quaternary glaciations in the Tianger Range, eastern Tian Shan, China, investigated using 10Be surface exposure dating. *Quaternary Science Reviews*, **98**, 7–23.

Lichtenecker, N. (1938). Die gegenwartige und die eiszeit liche Schneegrenze in den Ostalpen. *Verhandlungsband der III. Internationalen Quartarkonferenz, Wien*, **1936**, 141–147.

Lifton, N.A., Bieber, J.W., Clem, J.M., Duldig, M.L., Evenson, P., Humble, J.E. & Pyle, R. (2005). Addressing solar modulation and long-term uncertainties in scaling secondary cosmic rays for in situ cosmogenic nuclide applications. *Earth and Planetary Science Letters*, **239**, 140–161.

Liu, J., Yi, C., Li, Y., Bi, W., Zhang, Q. & Hu, G. (2017). Glacial fluctuations around the Karola Pass, eastern Lhagoi

Kangri Range, since the Last Glacial Maximum. *Journal of Quaternary Science*, **32**, 516–527.

Loibl, D.M. & Lehmkuhl, F. (2015). Glaciers and equilibrium line altitudes of the eastern Nyainqêntanglha Range, SE Tibet. *Journal of Maps*, **11**, 575–588.

Louis, H. (1955). *Schneegrenze und Schneegrenzbestimmung*. Geographisches Taschenbuch.

Lutz, A.F., Immerzeel, W.W., Shrestha, A.B. & Bierkens, M.F.P. (2014). Consistent increase in High Asia's runoff due to increasing glacier melt and precipitation. *Nature Climate Change*, **4**, 587–592.

Mann, D.H., Sletten, R.S. & Reanier, R.E. (1996). Quaternary glaciations of the Rongbuk Valley, Tibet. *Journal of Quaternary Science*, **11**, 267–280.

Maussion, F., Scherer, D., Mölg, T., Collier, E., Curio, J., Finkelnburg, R., Maussion, F., Scherer, D., Mölg, T., Collier, E., Curio, J. & Finkelnburg, R. (2014). Precipitation Seasonality and Variability over the Tibetan Plateau as Resolved by the High Asia Reanalysis*. *Journal of Climate*, **27**, 1910–1927.

McCarroll, D. (1987). The Schmidt hammer in geomorphology : five sources of instrument error. *British Geomorphological Research Group Technical Bulletin*, **36**, 16–27.

Meierding, T.C. (1982). Late Pleistocene Glacial Equilibrium-Line Altitudes in the Colorado Front Range: A Comparison of Methods. *Quaternary Research*, **18**, 289–310.

Miehe, G. (2004). *Gebirge der Erde: Landschaft, Klima, Pflanzenwelt*. Germany: Ulmer.

Muller, F. (1980). Present and late Pleistocene equilibrium line altitudes in the Mt. Everest region - An application of the glacier inventory. *Proceedings of the Riederalp Workshop*, **126**, 75–94.

Murakami, T. (1987). Effects of the Tibetan Plateau. *Monsoon Meteorology*, 235–270.

Murari, M.K., Owen, L.A., Dortch, J.M., Caffee, M.W., Dietsch, C., Fuchs, M., Haneberg, W.C., Sharma, M.C. & Townsend-Small, A. (2014). Timing and climatic drivers for glaciation across monsoon-influenced regions of the Himalayan–Tibetan orogen. *Quaternary Science Reviews*, **88**, 159–182.

Nishiizumi, K., Imamura, M., Caffee, M.W., Southon, J.R., Finkel, R.C. & McAninch, J. (2007). Absolute calibration of 10Be AMS standards. *Nuclear Instruments and Methods in Physics Research Section B: Beam Interactions with Materials and Atoms*, **258**, 403–413.

Nuimura, T., Sakai, A., Taniguchi, K., Nagai, H., Lamsal, D., Tsutaki, S., Kozawa, A., Hoshina, Y., Takenaka, S., Omiya, S., Tsunematsu, K., Tshering, P. & Fujita, K. (2015). The GAMDAM glacier inventory: a quality-controlled inventory of Asian glaciers. *The Cryosphere*, **9**, 849–864.

Oerlemans, J. (2001). *Glaciers and Climate Change*. 1st edn. A.A. Balkema Publishers.

Oerlemans, J. (2005). Extracting a Climate Signal from 169 Glacier Records.

Ogilvie, A.E.J. & Jónsson, T. (2001). "Little Ice Age" Research: A Perspective from Iceland. *Climatic Change*, **48**, 9–52.

Oguchi, C.T. (2001). Formation of weathering rinds on andesite. *Earth Surface Processes and Landforms*, **26**, 847–858.

Owen, L.A., Caffee, M.W., Finkel, R.C. & Seong, Y.B. (2008). Quaternary glaciation of the Himalayan-Tibetan orogen. *Journal of Quaternary Science*, **23**, 513–531.

Owen, L.A. & Dortch, J.M. (2014). Nature and timing of Quaternary glaciation in the Himalayan–Tibetan orogen. *Quaternary Science Reviews*, **88**, 14–54.

Owen, L.A., Finkel, R.C. & Caffee, M.W. (2002a). A note on the extent of glaciation throughout the Himalaya during the global Last Glacial Maximum. *Quaternary Science Reviews*, **21**, 147–157.

Owen, L.A., Finkel, R.C., Caffee, M.W. & Gualtieri, L. (2002b). Timing of multiple late Quaternary glaciations in the Hunza Valley, Karakoram Mountains, northern Pakistan: Defined by cosmogenic radionuclide dating of

moraines. *Geological Society of America Bulletin*, **114**, 593–604.

Owen, L.A., Robinson, R., Benn, D.I., Finkel, R.C., Davis, N.K., Yi, C., Putkonen, J., Li, D. & Murray, A.S. (2009). Quaternary glaciation of Mount Everest. *Quaternary Science Reviews*, **28**, 1412–1433.

Penck, A. & Brückner, E. (1901). *Die Alpen im Eiszeitalter*. Tauchnitz: Leipzig.

Pfeffer, W.T., Arendt, A.A., Bliss, A., Bolch, T., Cogley, J.G., Gardner, A.S., Hagen, J.-O., Hock, R., Kaser, G., Kienholz, C., Miles, E.S., Moholdt, G., Mölg, N., Paul, F., Radić, V., Rastner, P., Raup, B.H., Rich, J., Sharp, M.J. & Consortium, T.R. (2014). The Randolph Glacier Inventory: a globally complete inventory of glaciers. *Journal of Glaciology*, **60**, 537–552.

Phillips, W.M., Sloan, V.F., Shroder, J.F., Sharma, P., Clarke, M.L. & Rendell, H.M. (2000). Asynchronous glaciation at Nanga Parbat, northwestern Himalaya Mountains, Pakistan. *Geology*, **28**, 431.

Porter, S.C. (1983). Late Quaternary Environments of the United States. *Minneapolis*, 71–111.

Porter, S.C., Pierce, K.L. & Hamilton, T.D. (1983). Late Pleistocene glaciation in the western United States.

Prell, W.L. & Kutzbach, J.E. (1987). Monsoon variability over the past 150,000 years. *Journal of Geophysical Research*, **92**, 8411.

Prell, W.L. & Kutzbach, J.E. (1992). Sensitivity of the Indian monsoon to forcing parameters and implications for its evolution. *Nature 1992 360:6405*, **360**, 647.

Price, R.J. (1970). Moraines at Fjallsjökull, Iceland. *Arctic, Antarctic and Alpine Research*, **2**, 27–42.

Putkonen, J. & Swanson, T. (2003). Accuracy of cosmogenic ages for moraines. *Quaternary Research*, **59**, 255–261.

Qiao, B. & Yi, C. (2017). Reconstruction of Little Ice Age glacier area and equilibrium line attitudes in the central and western Himalaya. *Quaternary International*, **444**, 65–75.

Rabatel, A., Francou, B., Jomelli, V., Naveau, P. & Grancher, D. (2008). A chronology of the Little Ice Age in the tropical Andes of Bolivia (16°S) and its implications for climate reconstruction. *Quaternary Research*, **70**, 198–212.

Radić, V. & Hock, R. (2014). Glaciers in the Earth's Hydrological Cycle: Assessments of Glacier Mass and Runoff Changes on Global and Regional Scales. *Surveys in Geophysics*, **35**, 813–837.

Raper, S.C.B. & Braithwaite, R.J. (2009). Glacier volume response time and its links to climate and topography based on a conceptual model of glacier hypsometry. *The Cryosphere*, **3**, 183–194.

Raup, B., Racoviteanu, A., Khalsa, S.J.S., Helm, C., Armstrong, R. & Arnaud, Y. (2007). The GLIMS geospatial glacier database: A new tool for studying glacier change. *Global and Planetary Change*, **56**, 101–110.

Rupper, S., Roe, G. & Gillespie, A. (2009). Spatial patterns of Holocene glacier advance and retreat in Central Asia. *Quaternary Research*, **72**, 337–346.

Sakai, A. (2018). Brief Communication: Updated GAMDAM Glacier Inventory over the High Mountain Asia. *The Cryosphere Discussions*, 1–12.

Sati, S.P., Ali, S.N., Rana, N., Bhattacharya, F., Bhushan, R., Shukla, A.D., Sundriyal, Y. & Juyal, N. (2014). Timing and extent of Holocene glaciations in the monsoon dominated Dunagiri valley (Bangni glacier), Central Himalaya, India. *Journal of Asian Earth Sciences*, **91**, 125–136.

Scherler, D., Bookhagen, B., Strecker, M.R., Blanckenburg, F. von & Rood, D. (2010). Timing and extent of late Quaternary glaciation in the western Himalaya constrained by 10Be moraine dating in Garhwal, India. *Quaternary Science Reviews*, **29**, 815–831.

Scherler, D., Wulf, H. & Gorelick, N. (2018). Global Assessment of Supraglacial Debris-Cover Extents. *Geophysical Research Letters*, **45**, 11,798-11,805.

Schlüchter, C. (2004). *The Swiss glacial record - a schematic summery*. Elsevier.

Schmidt, E. (1951). A non-destructive concrete tester. *Concrete*, **59**, 34–35.

Sharma, M.C. & Owen, L.A. (1996). Quaternary Glacial History of NW Garhwal, Central Himalayas. *Quaternary Science Review*, **15**, 335–365.

Shi, Y., Zheng, B. & Li, S. (1992). *Last Glaciation and Maximum Glaciation in the Qinghai-Xizang (Tibet) Plateau: A Controversy to M.Kuhle's Ice Sheet Hypothesis*. Science Press.

Shindell, D.T. (2009). Little Ice Age. *Encyclopedia of Paleoclimatology and Ancient Environments*.

Shiraiwa, T., Watanabe, T. & Shiraiwa, T.A. (1991). Late Quaternary Glacial Fluctuations in the Langtang Valley, Nepal Himalaya, Reconstructed by Relative Dating Methods. *Arctic , Antarctic and Alpine Research*, **23**, 404–416.

Shiyin, L., Wenxin, S., Yongping, S. & Gang, L. (2003). Glacier changes since the Little Ice Age maximum in the western Qilian Shan, northwest China, and consequences of glacier runoff for water supply. *Journal of Glaciology*, **49**, 117–124.

Sinha, A., Berkelhammer, M., Stott, L., Mudelsee, M., Cheng, H. & Biswas, J. (2011). The leading mode of Indian Summer Monsoon precipitation variability during the last millennium. *Geophysical Research Letters*, **38**.

Soman, M.K. & Slingo, J. (1997). Sensitivity of the asian summer monsoon to aspects of sea-surface-temperature anomalies in the tropical pacific ocean. *Quarterly Journal of the Royal Meteorological Society*, **123**, 309–336.

Stone, J.O. (2000). Air pressure and cosmogenic isotope production. *Journal of Geophysical Research: Solid Earth*, **105**, 23753–23759.

Su, Z. & Shi, Y. (2002). Response of monsoonal temperate glaciers to global warming since the Little Ice Age. *Quaternary International*, **97**–**98**, 123–131.

Sumner, P. & Nel, W. (2002). The effect of rock moisture on Schmidt hammer rebound: tests on rock samples from Marion Island and South Africa. *Earth Surface Processes and Landforms*, **27**, 1137–1142.

Tomkins, M.D., Dortch, J.M. & Hughes, P.D. (2016). Schmidt Hammer exposure dating (SHED): Establishment and implications for the retreat of the last British Ice Sheet. *Quaternary Geochronology*, **33**, 46–60.

Tuniz, C. (Claudio). (1998). *Accelerator mass spectrometry : ultrasensitive analysis for global science*. CRC Press.

Viles, H., Goudie, A., Grab, S. & Lalley, J. (2011). The use of the Schmidt Hammer and Equotip for rock hardness assessment in geomorphology and heritage science: a comparative analysis. *Earth Surface Processes and Landforms*, **36**, 320–333.

Wagner, G.A. (1998). Cosmogenic Nuclides. Pp. 113–194. Springer, Berlin, Heidelberg.

Wang, Y.J., Cheng, H., Edwards, R.L., An, Z.S., Wu, J.Y., Shen, C.C. & Dorale, J.A. (2001). A high-resolution absolute-dated late Pleistocene Monsoon record from Hulu Cave, China. *Science (New York, N.Y.)*, **294**, 2345–8.

Weissert, H. & Stössel, I. (2015). *Der Ozean im Gebirge*. 3rd edn. Vdf Hochschulverlag.

Winkler, S. (2005). New Zealand Journal of Geology and Geophysics The Schmidt hammer as a relative-age dating technique: Potential and limitations of its application on Holocene moraines in Mt Cook National Park, Southern Alps, New Zealand The Schmidt hammer as a relative-ag. *New Zealand Journal of Geology and Geophysics*, **48**, 105–116.

Yao, T., Shi, Y. & Thompson, L.G. (1997). High resolution record of paleoclimate since the Little Ice Age from the Tibetan ice cores. *Quaternary International*, **37**, 19–23.

Yasunari, T. & Inoue, J. (1978). Characteristics of Monsoonal Precipitation around Peaks and Ridges in Shorong and Khumbu Himal. *Journal of the Japanese Society of Snow and Ice*, **40**, 26–32.

Yin, A. & Harrison, T.M. (2000). Geologic Evolution of the Himalayan-Tibetan Orogen. *Annual Review of Earth and Planetary Sciences*, **28**, 211–280.

Zech, R., Glaser, B., Sosin, P., Kubik, P.W. & Zech, W. (2005). Evidence for long-lasting landform surface instability on hummocky moraines in the Pamir Mountains (Tajikistan) from 10Be surface exposure dating. *Earth and Planetary Science Letters*, **237**, 453–461.

Zech, R., Röhringer, I., Sosin, P., Kabgov, H., Merchel, S., Akhmadaliev, S. & Zech, W. (2013). Late Pleistocene glaciations in the Gissar Range, Tajikistan, based on 10Be surface exposure dating. *Palaeogeography, Palaeoclimatology, Palaeoecology*, **369**, 253–261.

Zech, R., Zech, M., Kubik, P.W., Kharki, K. & Zech, W. (2009). Deglaciation and landscape history around Annapurna, Nepal, based on10Be surface exposure dating. *Quaternary Science Reviews*, **28**, 1106–1118.

10. PERSONAL DECLARATION

I hereby declare that the material contained in this thesis is my own original work. And quotation or paraphrase in this thesis from the published or unpublished work of another individual or institution has been duly acknowledged. I have not submitted this thesis, or any part of it, previously to any institution for assessment purposes.

Buonas, 30.04.2019, Laura Büchler

11. APPENDIX
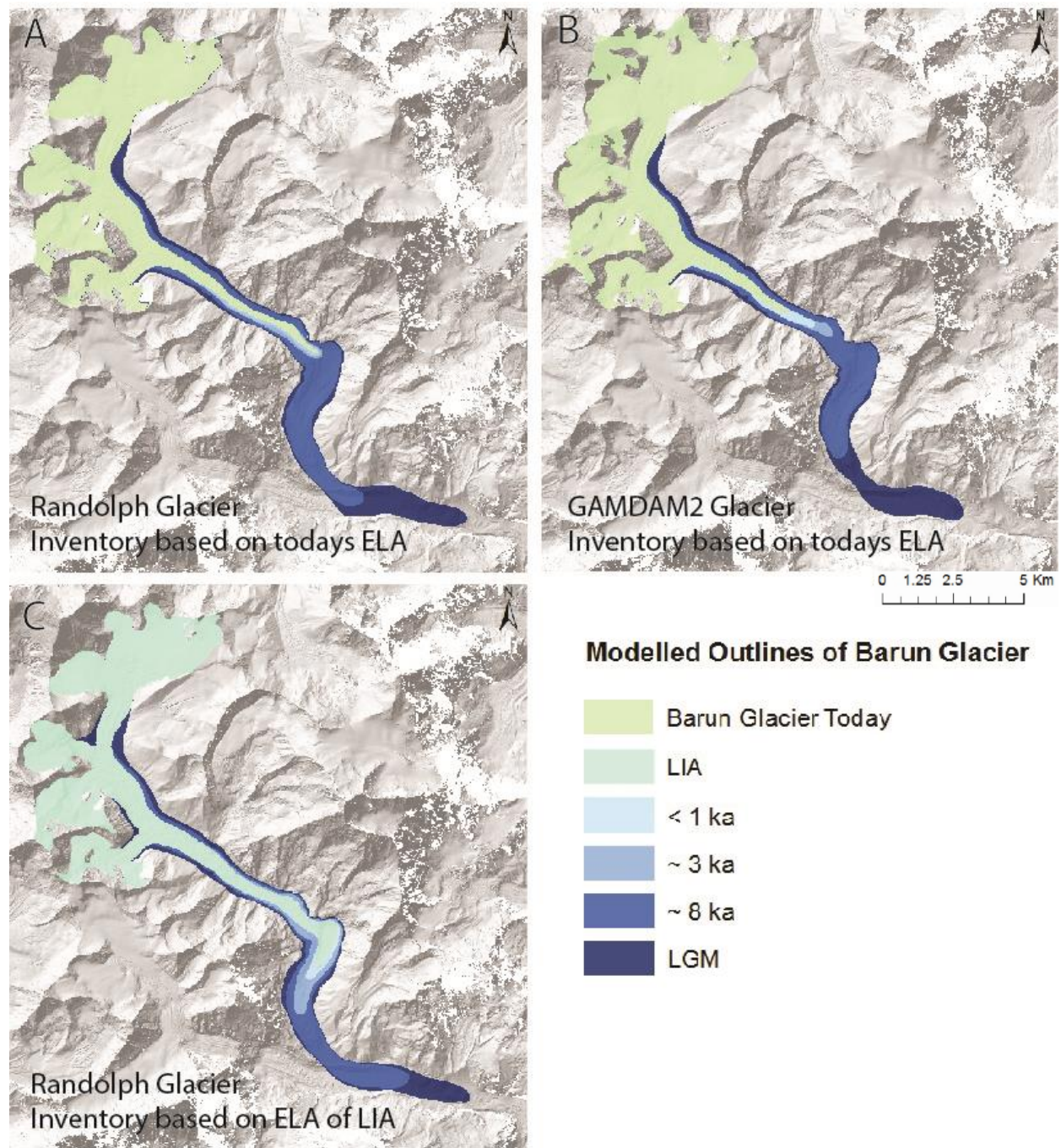
Fig. 33: Reconstructed glacial extents of Barun Glacier with two different inventories and based on the ELA of today and the ELA of the LIA.

Table 9: Calculated ELAs and former glacier terminus of Barun Glacier with the headwall altitude estimated separate for each basin.

		LIA	3ka	Δ ELA [m]	8ka	Δ ELA [m]	LGM	Δ ELA [m]
Barun Glacier								
	Inventory Date	RGI						
	Area [km2]	32.2						
	Method	separate for each basin						
Headwall	Basin 1	6905	6905		6905		6905	
	Basin 2	7056	7056		7056		7056	
	Basin 3	6316	6316		6316		6316	
	Basin 4	6317	6317		6317		6317	
	Toe [m]	4801	4763		4537		4222	
	Slope [°]							
	Aspect [°]	122						
	Lmax [km]							
ELA [m]								
Basin 1	THAR 0.5	5853	5834	-19	5721	-132	5563	-289
Basin 2	THAR 0.5	5929	5909	-19	5797	-132	5639	-289
Basin 3	THAR 0.5	5558	5539	-19	5427	-132	5269	-289
Basin 4	THAR 0.5	5559	5540	-19	5427	-132	5269	-289
Basin 1	THAR 0.6	6063	6048	-15	5958	-106	5832	-232
Basin 2	THAR 0.6	6154	6139	-15	6049	-106	5923	-232
Basin 3	THAR 0.6	5710	5695	-15	5604	-106	5478	-232
Basin 4	THAR 0.6	5710	5695	-15	5605	-106	5479	-232
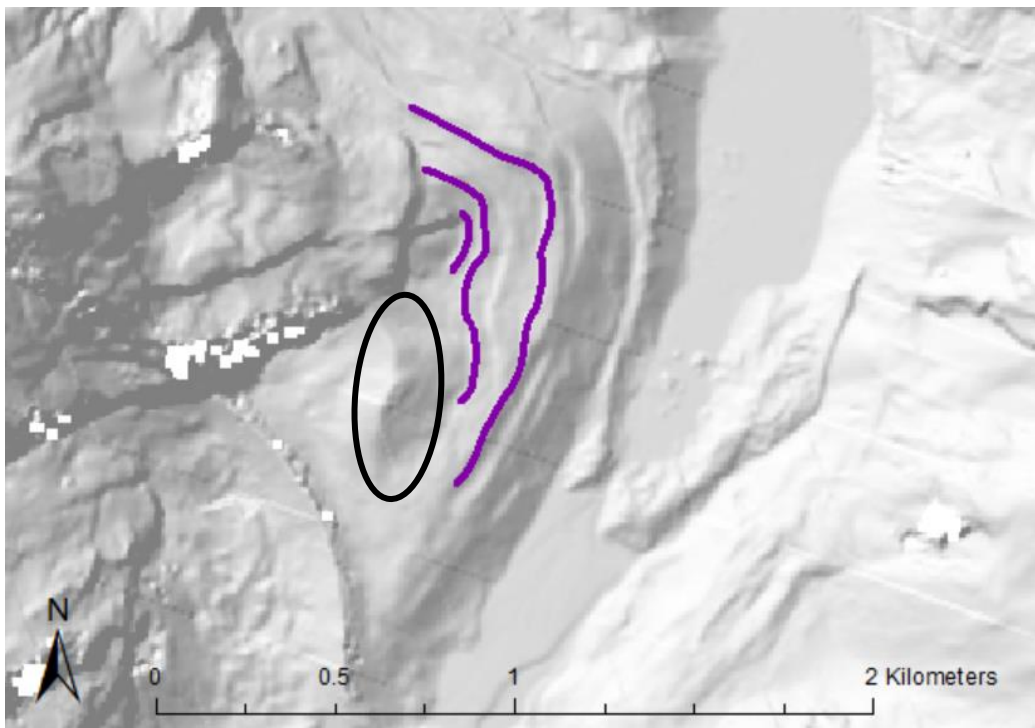
Fig. 34: Interesting feature, possibly the LGM moraine (black); purple : dated moraines.

Table 10: Calculated ELAs and ΔELAs from the Khumbu Valley with the THAR method (RGI + GAMDAM2) based on today.

	Today RGI	Today GAMDAM2	<1ka RGI	<1ka GAMDAM2	<1ka RGI Δ ELA	<1ka GAMDAM2 Δ ELA	3ka RGI	3ka GAMDAM2	3ka RGI Δ ELA	3ka GAMDAM2 Δ ELA	8ka RGI	8ka GAMDAM2	8ka RGI Δ ELA	8ka GAMDAM2 Δ ELA	LGM RGI	LGM GAMDAM2	LGM RGI Δ ELA	LGM GAMDAM2 Δ ELA
Barun Glacier																		
Date	36829	36277																
Area [km2]	30	35	31	35			31	36			40	44			47	52		
Headwall [m]	7056	7417	7056	7417			7056	7417			7056	7417			7056	7417		
Toe [m]	4875	5016	4857	4995			4834	4976			4597	4734			4272	4411		
Slope [°]	14																	
Aspect [°]	122	122																
Lmax [km]	14																	
ELA [m]																		
THAR 0.5	5965	6216	5957	6206	-9	-10	5945	6196	-20	-20	5827	6075	-139	-141	5664	5914	-301	-302
THAR 0.6	6184	6456	6177	6448	-7	-8	6167	6440	-16	-16	6073	6344	-111	-113	5943	6215	-241	-242
THAR 0.7	6402	6696	6396	6690	-5	-6	6390	6684	-12	-12	6318	6612	-83	-85	6221	6515	-181	-181
Lower Barun Glacier																		
Date	36829	36277																
Area [km2]	24	26																
Headwall [m]	6710	7196																
Toe [m]	4488	4488																
Slope [°]	13																	
Aspect [°]	104	104																
Lmax [km]	14																	
ELA [m]																		
THAR 0.5	5599	5842																
THAR 0.6	5821	6112																
THAR 0.7	6043	6383																
Ama Dablam Glacier																		
Date	36829	36277																
Area [km2]	5	5																
Headwall [m]	5873	6362	5873	6362							5873	6362						
Toe [m]	4768	4776	4766	4766							4514	4514						
Slope [°]	19																	
Aspect [°]	338	338																
Lmax [km]	4																	
ELA [m]																		
THAR 0.5	5320	5569	5319	5564	-1	-5					5193	5438	-127	-131				
THAR 0.6	5431	5728	5430	5724	-1	-4					5329	5623	-101	-105				
THAR 0.7	5541	5886	5541	5883	0	-3					5465	5807	-76	-79				
Nuptse Glacier																		
Date	37261	36277																
Area [km2]	4	3																
Headwall [m]	5786	5814	5786	5814			5786	5814										
Toe [m]	4958	4958	4958	4958			4929	4929										
Slope [°]	12																	
Aspect [°]	199	199																
Lmax [km]	6																	
ELA [m]																		
THAR 0.5	5372	5386	5372	5386	0	0	5358	5372	-15	-15								
THAR 0.6	5455	5472	5455	5472	0	0	5443	5460	-12	-12								
THAR 0.7	5538	5557	5537	5557	0	0	5529	5549	-9	-9								

Hillary Glacier																	
Date	37261	36277															
Area [km2]	3	3															
Headwall [m]	7217	7162					7217	7162										
Toe [m]	4941	4941					4890	4890										
Slope [°]	22																	
Aspect [°]	196	196																
Lmax [km]	4																	
ELA [m]																		
THAR 0.5	6079	6051					6053	6026	-26	-26								
THAR 0.6	6306	6274					6286	6253	-20	-20								
THAR 0.7	6534	6496					6518	6480	-15	-15								
Kyubo Glacier																	
Date	37181	36277															
Area [km2]	1	0															
Headwall [m]	5096	5989									5096	5989			5096	5989		
Toe [m]	4748	4752									4631	4631			4229	4229		
Slope [°]	14																	
Aspect [°]	307	307																
Lmax [km]	2																	
ELA [m]																		
THAR 0.5	4922	5371									4863	5310	-58	-61	4662	5109	-259	-262
THAR 0.6	4956	5494									4910	5446	-47	-48	4749	5285	-207	-209
THAR 0.7	4991	5618									4956	5582	-35	-36	4836	5461	-156	-157
Khumbu Glacier																	
Date	37261	36277															
Area [km2]	32	40															
Headwall [m]	7832	7999	7832	7999							7832	7999			7832	7999		
Toe [m]	4881	4881	4831	4831							4419	4419			4195	4195		
Slope [°]	18																	
Aspect [°]	262	262																
Lmax [km]	15																	
ELA [m]																		
THAR 0.5	6356	6440	6331	6415	-25	-25					6125	6209	-231	-231	6013	6097	-343	-343
THAR 0.6	6651	6752	6631	6732	-20	-20					6467	6567	-185	-185	6377	6478	-274	-274
THAR 0.7	6946	7064	6931	7049	-15	-15					6808	6925	-139	-139	6741	6858	-206	-206
Mean ELA depression THAR 0.5					-9	-10			-20	-20			-139	-141			-301	-302
THAR 0.6					-7	-8			-16	-16			-111	-113			-241	-242
THAR 0.7					-5	-6			-12	-12			-83	-85			-181	-181

Table 11: Cronus Earth input data.

1. Datierung

Sample name	Latitude (DD)	Longitude (DD)	Elevation (m)	Elv/pressure flag	Thickness (cm)	Density (g cm-2)	Shielding correction	Erosion rate (cm yr-1)	[Be-10] atoms g-1	+/- atoms g-1	Be AMS standard	[Al-26] atoms g-1	+/- atoms g-1	Al AMS standard
OHNE SCHNEEFAKTOR														
MAKA1A	27.8424	87.07313	5026	std	2	2.7	0.932	0.0001	625716.573	17197.0184	07KNSTD	0.000E+00	0.000E+00	KNSTD
MAKA2A	27.84275	87.07393	5034	std	2.5	2.7	0.959687	0.0001	433871.919	24819.256	07KNSTD	0.000E+00	0.000E+00	KNSTD
MAKA2B	27.84288	87.07372	5040	std	2.25	2.7	0.963839	0.0001	451397.196	12413.0695	07KNSTD	0.000E+00	0.000E+00	KNSTD
MAKA3A	27.8377	87.07373	4995	std	1.75	2.7	0.972529	0.0001	173754.81	8478.07125	07KNSTD	0.000E+00	0.000E+00	KNSTD
MAKA3B	27.8382	87.07402	5001	std	1.75	2.7	0.971193	0.0001	306421.238	10190.458	07KNSTD	0.000E+00	0.000E+00	KNSTD

MIT SCHNEEFAKTOR   2m over 6months with density of 0.3

Sample name	Latitude (DD)	Longitude (DD)	Elevation (m)	Elv/pressure flag	Thickness (cm)	Density (g cm-2)	Shielding correction	Erosion rate (cm yr-1)	[Be-10] atoms g-1	+/- atoms g-1	Be AMS standard	[Al-26] atoms g-1	+/- atoms g-1	Al AMS standard
MAKA1A	27.8424	87.07313	5026	std	13.1	2.7	0.932	0.0001	694545.396	17197.0184	07KNSTD	0.000E+00	0.000E+00	KNSTD
MAKA2A	27.84275	87.07393	5034	std	13.6	2.7	0.959687	0.0001	485936.549	24819.256	07KNSTD	0.000E+00	0.000E+00	KNSTD
MAKA2B	27.84288	87.07372	5040	std	13.35	2.7	0.963839	0.0001	503307.873	12413.0695	07KNSTD	0.000E+00	0.000E+00	KNSTD
MAKA3A	27.8377	87.07373	4995	std	12.85	2.7	0.972529	0.0001	192520.329	8478.07125	07KNSTD	0.000E+00	0.000E+00	KNSTD
MAKA3B	27.8382	87.07402	5001	std	12.85	2.7	0.971193	0.0001	339514.731	10190.458	07KNSTD	0.000E+00	0.000E+00	KNSTD

2.Datierung

Sample name	Latitude (DD)	Longitude (DD)	Elevation (m)	Elv/pressure flag	Thickness (cm)	Density (g cm-2)	Shielding correction	Erosion rate (cm yr-1)	[Be-10] atoms g-1	+/- atoms g-1	Be AMS standard	[Al-26] atoms g-1	+/- atoms g-1	Al AMS standard
OHNE SCHNEEFAKTOR														
MAKA-1Ar	27.8424	87.07313	5026	std	2	2.7	0.932	0.0001	654661.997	15992.4871	07KNSTD	0.000E+00	0.000E+00	KNSTD
MAKA-2Ar	27.84275	87.07393	5034	std	2.5	2.7	0.959687	0.0001	378175.362	13490.7948	07KNSTD	0.000E+00	0.000E+00	KNSTD
MAKA-2Br	27.84288	87.07372	5040	std	2.25	2.7	0.963839	0.0001	434181.99	12059.5773	07KNSTD	0.000E+00	0.000E+00	KNSTD
MAKA-3Ar	27.8377	87.07373	4995	std	1.75	2.7	0.972529	0.0001	159497.345	10746.5914	07KNSTD	0.000E+00	0.000E+00	KNSTD
MAKA-3Br	27.8382	87.07402	5001	std	1.75	2.7	0.971193	0.0001	293959.29	9162.92336	07KNSTD	0.000E+00	0.000E+00	KNSTD

MIT SCHNEEFAKTOR   2m over 6months with density of 0.3

Sample name	Latitude (DD)	Longitude (DD)	Elevation (m)	Elv/pressure flag	Thickness (cm)	Density (g cm-2)	Shielding correction	Erosion rate (cm yr-1)	[Be-10] atoms g-1	+/- atoms g-1	Be AMS standard	[Al-26] atoms g-1	+/- atoms g-1	Al AMS standard
MAKA-1Ar	27.8424	87.07313	5026	std	13.1	2.7	0.932	0.0001	726674.816	15992.4871	07KNSTD	0.000E+00	0.000E+00	KNSTD
MAKA-2Ar	27.84275	87.07393	5034	std	13.6	2.7	0.959687	0.0001	423556.405	13490.7948	07KNSTD	0.000E+00	0.000E+00	KNSTD
MAKA-2Br	27.84288	87.07372	5040	std	13.35	2.7	0.963839	0.0001	484112.919	12059.5773	07KNSTD	0.000E+00	0.000E+00	KNSTD
MAKA-3Ar	27.8377	87.07373	4995	std	12.85	2.7	0.972529	0.0001	176723.058	10746.5914	07KNSTD	0.000E+00	0.000E+00	KNSTD
MAKA-3Br	27.8382	87.07402	5001	std	12.85	2.7	0.971193	0.0001	325706.894	9162.92336	07KNSTD	0.000E+00	0.000E+00	KNSTD

Table 12: Raw data of weathering rind and Schmidt-Hammer measurements.

Weathering Rind Thickness [mm]			Schmidt-Hammer measurements [r-value]				
MAKA_1.A	MAKA_2.A	MAKA_2.B	MAKA_1.A	MAKA_2.A	MAKA_2.B	MAKA_3.A	MAKA_3.B
0.2	0.1	0.3	43	52	36	39	36
0.3	0.1	0.1	44	32	26	52	50
0.1	0.2	0.8	40	48	18	44	48
0.2	0.2	0.4	42	34	42	44	29
0.4	0.2	0.1	40	40	30	42	40
0.1	0.1	0.2	34	40	46	46	33
0.3	0.1	0.1	28	54	30	40	40
0.1	0.1	0.4	30	50	20	46	36
0.1	0.1	0.8	40	54	36	40	28
0.6	0.1	0.2	43	42	22	38	42
0.1	0.1	0.3	41	38	54	49	48
0.1	0.1	0.2	49	36	26	53	47
0.8	0.2	0.1	38	39	38	50	48
0.1	0.1	0.4	32	39	22	46	34
0.6	0.2	0.1	31	39	26	44	48
0.8	0.1	0.8	44	42	48	54	47
0.1	0.1	0.7	39	36	30	34	50
0.5	0.1	0.4	40	33	42	40	40
0.4	0.2	0.1	36	46	42	36	46
0.2	0.2	0.6	42	46	42	46	50
	0.2	0.1	36	54	36	22	54
	0.4	0.5	26	46	30	41	52
	0.3	0.1	18	48	22	39	42
	0.1	0.6	44	44	28	27	36
	0.3	0.1	20	50	34	26	34
	0.8	0.5	38	44	40	51	34
	0.6	0.4	24	44	20	42	39
	0.8	0.1	30	36	36	22	43
	0.4	0.8	34	34	22	31	32
	0.6	0.1	24	42	42	29	28
	0.8	0.2	36	43	34	23	34
	0.1	1	22	36	44	45	43
	0.1	0.1	26	38	44	42	35
	0.1	0.1	28	39	28	37	48
	0.1	0.1	34	31	24	34	38
	0.1	0.1	34	40	20	47	48
	0.4	0.4	34	38	22	28	55
	0.2	0.1	30	48	22	40	42
	0.1	0.1	34	40	24	37	34
	0.1	0.1	30	48	34	46	35
	0.1	0.2	24	50	30	16	55
	0.1	0.1	24	48	24	41	32
	0.1	0.1	26	48	32	29	56
	0.1	0.1	38	48	42	34	53
	0.2	0.3	28	40	38	26	50
	0.1	0.1	30	47	34	44	40
	0.1	0.1	32	44	38	19	49
	0.1	0.6	42	39	30	29	44
	0.2	0.3	48	46	36	42	43
	0.2	0.1	44	41	40	47	26

Table 13: Raw data of the topographic shielding measurements.

Shielding Azimuth	MAKA_1.A	MAKA_2.A	MAKA_2.B	MAKA_3.A	MAKA_3.B
0	20.8	21.8	21.8	19.3	20.8
10	26.6	29.2	26.6	28.8	26.6
20	31.0	32.2	31.0	28.8	31.0
30	31.0	31.0	31.4	26.6	31.0
40	24.7	24.7	25.2	26.6	24.7
50	24.7	22.8	21.1	26.6	24.7
60	24.7	23.3	21.1	24.2	24.7
70	24.7	23.7	21.1	21.3	24.7
80	24.7	15.6	21.1	18.3	24.7
90	24.7	15.6	21.1	16.7	24.7
100	17.7	15.6	16.7	14.0	17.7
110	11.3	15.6	11.3	11.3	11.3
120	9.1	15.6	8.5	11.3	9.1
130	6.8	15.6	8.5	11.3	6.8
140	6.8	6.8	6.3	11.3	6.8
150	5.7	5.7	5.7	8.5	5.7
160	6.8	11.3	9.1	12.4	6.8
170	11.3	11.3	10.2	12.4	11.3
180	11.3	9.6	10.2	11.3	11.3
190	16.2	2.3	3.4	18.0	16.2
200	16.2	11.6	10.2	18.0	16.2
210	16.2	11.6	10.2	18.0	16.2
220	20.8	20.3	10.2	18.0	20.8
230	26.6	26.6	10.2	18.0	26.6
240	28.8	27.7	16.7	18.0	28.8
250	28.8	27.7	22.8	18.0	28.8
260	31.0	27.7	25.2	18.0	31.0
270	33.0	27.7	31.0	18.0	33.0
280	35.0	28.8	31.0	18.0	35.0
290	40.0	28.8	31.0	18.0	40.0
300	38.7	26.6	28.8	18.0	38.7
310	36.9	21.8	24.2	24.2	36.9
320	33.0	18.8	19.3	24.2	33.0
330	33.0	19.3	19.3	17.7	33.0
340	28.8	17.2	18.8	16.7	28.8
350	21.8	18.3	19.3	16.7	21.8